AN ABSTRACT OF THE THESIS OF

Derek Bean for the degree of Doctor of Philosophy in Mechanical Engineering presented on June 7, 2022.

Title: Ignition of Fuel Beds by Firebrands

Abstract approved: _____
David Blunck

The severity of wildfires around the globe is increasing. At the same time, urban development is expanding outward into areas where severe fires occur. There is an increased risk of home loss to fires in areas where severe fires and urban expansion meet. Ignition of homes or nearby fuel is a significant mechanism of home loss. To date, a general model for ignition has proven elusive due to the limited quantification of parameters that control ignition. Thus, understanding and quantifying the processes and parameters that control ignition is essential to reducing home losses. This work considered the influence of fuel bed properties (i.e., particle size and chemical composition), environmental conditions near the ignition site (i.e., wind speed and direction), and variations of ignition sources (i.e., spacing, count, and energy deposition) on the likelihood of ignition. A combination of experimental and computational approaches were conducted to determine the influence of the parameters studied on ignition. Ignition propensity increased when conduction was favored due to small particle sizes compared to radiation-driven heat transfer to fuel beds with larger particle sizes. Ignition was also sensitive to fuel bed species. Fuels high in lignin were not able to be ignited, and increased wind speed decreased the ignition threshold for some, but not all, materials. The formation of recirculation zones caused by wind decreased the ignition threshold. The propensity of wind orientation with respect to the ignition source influenced the formation of recirculation zones. As the size of the recirculation zone increased, the ignition threshold decreased. In windy conditions, the presence of multiple firebrands had little influence on the ignition threshold. However, at low wind speeds, interactions between additional firebrands significantly influenced

ignition. Finally, results from all ignition tests conducted in this work were aggregated, and an ignition model was created. It is anticipated that the insights gained from these studies and the subsequent model may act as a novel framework for predicting ignition.

Ignition of Fuel Beds by Firebrands

by

Derek Bean

A THESIS

submitted to

Oregon State University

in partial fulfillment of
the requirements for the
degree of

Doctor of Philosophy

Presented June 7, 2022
Commencement June 2023

Doctor of Philosophy thesis of Derek Bean presented on June 7, 2022.

APPROVED:

Major Professor, representing Mechanical Engineering

Head of the School of Mechanical, Industrial, and Manufacturing Engineering

---

Dean of the Graduate School

I understand that my thesis will become part of the permanent collection of Oregon State University libraries. My signature below authorizes release of my thesis to any reader upon request.

Derek Bean, Author

ACKNOWLEDGEMENTS

I have been fortunate to be perpetually surrounded by people who have given me an immense amount of support and guidance throughout my life. This has been especially true in my studies. This period of my life has been truly transformative. It would not have been possible without all of the wonderful people in my life. I owe the greatest thanks to my family, whose unwavering support, encouragement, and guidance have been invaluable. I would not be who I am or where I am today if it was not for you all. It is impossible to express how much I appreciate everything you have done for me. To Heather, thank you for being my partner through the toughest parts of this journey, for asking so many great questions, and for encouraging me to keep going so that I may reach my goals. I doubt I would have made it this far without you.

Thank you to Dr. David Blunck for giving me the opportunity to conduct this work. With the graduate school experience you have facilitated, I have achieved things I did not know I was capable of. I have the deepest gratitude for your guidance, insight, and the example that you set. I owe a similar debt of gratitude to my friends and colleagues. I have made many lifelong friendships and created many fond memories. Thank you all for guiding me to who I am today, and I am excited to see where life takes us.

This work was supported by the National Institute of Standards and Technology as part of project number 70NANB17H281.

TABLE OF CONTENTS

TABLE OF CONTENTS (Continued)

Page

LIST OF FIGURES

Figure Page

LIST OF FIGURES (Continued)

Figure Page

LIST OF FIGURES (Continued)

Figure Page

LIST OF FIGURES (Continued)

Figure Page

Chapter 1: Introduction

Wildfires are inevitable and are often beneficial in many ecosystems around the globe. However, wildfires are also a significant source of destruction, especially when they transition from fire-adapted ecosystems to the built environment where homes, structures, and sometimes whole communities are consumed. In recent years the number of homes and structures lost to wildfires has increased and is likely to further increase due to three factors. Climate change is currently and is anticipated to be a driving factor for increased fire severity [1]. Wildfire exclusion has led to significant changes in ecosystems, promoting more severe fires [2, 3] and the expansion of the Wildland Urban Interface (WUI) has increased the number of homes in the path of fires [4, 5]. While the risk of loss due to fires is likely to increase for the foreseeable future, adapting structures to the increased risk by accurately predicting risks both before and during fires may reduce the number of structures lost [6].

A significant mode of structure ignition is by firebrands [7]. A firebrand, alternatively called an ember, is a hot combusting particle of biomass that travels from an active fire to another surface or biomass (e.g., pine needles, leaves, or a crevice in a deck). If the firebrands have sufficient energy, they may ignite the material they land on, leading to ignition, spot fires, and potentially the destruction of a structure. Characterization of firebrand and spot fire processes typically involve three parts: the generation of a firebrand in the fire itself, transport of a firebrand from the fire to the eventual landing point, and the interaction of the firebrand with the surrounding material [8].

The overall goal of this work is to identify parameters and processes that control the ignition of a fuel bed when an firebrand lands on it. Four specific objectives were addressed to provide a framework for achieving the overall goal based on the current knowledge of fuel bed ignition. The specific objectives of this work are as follows:

1. Determine the effects of sizes of the recipient fuels on ignition behavior,
2. Ascertain ignition dependence on heating location(s), mode, and rate,
3. Identify and quantify the influence of wind on ignition propensity,

4. Identify the influence of fuel bed chemical composition on flaming ignition

The structure of this dissertation is as follows. First, the current state of knowledge of fuel bed ignition modeling is summarized as it applies to this work (Chapter 2). A literature review specific to each objective is contained in the corresponding manuscripts. The results of this effort are then presented in manuscript form, followed by the conclusions, suggestions for future work, and appendices. The first manuscript addresses sensitivities of ignition to the particle size of the fuel bed materials (Chapter 3). The second manuscript explores the influence of wind and fluid phenomena around the firebrands in the presence of a heat source unaffected by wind (Chapter 4). The third manuscript identifies sensitivities to ignition related to chemical composition and thermal properties in both quiescent conditions and with wind (Chapter 5). The fourth manuscript identifies changes in ignition propensity when multiple firebrands are located close to the fuel bed (Chapter 6). Chapter 7 summarizes the conclusions of each manuscript and introduces an ignition model developed from the conclusions and data collected. The model is then applied and extended to other ignition experiments from the literature to evaluate the accuracy of ignition predictions across different ignition conditions. The model proposed in Chapter 7 provides a framework to allow the prediction of ignition across various firebrand and fuel bed combinations both in the laboratory and in the field.

It is anticipated that this work will provide insights and a basis for the creation of a simplified model that can accurately predict ignition. For example, in a recent conversation with a developer of the Fire Dynamics Simulator (FDS), the need was expressed for an accurate and low computational cost methodology or model to predict ignition for better fire spread predictions. Due to the large scales in fire simulations (10m grid size) a detailed model of ignition (<1mm grid size) is not feasible. Similarly, risk management personnel or homeowners are not likely to have the capability to create detailed models to predict risk around structures and homes they are tasked with protecting. The model proposed in Chapter 7 is anticipated to become or act as a framework for an easily implemented model that can be used by the fire scale modelers, firefighting personnel, or homeowners to accurately evaluate the risk of ignition due to firebrands. Thus, closing a significant gap in the current knowledge of ignition.

Chapter 2: Background

This chapter provides a discussion of the background and motivation of this work in further depth than the manuscripts presented later in this dissertation. Here, a general overview of ignitions as a threat to structures and fire spread and the current state of knowledge and predictive capabilities is communicated. Each manuscript includes a relevant and more detailed literature review pertaining to the specific objective of the chapter.

2.1 Widlfires and the WUI

Wildfires have been an integral part of many ecosystems for millennia and are often beneficial or required for maintaining a healthy ecosystem. As beneficial as they may be to the natural environment, wildfires pose a significant risk to the built environment. As communities around the world have expanded communities outward into environments that support wildfires (e.g., forests and grasslands), the risk of destruction of structures by wildfires has increased [5]. In the United States, 91% of the Wildland Urban Interface (WUI) growth of 189,000km^2 (larger than the state of Washington) development between 1990 and 2010 is occupied by homes [9] and has continued to grow on recent years. The increased development in these areas means that an excess of 40 million homes are located in areas that may be threatened by a wildfire.

In addition to the increase of homes in the WUI, the intensity and severity of fires have increased. California is an example of the increased fire severity where 13 of the 20 most destructive fires have occurred since 2010, and 7 of the 20 most destructive occurred in 2020 and 2021 [10]. Increasingly severe fires are not just limited to California. Texas and Tennessee each had one of the top ten most severe fires in the United States between 2005 and 2020. Colorado, Oregon, Washington, Oklahoma, and Florida have also seen highly destructive fires in recent years [11]. The United States is not unique in the presence of wildfires that destroy homes. Australia's Black Summer in 2019-2020 was one of the most severe fire seasons in the country's history [1] where over 3000 homes

and greater than 46 million acres burned [12], which is approximately equivalent to 75% of Oregon's land area. The Mediterranean countries of Portugal, Spain, France, Italy, and Greece are also either experiencing greater losses or are a risk for greater losses due to wildfires in recent years. Similar trends are also present in many Asian and South American countries [13]. Wildfires that threaten lives, homes, and structures are truly a global phenomenon, and it is essential to understand how homes are ignited and destroyed in wildfires to better prevent losses from occurring.

2.2 The Problem of Ignition

Ignition of a home in a WUI fire is attributed to three primary mechanisms; direct flame contact, ignition by radiative heating, and ignition by firebrands. Of these methods, ignition by firebrands is considered to be a primary threat to homes [14–16]. Case studies of WUI fires have consistently attributed structural losses to firebrand ignition [17, 18] with one study attributing at least 2/3 of home losses to firebrands [19]. With the majority of ignitions occurring due to firebrand ignition, it is imperative to understand the mechanism of firebrand ignition to reduce home losses. An analysis of structures burned in California wildfires from 2013 to 2018 found that many of the homes lost would have been considered "fire-safe" by current standards but were still ignited by firebrands [20]. Codes, standards, and best practices built upon a better understanding of ignition by firebrands would help provide better resilience to firebrand attacks [7] reducing the number of homes lost in wildfires. Examples of these changes may include adjustments in building and landscaping materials favoring the selection of harder to ignite species or housing geometry constraints to reduce the collection of flammable materials or firebrands. Without a comprehensive knowledge of the ignition process, creating the codes and standards to reduce the risk of home loss is challenging at best and may even be counterproductive.

The general mechanism for firebrand ignition is considered to be a three-step process that starts within the fire itself, often at a significant distance from the ignition point. First, a firebrand is generated as burning material breaks off or is lofted into the air. Second, the firebrand is then lofted through the air and transported to the ignition site. Third, a firebrand lands on a recipient fuel bed, and then ignition occurs if the criteria for ignition are met [8]. When considering the possibility of ignition during a

fire event, all three processes must be considered as each process significantly influences the properties of a firebrand landing on a fuel bed. For example, the number, energy content, and size of firebrands that may land on a fuel bed are significantly influenced by the surrounding foliage [21] and moisture content of the foliage [22] which introduces significant variability in ignition sources a fuel bed may encounter. Similarly, the winds transporting a firebrand significantly influence the path of travel and time of flight, which influences the energy content [23, 24] and localized winds around structures may lead to firebrand accumulation [25–27]. Unfortunately, the generation and ignition processes are significantly less understood than the transport processes [7]. The work contained in this dissertation is focused on the ignition process of the fuel bed by a firebrand and does not consider the generation of firebrands. For further information on firebrand generation processes, the reader is referred to review papers considering this process by Fernandez-Pello [28], Manzello et al. [7] and Babrauskas [8].

Firebrands have been identified as a source of structure loss as early as the 1600s [29] however, studies of firebrand ignition have only begun recently. Perhaps one of the first studies published to specifically address firebrands within the scope of structure loss was conducted by Waterman in 1969 [30]. However, research remained sparse until the early 2000s. Early research and a significant portion of current research have been conducted by dropping combusting firebrands [31–35] (either flaming or glowing) or hot metal particles [36–39] onto fuel beds in varying configurations that simulate conditions in a wildfire and observing ignition or no ignition outcomes. These works have identified some parameters that appear to control ignition but models created from these studies only provide qualitative predictions of ignition. The lack of models of quantitative accuracy was identified by Finney et al. in 2013, who identified the lack of a fundamental understanding of what processes occur and how they interact as a primary gap in the knowledge of ignition [40]. A similar need was identified by Manzello et al. in 2018 [13] and again in 2020 [7]. As fires increase in severity and the WUI continues to expand, the number of homes lost to wildfires is likely to increase in the near future significantly. Thus, the need for accurate predictions of ignition has never been higher.

2.3 Modeling Efforts

Creating a model with quantitative accuracy of ignition requires a thorough understanding of the processes and relative importance of each process leading up to ignition. Figure 2.1 illustrates the different factors that can influence the ignition process. To better understand how these parameters affect the ignition process can be considered as a series of three processes. The first is the heat transfer to the fuel bed from the firebrand. The second is the pyrolysis of the fuel bed material and the subsequent release of pyrolyzates into the air above the fuel bed. The third step is the mixing of the pyrolyzates with air above the fuel bed and subsequent gas-phase ignition. It is important to note that all three of these processes may occur simultaneously throughout the ignition process and are often interconnected. For example, as heat is transferred from the firebrand to the fuel bed, the thermal conductivity of the fuel bed changes with temperature both before and after pyrolysis begins [41]. Furthermore, the heat transfer mode and thermal resistance between the firebrand and fuel continuously change as mass is released due to pyrolysis, which may influence ignition [42]. With the interconnection of the processes that occur during ignition and the inherent variability of fuel beds and biomass fuels in general, the quantification of parameters that influence ignition is quite challenging. Despite these challenges, results of previous research have identified influential parameters that have consistently been observed to control ignition. This work considers these parameters as belonging to one of three categories, namely, thermo-physical properties of the fuel bed, energy supplied by the firebrand, and environmental conditions near the ignition point. Detailed reviews of each category are provided in the relevant manuscripts and are not reproduced here. The remaining sections of this review address the predictive models of ignition that have been created from the current state of knowledge. The accuracy and applicability of each model are discussed in turn, and the remaining challenges are identified as they have motivated the objectives of this work.

Perhaps the first model to be considered for the ignition of wildland fuels is the hot spot theory. The hot spot model considers the ignition of a fuel bed by a heat source (firebrand) by determining the energy required for a thermally explosive reaction in the fuel [43, 44]. The minimum hot particle size for ignition of a fuel bed, as presented by Hadden et al. [39], is shown in Equation 2.1.

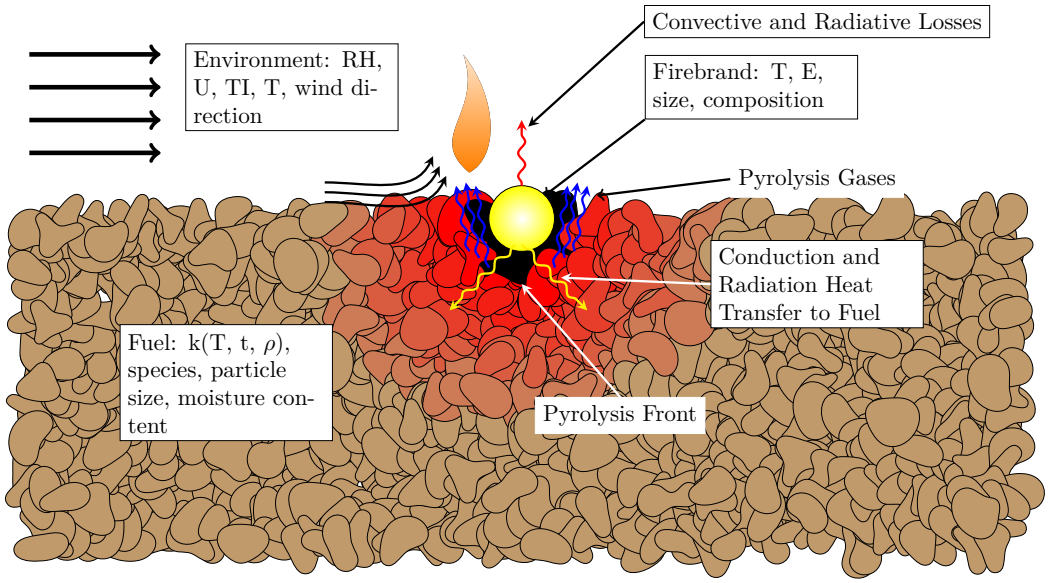

Figure 2.1: Illustration of key features of fuel bed ignition and parameters/characteristics that may influence ignition. The black region near the firebrand represents char formed as the result of pyrolysis.

$$r_{cr} = \delta_{cr}\sqrt{\frac{k}{\rho A \Delta H}\frac{RT_{p0}^2}{E}exp\left(\frac{E}{RT_{p0}}\right)} \tag{2.1}$$

In this equation, δ_{cr} is defined as the critical Frank-Kamenetskii hot spot parameter and is determined from calculations [45]. δ_{cr} is dependent on the ratio of volumetric heat capacities of the ignition source and the material, the activation energy of the material, and the temperature of the hot particle. In Equation 2.1 $k, \rho A, E$, and ΔH are the thermal conductivity, density, pre-exponential factor, activation energy, and heat of combustion of the fuel bed material, respectively. R is the universal gas constant, and T_{p0} is the initial temperature of the heat source. Ultimately, Equation 2.1 defines the particle energy needed to raise the temperature of a fuel bed region such that thermal runaway and subsequent ignition occurs. The hot spot theory has some limitations that prevent quantitative predictions of ignition in a wildfire setting. A discussion of the shortcomings of the hot spot theory is presented by Thomas [44] and more recently presented by Hadden et al. [39] with respect to wildfires. The two most significant shortcomings addressed by the previous works are neglecting heat losses to the surroundings and considering the pyrolysis and ignition phenomena as single-step, infinitely fast reactions. Hadden et al. attribute these shortcomings as a significant source of error for quantitative ignition predictions. This assertion is reinforced in a review by Fernandez-Pello [28] who concluded that in instances where hot spot theory has been applied, only qualitatively accurate predictions of ignition had been obtained. A similar model to hot spot theory but with a more comprehensive inclusion of heat loss from the firebrand was developed by Yin et al. [46]. A correlation between fuel properties, the energy transferred to the fuel bed, and the time to ignition was proposed and is shown in Equation 2.2.

$$\sqrt{t_{ig}} \approx \frac{q\sqrt{\frac{\rho_f k}{c_p}}}{\frac{\rho Z \Delta H_c}{t_b} - h_T(T_f - T_0)} \tag{2.2}$$

Comparing the correlations presented in Equations 2.1 and 2.2, Equation 2.2 includes properties of the fuel bed (ρ, k, c_p, Z, T_0) and firebrand (ρ_f, $\Delta H_c/t_b$, T_f) as well as the energy required for ignition (q) mirroring the Frank-Kamenetskii critical hot spot diameter. The addition of heat losses to the ambient is the most significant difference

from the hotspot parameter and addresses a key shortcoming of the hot spot theory. However, the model does not consider the combustion of the fuel bed other than the critical energy for ignition, leaving the second key gap for the hot spot theory unaddressed. Perhaps due to the omission of combustion, this model suffers a similar fate as the hot spot theory and follows qualitative trends but is not quantitative. Ultimately, the hot spot theory and similar models do not capture the complexity and variability inherent to ignition [7].

Another approach that has been used to predict the onset of ignition in fuels is defining the critical mass flux for ignition. The critical mass flux model asserts that if energy is transferred into a fuel bed at such a rate or quantity that the mass flux of pyrolysis products released is above the "critical" value, ignition will occur [47]. The critical mass flux approach has been primarily considered for the ignition of solid materials such as PMMA [48] and wood slabs [49, 50]. In these studies, the critical mass flux was well correlated with ignition; however, a general model that predicts ignition across materials and experiments is lacking. One shortcoming is the sensitivity to environmental conditions and material properties. In work conducted by McAllister for wooden plates, sensitivities to thermal boundary conditions were anticipated to be magnified in consideration of fuel beds made of particles. Differences in pyrolysis between the materials were also of concern as oxygen availability and boundary layer effects of the particle fuel beds were postulated to have a significant effect [50]. Numerical studies considering the critical mass flux for a piloted ignition reported that the mass flux at ignition was sensitive to the Damkolher number above the fuel bed [51] giving further support to the sensitivity to boundary conditions (i.e., wind near the ignition source). While further study and development of the critical mass flux could potentially be expanded to address its shortcomings, other models have been developed that are more promising.

Proposed ignition models that provide greater accuracy than the hot spot and critical mass flux models do so at the expense of complexity and computational cost. The majority of these models and modeling efforts use a two-part approach to join a pyrolysis-specific solver to address the chemical kinetics of an existing or custom computation fluid dynamics solver. This approach requires selecting a combination of three parts, each of which has limitations and considerations which may affect the accuracy of ignition predictions. First, an appropriate chemical kinetic mechanism must be chosen based on the computational resources available. For example, many early works [52] and some

more recently [53, 54] have considered pyrolysis to occur as a single step process or as a process of few reactions (approximately ten or fewer). Newer kinetic mechanisms have been developed to more completely capture the processes of pyrolysis and are much more complex. Perhaps the most comprehensive mechanisms are extended forms of the mechanism developed by Ranzi et al. [55]. Additions to this mechanism have expanded the method to include extractives to cover a greater variety of biomass [56] and the addition of reactions to address gas-phase reactions previously not considered [57]. For a more detailed discussion of the progression and challenges of biomass pyrolysis, the reader is referred to review articles by Di Blasi [58] and more recently by Haberle et al. [59].

One of the most recent and most promising tools for ignition modeling and pyrolysis is Gpyro which is a pyrolysis solver specifically designed to handle both the condensed (solid) and gas phase of biomass combustion [60]. Gpyro is often coupled with the Fire Dynamics Simulator (FDS) [61], an LES solver specifically designed to capture physics relevant to fires, to form a complete computational package. The combination of Gpyro and FDS has been utilized to observe combustion sensitivities and ignition sensitivities. For example, a study of the effects of moisture content on ignition using Gpyro/FDS suggested that moisture in the fuel affected ignition, gas-phase combustion, and pyrolysis of the fuel [62]. Other studies using Gpyro/FDS have been conducted to predict ignition and observe controlling parameters [38, 63, 64]. Unfortunately, the Gpyro/FDS modeling requires significant computational expenditure. The high computational cost of tools like Gpyro/FDS prevents them from practical application across the vast number of configurations and possible ignition threats present in the wildland urban interface.

To balance the need for accuracy and computational cost, a usable and accurate model is anticipated to be between the critical mass flux and the full CFD model with respect to complexity. The understanding of the effects (e.g., environmental conditions, fuel bed properties.) that are most influential to ignition is not complete enough to develop such a model. Bridging this knowledge gap by identifying and quantifying which parameters are the most influential to ignition or non-ignition outcome is the overall goal of this work. The identification of the most influential parameters is anticipated to enable the creation of a model that can predict ignition across a variety of fuel beds, firebrands, and environmental configurations.

Chapter 3: Sensitivities of Porous Beds and Plates to Ignition by Firebrands

Derek Bean, David L. Blunck

My contributions to this work included the design of the experiments, fabrication of the experimental apparatus, collecting data and/or supervising undergraduates who collected data, data analysis, conducting modelling efforts, and preparation of the manuscript.

Further details of the modeling conducted in this manuscript are contained in Chapter 4.

Frontiers in Mechanical Engineering
Vol. 7, 1-11, 2021.
https://doi.org/10.3389/fmech.2021.653810

3.1 Abstract

The increasing occurrence of severe wildfires, coupled with the expansion of the wildland urban interface has increased the number of structures in danger of being destroyed by wildfires. Ignition by firebrands is a significant avenue for fire spread and structure loss; thus, understanding processes and parameters that control the ignition of fuel beds by firebrands is important for reducing these losses. In this study the effect of fuel bed characteristics (i.e., particle size and porous or solid fuel bed) on ignition behavior was considered. Modelling and analysis was conducted to better understand parameters that are dominant in controlling ignition. The fuel beds, made from Douglas-fir shavings, Douglas-fir plates, or cardboard plates, were heated with a cartridge heater (i.e., surrogate firebrand) to observe ignition. Smaller particles were observed to ignite more readily in porous beds than larger particles when heat transfer from the heater is primarily through conduction. This occurs in large part due to differences in contact area between the fuel bed and the heater coupled with thermal properties of the fuel bed. As particle sizes increased, ignition was more likely to occur at extended times (>100s) due to the increased importance of radiation heat transfer. Douglas-fir plates were primarily observed to ignite at times where conduction was the dominant mode of heat transfer (<10s). Heat flux delivered to the fuel bed was observed to be a more accurate predictor of ignition likelihood and ignition time than heater temperatures. The characteristic ratio of transport and chemical timescales can be used, in conjunction with the measured heat flux and thermal diffusivity of the fuel beds, as a first approximation to predict ignition for the porous fuel beds. This suggests that future work focusing on these parameters may produce a general characterization of fuel bed ignition probability across fuel beds materials and morphologies.

3.2 Introduction

Increasing urban expansion into the wilderness has increased the area of the wildland urban interface (WUI). The increase of the WUI, coupled with global climate change has resulted in fires of increasing severity, size, and impact to humans. For example, consider the state of California in the United States, where four of the five largest fires and three of the five most destructive fires have occurred in the past decade [10, 65].

These fires highlight a trend in the increasing severity of wildfires. Of particular concern with the increasing severity of wildfires is the severity of fires in the WUI. The 2018 Camp fire, where residential property losses amounted to more than twice the reported costs for nationwide federal suppression efforts during the same year [66, 67], is a stark example of how severe a fire that occurs in the WUI can be. A significant mechanism for the spread of fires into the WUI, or even within the WUI, is the ignition of fuel beds by firebrands [15, 68]. Ignition by firebrands in wildfires occurs when a hot combusting particle is generated within the fire and transported, typically by wind, to a recipient fuel bed [69]. Structures in the WUI often have geometry conducive to the collection of firebrands, further increasing the risk of ignition [29]. Hence, efforts to mitigate the destruction that can be caused by fires in the WUI must consider the role of ignition by firebrands.

Three primary processes control the ignition of fuel beds by firebrands. Specifically, heat transfer between the fuel bed and the firebrand, pyrolyzate generation in the fuel bed, and the mixing of the pyrolyzates above the bed at sufficient temperatures for ignition to occur [8]. A recent review of the role of firebrands in the spread of fires by Manzello et al. [7] identified that research into the ignition behavior of fuel beds by firebrands is critical to improving preventative measures. Work conducted by Manzello et al. [34, 35, 70] studying ignition of various fuel bed materials (e.g., cut grass and pine needle beds) concluded that the most influential factors for ignition were the number flux of firebrands to the fuel bed, the size of the firebrands, and the airflow over the fuel bed. Similar conclusions were found by Urban et al. [71], who found that larger firebrands were more likely to ignite fuel beds (i.e., fine sawdust) across a range of fuel moisture contents. These observations illustrate the critical role of heat transfer to the fuel bed in causing ignition. What is not clear from studies such as these is how ignition behavior would change for fuel beds other than those tested, even if identical firebrands were used. Even how the size of fuel particles alter ignition is not clear. Such knowledge is needed to help transition knowledge to a variety of fuel beds that can be present near the WUI (e.g., wood shavings, needles, leaves, etc.).

Essential to understanding the ignitablility of fuel beds is understanding how the role of heat transfer and energy of a firebrand influences ignition. Hadden et al. [39] found that as the energy content of hot metal particles increased the ignition probability increased. It was also observed that the particle energy alone is not a sufficient condition

for ignition to occur and that a minimum particle temperature is required. Similarly, Zak et al. [72] observed that the energy of a metal particle was not a sufficient parameter for ignition and minimum values for particle energy and temperature are required; the values of which are dictated by the ability of hot particles to generate sufficient amounts of hot pyrolyzates in fuel beds. Further studies by Fernandez-Pello et al. [38] added to the understanding of these factors concluding that heat losses from the hot particle, which reduce the heat flux to the fuel bed, can have a significant impact on the ignition of fuel beds. Additional studies conducted by Urban et al. [37, 73] found that the timescale of flaming ignition can be relatively short ($\leq$ 100 ms). Furthermore, smaller fuel bed particles tended to ignite at lower metal particle temperatures. A sensitivity of ignition to the chemical composition of the fuel bed was also observed. While sensitivities to fuel bed particle size, ember particle size, and ember energy have been observed, the relative effect of each parameter on ignition limits and a general application of these sensitivities across various fuel beds and embers remains elusive.

Studies evaluating the heat flux of firebrands and the critical heat flux for ignition have yielded further insights into the ignition process. Hakes et al. [74] found that, for a single cylindrical firebrand and piles of firebrands, peak heat flux values ranged between 20 and 60 kW/m^2 with average heat fluxes between 12 and 25 kW/m^2. The mass of the firebrands or piles of firebrands had little effect on the peak heat flux but directly influenced the total energy released. Tao et al. [75] and observed similar heat fluxes for various of natural and manufactured firebrands. Bearinger et al. [76] observed similar average heat fluxes but observed higher heat peak heat fluxes for firebrands deposited on a steel plate. Hakes et al. [74], Tao et al. [75], and Bearinger et al. [76] observed that an increase in wind speed significantly increased the measured heat flux. Hernandez et al. [77] found that Monterey Pine (*pinus radiata*) needles ignited under heat flux as low as 10 kW/m^2 with ignition time decreasing proportionally to the inverse square of increasing heat flux. In similar tests but with different fuels, Rivera et al. [78] observed that critical heat fluxes for ignition were highly dependent on fuel bed properties with the critical radiative heat flux increasing as the porosity decreased. Reported critical values ranged from 6.64 kW/m^2 to 20.85kW/m^2 for Monterey Pine needles with porosities of 0.09 and 0.01, respectively. It has been observed that a variety of firebrands are capable of producing heat fluxes well above the critical heat flux values long enough for ignition in some fuels. However, upon comparing these values to other studies, ignition is not

guaranteed if the critical heat flux rate and duration are met. For example, experiments conducted by Manzello et al. [70] used firebrands similar to Hakes et al. [74] and Tao et al. [75] with fuels similar to Hernandez et al. [77] and Rivera et al. [78] (e.g., wooden disks on pine needles) but did not observe ignition under conditions that would be anticipated to produce ignition. It should be noted that the studies conducted by Hernandez et al. and Rivera et al. were conducted under quiescent conditions and those by Manzello et al. between 0.5m/s and 1.0m/s. Nevertheless, the reported values of firebrand heat flux at 0.5m/s and 1.2m/s conditions by Tao et al. suggest ignition is likely to occur for instances where no ignition was observed. Not observing ignition under conditions at the apparent intersection of these findings suggests that other factors may be as important as heat flux and duration of heating.

Given this background and motivation the objective of this work is to identify how the size of fuel particles influences ignition and to ascertain changes in ignition of porous and solid fuels. Time to ignition tests with a cartridge heater were conducted to elucidate this sensitivity. It is anticipated that the observations from this study will enhance the understanding of fuel bed ignition and enable more focused studies regarding additional effects of fuel bed properties on ignition.

3.3 Methodology

The time to ignition was measured for five different fuel bed conditions with varying surface temperatures of a resistance heater. The time to ignition was the metric used to evaluate the ignition propensity. The experimental apparatus, as illustrated in Figure 3.1, was designed to replicate both conduction and radiation that may occur when a firebrand lands on the fuel bed. The heater was held in place by a lever arm that, when lowered, positioned the heater at a fixed location for the duration of the test. The firebrand was represented by a 6.35mm diameter 51mm long cartridge heater capable of a 250W output. The heater was inserted 3mm into the bed (approximately half the diameter) in the porous media tests and on top of the plates for the other experiments. The temperature of the heater was continually recorded via a type-K thermocouple attached to the top of the heater. An important distinction between using the lever arm holder and a naturally occurring firebrand is that the location of the heater remained fixed and, for times greater than roughly 10s, could lose contact with the fuel bed as material

was lost because of pyrolysis. Thus, for the longer ignition experiments the arrangement mimicked a firebrand with a gap between it and the fuel bed, instead of a firebrand that maintained consistent contact. The rationale in using the lever arm was to ensure that the heater was placed a consistent depth within the fuel bed since sensitivities of ignition to heat source penetration depth have been observed by Wang et al. [79]. The temperature of the heater was held to within ± 6% of the set point using PID control implemented in LabVIEW. Power delivery to the heater was measured at a rate of 1kHz for all tests. Admittedly, the temperature and heat transfer from an actual firebrand to a fuel bed may vary more than that of a controlled heater, nor does the heater have a piloted ignition source. Nonetheless, trends of ignition propensity are expected to be similar between the heater and firebrands since the heat transfer rates calculated in these experiments are in the range of 1kW/m^2 to 21kW/m^2 which are comparable to heat flux values reported by Hakes et al. [74] and Tao et al. [75] for combustion of glowing firebrands on an instrumented surface. The advantage of using a heater was that it allowed sensitivities of ignition to the fuel beds and controlling processes to more readily be identified because the boundary conditions were measured, controlled, and consistent.

Wood particles and flat plates were used as the fuel bed materials. The fuel particles were Douglas-fir (*Pseudotsuga menziesii*) shavings sorted into three size classes: L_c <1mm, 4mm < L_c < 6mm, and 6mm < L_c < 12mm to allow sensitivities of ignition to be identified. Fuel particles were generated by processing Douglas-fir lumber through a planer and then sorted by screening and/or granulating to achieve the desired size distribution. The fuels were placed in a glass container with a diameter 140mm and a depth of 70mm. The container was filled to the rim for the porous media tests, but the fuels were not packed. The materials used for the tests with flat plates were Douglas-fir and corrugated cardboard processed into 75mm-by-75mm squares. The thickness of the Douglas-fir and cardboard plates were 5mm and 6mm respectively. For plate ignition tests, the plates were stacked in the container to be level with the rim, replicating the porous media tests as close as possible.

The time to ignition was determined from the signal emitted from a BPX65 photodiode positioned to capture the lowering of the cartridge heater and the flames resulting from ignition. This measurement approach only considered flaming ignition. The time to ignition was defined as the time between the maximum light intensity gradients, which corresponds to lowering the heater onto the fuel bed and the ignition event. The pho-

todiode was sampled at 1kHz. Consistency in airflow, and thus oxygen availability, was achieved by maintaining the apparatus in the same orientation in a fume hood with the same airflow settings for every test. The average air velocity over the fuel bed was measured using a hot wire anemometer (TSI IFA300). Measurements were taken with the sample bowl filled with fuel particles and the heater in the lowered testing position at room temperature with the probe positioned approximately 16mm above the fuel bed. The average air velocity over the fuel bed was 0.1m/s.

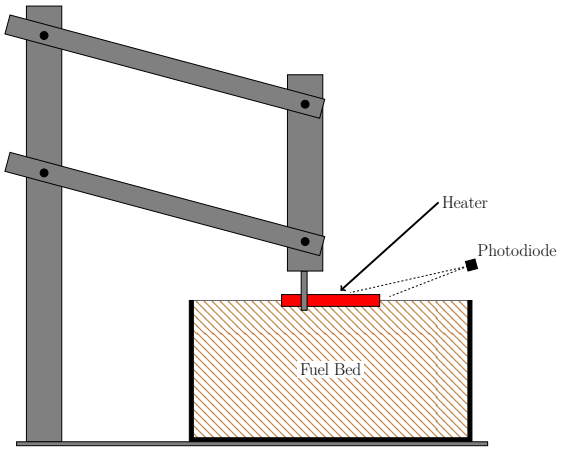

Figure 3.1: Experimental apparatus for the ignition propensity tests. The lever arm used to lower the apparatus into the fuel bed, the fuel bed size relative to the heater, and the location of the photodiode are illustrated.

The heat transfer to the fuel bed was estimated by applying an energy balance around the heater using the supplied (measured) power to the heater and subtracting the calculated infrared radiation losses to the surroundings. The heat flux was determined by normalizing the heat transfer to the heater by one-half of the surface area of the heater. This surface area was justified as the heater was inserted to a depth of half the diameter for each test. Heat loss to the surroundings was estimated by measuring temperatures along the length of the heater but with no fuel bed material in the apparatus. These temperature profiles were then used to estimate the heat losses to the ambient. The emissivity of the heater was taken to be 0.60 [80]. Heat flux values were calculated as an average for the duration of the test, and for a 200ms window when the heater made contact with the fuel bed. These two time scales allowed differences in sensitivities between average and initial

heat flux to be observed. The heat flux values provide insights into variations in the characteristic rate of heat transfer from the heater to the fuel bed for each of the materials tested. Combining the heat flux for each material with the estimated thermal conductivity of the fuel bed enabled representative temperature distributions within the fuel bed to be determined. It is acknowledged that the processes addressed in this work are transient, thus the thermal diffusivity of the materials is applicable. However, thermal conductivity is considered here because the calculation of the thermal conductivity relies on fewer correlations and is potentially more accurate. Additionally, the thermal properties of the materials are derived from literature such that both properties are directly proportional to the experimentally obtained bulk density. Thermal conductivity of the fuel bed materials were estimated using the mean of minimum and maximum effective thermal conductivity correlations in porous media [81]. The correlation for effective thermal conductivity is shown in Equation 3.1 where ϵ is defined as the proportion of volume occupied by air, as is shown in Equation 3.2.

$$k_{eff} = \frac{1}{2}\left(\frac{1}{(1-\epsilon)/k_{solid} + \epsilon/k_{air}} + \epsilon k_{air} + (1-\epsilon)\, k_{solid}\right) \tag{3.1}$$

$$\epsilon = 1 - \frac{\rho_{solid}}{\rho_{bed}} \tag{3.2}$$

The thermal conductivity of Douglas-fir plates and corrugated cardboard plates were obtained from literature [82, 83]. The bulk density of the porous material (ρ_{porous}) and the solid (ρ_{solid}) were obtained from experimental samples. Table 3.1 shows the mean bulk density for each material and the corresponding estimated thermal conductivity values for the porous materials and the solid plates. The values shown in Table 3.1 were used as inputs to the computational models, as discussed later.

Table 3.1: Measured ($\bar{\rho}$) and estimated (k) fuel bed properties

Material	$\bar{\rho}$ (kg/m^3)	k (W/(m K))
Douglas-fir plates	510	0.120
L_c <1mm	135	0.042
4mm < L_c < 6mm	69.9	0.034
6mm < L_c < 12mm	36.9	0.030
Cardboard plates	115	0.053

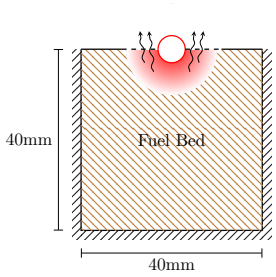

Figure 3.2: Diagram of the computational domain where black lines indicate domain boundaries, and red lines are boundaries defined by the heater. The arrows denote flow of pyrolysis products from the fuel bed into the air above the fuel bed.

Three simplified models were implemented to obtain further insights into the physical and chemical processes causing trends observed in the experimental ignition efforts. First, the temperature evolution of the fuel bed was modeled. Second, the time-averaged mass flux and species concentrations of the pyrolysis species leaving the fuel bed and entering the air were estimated using the calculated temperatures of the fuel bed. Third, the ignition delay times of the gaseous pyrolysis species estimated to depart the fuel bed were calculated. Time-averaged and spatially constant values were used for mass flux and mass fraction of pyrolysis products leaving the fuel bed. Figure 3.2 shows the computational domain representing the fuel bed. Figure 3.3 shows the data flow between the models where the rectangles indicate the implementation of a model or calculation, ellipses indicate an output of interest, and the rounded rectangles indicate an input from measurements or literature values. The dotted and dashed boxes outline which calculations pertain to each chemical mechanism used and the overlap shows the information that is transferred between the models. The fuel bed temperature was modeled using OpenFOAM [84]. Modeling of the pyrolysis was conducted using Cantera [85] with the BioPOx mechanism [57]. The Bio1412 mechanism [55, 86] was used for gas phase species exiting the fuel bed. The Bio1412 mechanism contains 137 species and 4533 reactions. The BioPox mechanism contains 710 species, 5035 reactions and includes both primary pyrolysis and secondary pyrolysis. The inclusion of secondary pyrolysis is important for the combustion of products in the fuel beds studied since the particle fuel beds contain air that may affect the composition of gases as they leave the fuel bed.

Modeling of the temperature evolution of the fuel bed was implemented to represent what occurs during the experiments. The domain size for the fuel bed was 40mm wide and 40mm in depth and ensured that wall effects did not influence the heat transfer over the 10s of simulations. The 10s time limit was chosen since the majority of experimental ignitions occurred before 10s, as explained shortly. Additionally, it was observed in experiments that the fuel bed began to lose contact with the heater beginning near 10s, potentially reducing the applicability of the model beyond this time. All sides of the fuel bed domain were treated as insulated, aside from the heater interface. The insulated sides and bottom of the domain are representative of experimental conditions, but the insulated top surface does not account for losses due to convection or radiation from the fuel bed materials. Nonetheless the calculated temperature distribution within the fuel beds are expected to be valid because heat transfer is dominated by conduction. Reactions and mass loss are not considered in determining the temperature distributions of the fuel beds. Despite these limitations, the calculated temperature distributions provide insights into the mass of each fuel bed material that undergoes pyryolysis which in turn is used for understanding the experimental results.

Combustion of the fuel bed materials was considered in two steps. Reactions occurring within the domain of the fuel bed were characterized with the BioPOx mechanism to include both pyrolysis and gas phase reactions. Reactions occurring at the exit of the fuel bed were considered solely gas phase, thus the Bio1412 mechanism was used. Chemistry calculations for both domains were performed in Cantera. A detailed chemistry model was considered to best capture the physics of the ignition process. However, a detailed discussion of differences in chemistry leading up to ignition are beyond the scope of this work. Instead, this work focuses on qualitative insights into ignition behavior. The mass of the fuel bed undergoing pyrolysis was defined as the mass of the fuel bed material above 220°C. 220°C was selected as it corresponds to the onset of hemicellulose pyrolysis [87] and is the lowest temperature estimated for reactions to occur encapsulating the potential breakdown of all constituents. The temperature at which pyrolysis occurred was taken as the average temperature of the fuel bed material above the temperature threshold. This step was necessary since the Cantera calculations performed were 0D. This approach provided an estimate of the average mass per unit time undergoing pyrolysis reactions. The exit area of the pyrolysis products was assumed to be constant for the duration of the test and was defined by the surface area of the fuel bed adjacent to the heater

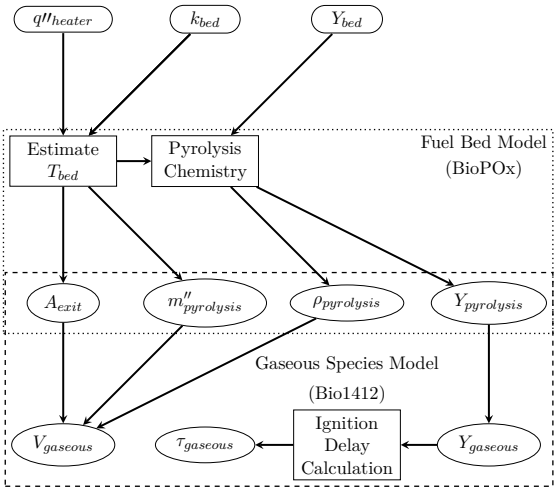

Figure 3.3: Illustration of the model used for the estimated heater flux (q''_{heater}), thermal conductivity of the fuel bed (k_{bed}), and chemical composition of the fuel bed (Y_{bed}), (e.g., cellulose) to calculate temperature (T) and pyrolyzate distribution above the fuel bed, and determine the resulting ignition delay times(τ). Here the subscript *bed* represents the properties of the fuel bed materials and *pyrolysis* represents the pyrolysis products leaving the fuel bed and entering the air above the fuel bed. For example, $V_{pyrolysis}$ represents the velocity of pyrolysis gases leaving the fuel bed and entering the quiescent air domain.

above the pyrolysis temperature at 10s. Species were anticipated to depart the fuel bed and participate in gas phase reactions if they were included in both mechanisms. The mass flux of species departing the fuel bed was defined as the mass fraction of the gas phase species in the fuel bed relative to the mass of the fuel bed undergoing pyrolysis (T>220°C) divided by the surface area of the fuel bed above the pyrolysis temperature as shown by the dashed lines in Figure 3.2. While in a physical experiment the mass flux and exit area would vary with time, all materials were treated equally in this study for simplicity and consistency in generating and understanding trends.

3.4 Results

The time required for flaming ignition to occur for the various fuel beds is shown in Figure 3.4 as a function of heater set point temperature. Four observations are noted. First, the ignition times generally occurred within the first 10s. If ignition did not occur after 10s then it would typically take between 100s and 1000s to ignite, if at all. Conditions where ignition did not occur are not included in Figure 3.4. A histogram of ignition times and the probability density for each material are shown in Figure 3.5 to further quantify the distribution of ignition times. The probability density of the $L_c <$ 1mm fuel particles, Douglas-fir plates, and cardboard plates are normally distributed with centers at 2.3s, 2.8s, and 3.9s. The $L_c <$ 1mm fuel particles have an outlier peak centered at 1000s. The 4mm $< L_c <$ 6mm and 6mm $< L_c <$ 12mm fuel particles are bimodal with highest density peaks at 1.7s and 113s respectively. The secondary peaks occur at 113s for the 4mm $< L_c <$ 6mm fuel particles and 2.1s for the 6mm $< L_c <$ 12mm fuel particles. Second, the probability of ignition at extended times increased as the particle sizes increased. Specifically, the proportion of ignition events in where $t_{ign} <$ 10s group were 90%, 77%, and 47% for the particles $L_c <$ 1mm, 4mm $< L_c <$ 6mm, and 6mm $< L_c <$ 12mm particle sizes, respectively. The third observation is that ignition was not observed beyond 100s for either of the solid plate fuel bed materials. Trends in ignition times for the plates were most similar to those for beds with the smallest particles. Fourth, for the ignition events that occurred within the first 10s there is no apparent relationship between time to ignition, temperature, particle size, and fuel bed type. Additionally, the long timescales of some ignition events suggest that smoldering initiates and then transitions to flaming combustion. Since the incidence of ignition

at extended times increases as the particle size increases the potential for smoldering to flaming transition is attributed to thermal and physical properties of the fuel bed. The different sensitivities of ignition just described are attributed to differences in the bulk thermal properties, the interface between the heater and fuel bed, and the global equivalence ratio of the fuel bed, as explained later.

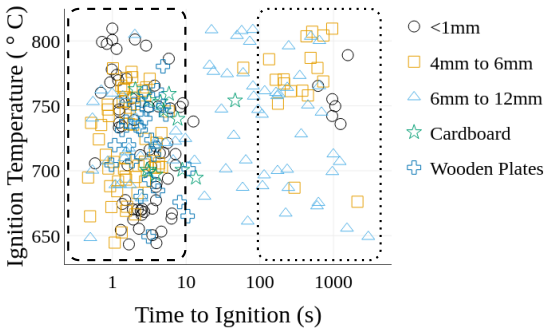

Figure 3.4: Time to ignition and heater temperature at ignition for all fuel bed materials. The dashed and dotted boxes emphasize the two general times-scales associated with ignition.

The clustering of ignition times in either the $t_{ign} < 10$s or 100s $< t_{ign} <$ 1000s time-scales is attributed to shifting of dominant heat transfer modes from conduction to radiation. This shift occurs because of the heater fixture apparatus and the physical properties of the fuel beds. Initially, the heater and the fuel bed are in contact. The beds with larger particles have lower bulk densities; larger fractions of the fuel bed consist of air and have less contact area between particles. As a result, the effective thermal conductivity of the fuel beds decreases as the particle size increases as is shown in Table 3.1. For a fixed heater temperature the higher effective thermal conductivity for the smaller particles would result in a higher mass of particles above the pyrolysis temperature (as supported by calculations) producing conditions more conducive to ignition. As particle sizes decrease the pyrolysis products are also in closer proximity to the heater increasing the chances of either heating or piloted ignition as the gas flows over the heater. As a result, a larger percentage of smaller particle fuel beds ignite within 10s, than the larger particle fuel beds (i.e., the second trend noted for Figure 3.4). As heating progresses, a

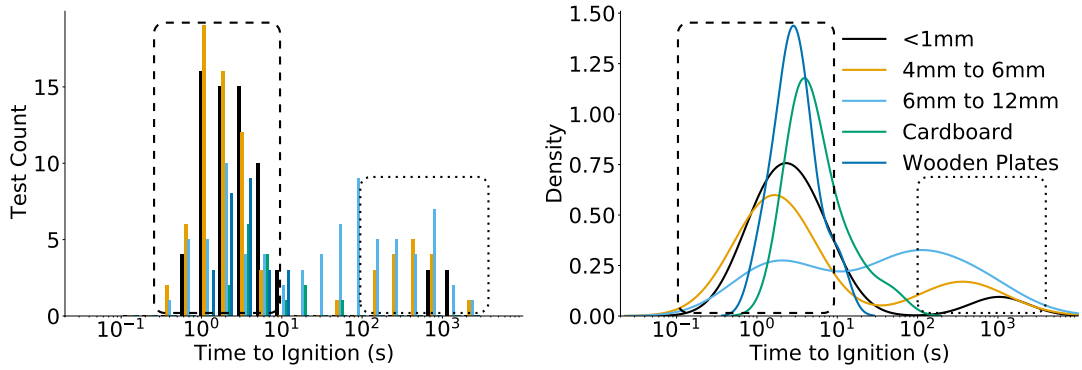

Figure 3.5: Ignition count (left) and probability density (right) of time to ignition for the fuel bed materials tested. The dashed and dotted boxes corresponding to the two zones of ignition from Figure 3.4.

separation between the fuel bed and heater occurred because the heater was held in a fixed location while the fuel bed height decreased because of pyrolysis. Anecdotally this separation was observed to occur after ≈10s for the various fuel beds. This separation causes the dominant mode of heat transfer to shift from conduction to infrared radiation. This change is significant because it corresponds to ignition times to shifting from being less than 10s to being generally greater than 100s, as shown in Figure 3.5. In addition, the larger particles tended to be longer thin particles which, on average, have a larger view factor per volume than the smaller particles. Hence, higher energy deposition per volume occurs for the larger particles when radiation is the dominant mode of heat transfer. As a result, the larger particle fuel beds more readily receive radiation and more readily ignite for t_{ign} >100s, consistent with the trends discussed previously. The shift in dominant modes of heat transfer also causes solid plate fuel beds to not ignite after 100s. As separation between the heater and fuel occurs and heat transfer shifts to being dominated by radiation, the higher thermal conductivity of the solid materials (i.e., $k_{solid} = 0.12\text{W}/(\text{m}\,\text{K})$ vs $k_{<1mm} \approx 0.042$ $\text{W}/(\text{m}\,\text{K})$) reduces the temperature gradients, peak temperatures, and the release of pyrolyzates.

Further analysis of the time to ignition results reaffirm the influence of the fuel bed properties and heat transfer between the heater and fuel bed. A random forest regression model was implemented using the scikit-learn python package [88] to identify which

parameters were most correlated to the incidence of ignition occurring at either less than or greater than 10s. The random forest regression model builds a series of independent decision trees based on experimental variables (e.g., average heat flux, particle size, etc.) and determines from those trees which variables have the largest influence on predicting the correct outcome (i.e., flaming ignition). A model is then assembled based on the specific values of each variable that best predict the desired outcome. Of the parameters recorded or calculated from experimental results, the incidence of ignition within each of the time scales was predicted with at least a 90% certainty (out of bag and R^2 validation) when considering the estimated heat flux to the fuel bed, the fuel bed density, the power delivered to the heater at the time of heater contact, and the heater temperature. The power delivered to the heater at the time of heater contact is included as it serves as a comparison for a an initial reference of heat flux by which a comparison between ignitions that occurred in the radiation dominated mode at extended times which may bias the average heat flux values. The importance of these factors highlight the dependencies previously discussed in that the fuel bed properties and heat transfer to the fuel bed significantly influence the time-scales associated with ignition. Moreover, the random forest analysis highlights a potential way that ignition may be predicted with a subset of information about the fuel bed.

The results and analysis just described focus on the characteristics of igniting cases; Figure 3.6 shows the probability of ignition for each of the fuel bed materials as a function of the heater temperature. The probability reported for each condition is based on the experiments being repeated at least five times. In general, the ignition probability increased as the heater temperature increased, as expected because of the higher energy deposition. It is noted that as the heater temperature increases the potential for piloted ignition of pyrolysis gases increases. However, ignition occurs both above and below the piloted ignition temperature region and there is not a significant shift in trends at higher heater temperatures. This suggests that the influence of piloted ignition on the results is less significant than the increase of heat transfer rates to the fuel beds at higher temperatures.

When considering differences in ignition between fuel bed types the fuel beds with smaller particles typically had higher ignition probabilities at a temperature than beds with larger particles. At the lower temperatures, the plates tended to have lower ignition probabilities than the porous beds, but the plates transitioned from no ignition to unity

ignition probability across a narrower range of temperatures than the porous fuel beds. It is noted that significant deviations from the overall trends (i.e., decreases in ignition probability) are apparent for the $L_c < 1$mm particles at 675°C and 750°C and for the 6mm $< L_c <$ 12mm particles at 700°C. The cause of these deviations are unclear, but it is plausible the changes are caused by differences in ablation of the fuels and shifts in the dominant mode of heat transfer depending on the temperature. The sensitivities in

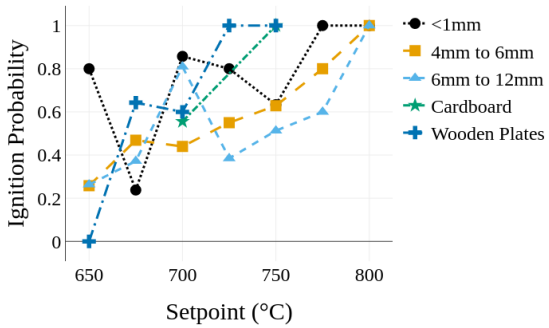

Figure 3.6: Probability of ignition for each material as a function of heater set point temperature

ignition probability to the fuel bed characteristics, as shown in Figure 3.6, are attributed to changes in area of the fuel bed in contact with the heater. Recall that the samples typically ignite within the first 10s; hence conduction and the area of the fuel in contact with the heater are important in causing pyrolysis. As the particle size of the fuel bed increases fewer particles come into contact with the the heater, reducing the overall contact area. Additionally, the average distance between the heater and particles not in contact with the heater increases as particle size increases due to the reduced packing density of the particles. This may result in heat transfer from infrared radiation occurring over a more distributed volume within the fuel bed. As particle sizes increase the reduction in contact area and more distributed heat flux from radiation likely decrease the temperature gradient in the fuel bed as well as the local heat flux rates immediately adjacent to the heater, ultimately resulting in lower ignition probabilities for a fixed temperature as the particle size increases.

With regards to ignition of the Douglas-fir plates, it is expected that the solid materials

behave similarly to the fuel beds with large particles (i.e., lower ignition probabilities at the lower temperatures) because the contact area between Douglas-fir plates and the cylindrical heater are more likely to be similar to the 6mm $< L_c <$ 12mm particles than the $L_c <$ 1mm particles. The Douglas-fir plates also have a much higher thermal conductivity and thermal mass than the particle fuel beds which is anticipated to result in similar temperature gradients between the largest particles and the plates. For the large particles infrared radiation to particles at greater distances from the heater, which would be occluded in the smaller particles, may act similarly to an increase in thermal conductivity and thus the similarity in ignition between the largest particles and Douglas-fir plates. The sharper transition from zero to unity ignition probability for the Douglas-fir plates is attributed to more consistent contact area between the heater and the plates from test to test. This uniformity is indicated in the narrower distribution of ignition times with only a $\approx$ 44s difference between the shortest and longest ignition times for the Douglas-fir plates compared to $\approx$ 1550s for the $L_c <$1mm particles. The narrower transition from non-ignition to ignition and the more consistent times to ignition of the Douglas-fir plates when compared to the particle fuel beds suggest that consistency in material properties and contact area between the heater and the fuel have a significant influence on ignition.

Similar to the time to ignition results, a random forest model was generated to gain insights into which parameters that are measured or derived are the most predictive of the occurrence of ignition of a fuel bed. The estimated heat flux to the fuel bed was the most influential parameter. With the addition of the fuel bed density, heater temperature, and heat flux at contact with the fuel bed the prediction accuracy for ignition was 80%. These values were achieved based a 50% test-train split of the entire dataset with out-of-bag and R^2 validation tests to measure predictive capabilities. The most noteworthy insight from this model is that the estimated average heat flux to the bed over the test duration has a much higher importance than the heater temperature for both porous and solid fuel beds. This is significant since the heat flux values, both upon contact and the overall average, encapsulate the effects of the heat transfer mode to the fuel bed unlike the surface temperature of the heater (or firebrand). A similar sensitivity of heat transferred to the fuel bed influencing ignition was observed by Fernandez-Pello et al.[38].

Figure 3.7 shows the derived average heat fluxes to the fuel bed for each of the materials and heater temperatures tested. Results for igniting cases are represented by

solid lines and non-igniting cases are represented with dashed lines. All the materials show two common trends except for cardboard plates, where not enough temperatures were evaluated to determine a trend. First, for tests where ignition occurred, and the heater setpoint was less than or equal to 750°C the heat flux to the fuel bed was higher than tests where ignition did not occur. Recall that the heater temperature is held constant, therefore variations in heat flux represent variations of heat transfer to the fuel. The implications of this are discussed in more detail later. Second, the heat flux values for tests where ignition occurred showed notable decreases in value for temperatures above 750°C, dropping lower than the values for the tests where ignition was not observed, in some cases. Higher heat fluxes for the igniting cases compared to the non-igniting cases

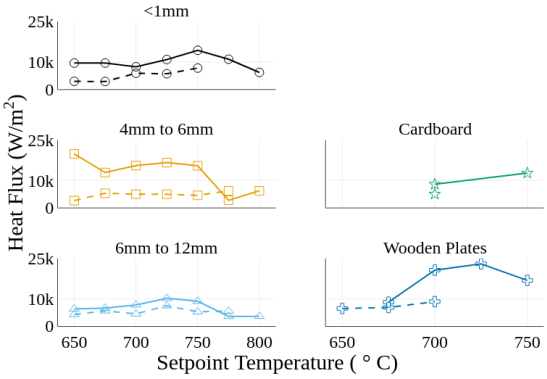

Figure 3.7: Comparison of estimated heat flux to the fuel bed for each material: dashed lines represents the mean of non-ignition tests and solid lines represent the mean of ignition tests for each heater temperature.

for the porous fuel beds are attributed to stochastic differences in contact area between the heater and the fuel bed particles. Seemingly, the tests with particles oriented in a manner that facilitates greater contact area have a higher heat flux due to increased conduction and are more likely to ignite. However, this assumption breaks down for high heater temperatures. At high heater temperatures (e.g., >750°C) the amount of heat transferred through infrared radiation appears be sufficient to counter differences in contact area and resulting conduction. Hence, this causes the reduction in the differences between igniting and non-igniting heat fluxes at the higher temperatures. A sensitivity

to the difference between igniting and non-igniting heat fluxes is noted depending on the particle sizes. Specifically, in Figure 3.7, the 4mm $< L_c <$ 6mm particles have greater differences in heat flux between the ignition and non-ignition cases when compared to the 6mm $< L_c <$ 12mm and L_c<1mm particles. The difference between igniting and non-igniting heat fluxes is correlated to the relative size of the particles compared to the diameter of the heater. For particles much smaller than the heater (<1mm) the random orientation of the particles would matter less than particles of similar size (4mm $< L_c <$ 6mm) as the heater. A similar phenomena is anticipated for particles larger than the heater (6mm $< L_c <$ 12mm), however, for the larger particles infrared radiation is anticipated to be more influential than conduction. Changes in contact between the heater and the fuel bed would then have a smaller effect on the rate of heat transfer as is shown by the spread in heat flux between ignition and non-ignition cases for the 6mm $< L_c <$ 12mm particles in Figure 3.7. The 4mm $< L_c <$ 6mm particles appear to represent a near critical case where the conduction is still the driving heat transfer mode but variation in contact area is high producing a larger spread in heat flux. For the wooden plates a smaller number of heater temperatures with both ignition and non ignition heat flux values is observed suggesting test to test variation in contact area is not significant enough to prevent ignition.

Results from OpenFOAM simulations of temperature profiles provide further insights into the effects of varying heat flux on ignition. Figure 3.8 shows regions of the fuel bed above the pyrolysis temperature for (row I) a fixed 750°C boundary condition, (row II) a heat flux boundary condition based on the average values from ignition tests at the 750°C, and (row III) a heat flux boundary conditions based on average heat fluxes for non-ignition tests at the 750°C. Column A shows the results for the fuel bed with $L_c <$ 1mm, column B with a bed of 4mm $< L_c <$ 6mm, and column C with a bed of 6mm $< L_c <$ 12mm particles. For the constant temperature boundary shown in row I, the region of the fuel bed above the pyrolysis temperature increases as particle sizes increase from left to right. Note, however, that the mass of the fuel bed material above the pyrolysis temperature decreases from left to right due to the decreasing density and thermal conductivity of the fuel bed as particle sizes increases. Specifically, the estimated mass of the fuel bed above the temperature for the onset of pyrolysis is 2.79µg, 1.59µg, and 1.55µg for columns (A), (B), and (C), respectively. As a result, it is expected that the fuel bed with the smallest particles would release the most pyrolzates.

Perhaps surprising, is the difference in area at elevated temperatures between columns A and B in row II. Recall from Figure 3.6 that at this heater temperature (750°C) the particles with $L_c <$ 1mm (i.e., column A), and the 4mm $< L_c <$ 6mm (i.e., column B) have nearly identical ignition probabilities; however, the calculated average temperatures and region undergoing pyrolysis are notably different (e.g., 175°C). More importantly, a 30% mass increase in pyrolyzates occurs from $L_c <$ 1mm to 4mm $< L_c <$ 6mm conditions. The corresponding ignition delay time, calculated using mass of pyrolyzates released and the average temperature of the pyrolysis region, was 0.5s for the $L_c <$1mm gaseous products compared to 0.06s for the 4mm $< L_c <$ 6mm products. The differences in ignition delay time results from differences in the average fuel bed temperature and in the global equivalence ratio as pyrolyzates are released. Physically, these ignition delay times correspond to the characteristics of the pyrolyzates exiting the fuel bed. The differences in ignition delay time would suggest that the particles with 4mm $< L_c <$ 6mm would ignite more readily, counter to the measured similar ignition probability. Note, however, that the calculated velocity of the gaseous products also varies, specifically $4.3{\cdot}10^{-3}$m/s for the $L_c <$1mm fuel compared to $2.6{\cdot}10^{-2}$m/s for the 4mm $< L_c <$ 6mm fuel bed. In short, consideration of both the ignition delay time and exit velocity of the gases maybe needed to more completely capture ignition probabilities.

The Damkohler number (Da), which represents the ratio of the transport to chemical times-scales, has been used previously to consider ignition behavior [51], and is now considered to help evaluate ignition behavior. In this work, the ratio of the heater diameter D normalized by the product of the exit velocity (V_{exit}) and ignition delay time (τ) were considered, to create a Damkohler number of ignition for porous beds. This analysis results in the non-dimensional values of 2.42, 4.04, and 7.66 for the smallest to largest particles (respectively) for the results just described in the previous paragraph. Note that the smaller the (Da) the smaller the transport time (relative to chemical time-scale) and the less time that a parcel of reactants is near the high temperatures of the heater. In its limit, rectants may diffuse/advect away from the fuel prior to ignition.

To further explore the potential role of using a (Da) to characterize ignition propensity or porous, Figure 3.9 shows the (Da) number for the gaseous products at the exit of the fuel bed for each particle size and heater set point. Data from the plates is excluded, as the supporting calculations were beyond the scope of the work. The abscissa is plotted relative to the average heat flux to the fuel bed multiplied by the thermal diffusivity of

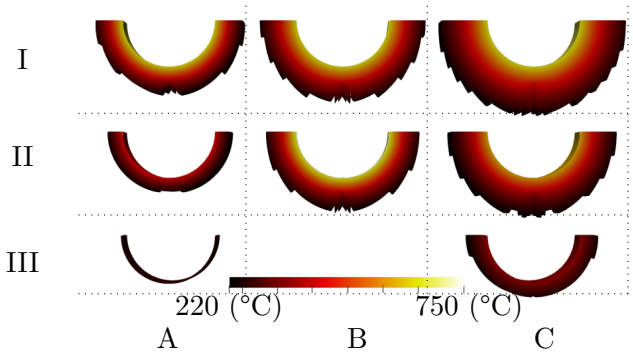

Figure 3.8: Calculated region of fuel bed above the pyrolysis temperature 10s after heater contact for a fixed 750°C boundary (I), ignition event heat flux (II), and non-ignition test event flux (III) for $L_c <$ 1mm (A), 4mm $< L_c <$ 6mm (B), and 6mm $< L_c <$ 12mm particles (C).

the fuel bed. These values were selected to include the influence of heat flux and thermal properties of the fuel beds in the characterization of ignition. Effectively, the chemical properties of the fuel bed and transport behavior are captured in the Da analysis and thermal properties are included in the heat flux and thermal diffusivity. The lower right area of the plot, labelled No Ignition, represents values estimated to be less conducive to ignition (i.e., longer ignition delay times) than those observed to produce ignition in experiments. The region where ignition is expected contains the remainder of the plot and represents values estimated to equally or more conducive to ignition (i.e., higher heat fluxes and shorter ignition delay times) than those observed in experiments. The relative similarity trends in ignition behavior when considering the (Da) indicate that considering the local transport conditions may be important to predicting ignition, in addition to considering the local heat flux and release of pyrolyzates.

3.5 Summary and Conclusions

Flaming ignition tests have been conducted for porous Douglas-fir beds, Douglas-fir plates, and cardboard plates. A cylindrical cartridge heater was used as a firebrand surrogate. Heater temperature and electrical power to the heater were collected throughout each test. The derived heat flux to the fuel bed was within the range reported in literature of heat fluxes delivered by firebrands. The time to ignition and probablity of ignition were

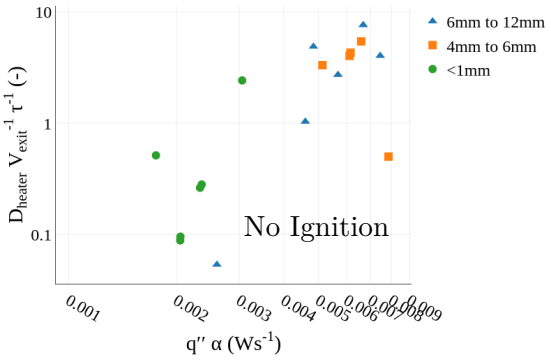

Figure 3.9: Comparison of non-dimensional chemical and flow timescale (for the igniting cases) as a function of heat flux time and thermal diffusivity. Conditions where ignition and non-ignition are anticipated are highlighted.

used to evaluate the ignition propensity for the various fuel beds and heater temperatures. A simplified heat transfer, pyrolysis, and ignition delay model was developed and used to provide further insights into the physical processes associated with ignition. The specific conclusions from this work are as follows.

1. Smaller particles ignite more readily in porous beds than larger particles when heat transfer from the heater is primarily through conduction. This was evident by higher ignition probabilities, in general, of the smaller particles for a fixed heater temperature. As particle sizes increase radiant heat transfer becomes more important and fuel beds with larger particles were more likely than smaller particles to ignite at extended times (>100s) due to the increased importance of radiant ignition.

2. Douglas-fir plates ignite at times where conduction is the dominant mode of heat transfer (<10s) due to the higher thermal conductivity of the solid plates. The ignition probability of plates was the most similar to the larger particle, in particular at lower heater temperatures, due to dispersed heating of the porous fuel bed through radiation and the increased thermal conductivity of the plates creating similar temperature profiles. The rise in ignition probability over a smaller heater temperature range time with temperature results from more consistent contact

between the heater and plate surface.

3. Heat flux delivered to the fuel bed, when compared to heater temperature, is more indicative of ignition likelihood and ignition time for porous fuel beds. Heat flux is a more significant predictor of ignition because it captures differences in heat transfer modes and particle contact that heater temperature values do not. While this finding is not new, what is novel is that the mixed mode of heating (conduction and radiation) has a significant impact on the flaming ignition of fuel beds.

4. Consideration of the transport characteristics of pyrolyzate gases near the high temperature source can be important for more fully predicting ignition propensity. A Da of ignition, in relation to the measured heat flux and thermal diffusivity of the fuel beds, is a promising relationship for predicting ignition for the porous fuel beds.

Further work is needed to verify that the Da may be used to predict ignition for solid surfaces and for porous fuel beds with varying chemical compositions. If proven valid, the (Da), measured/predicted heat fluxes, and fuel bed properties may be used to help predict ignition of fuel beds both in and out of the WUI, ultimately helping to increase the effectiveness of fire prevention and suppression efforts.

Chapter 4: Influence of Wind on Flaming Ignition of Porous Wood Fuel Beds

Derek Bean, David L. Blunck

My contributions to this work included the design of the experiments, fabrication of the experimental apparatus, collecting data, data analysis, conducting modelling efforts, and preparation of the manuscript.

Status: Under Review
Fire Safety Journal

4.1 Abstract

The increasing severity of wildfires and the expansion of the wildland urban interface has increased the need to better protect homes from fires. Ignition of fuels (e.g., needles, mulch, leaves) near or on homes by firebrands can be a significant risk factor for home loss. Understanding the environmental factors that control the ignition of fuel beds by firebrands is important to reducing the risk of home loss. This study evaluates the effect of the wind speed and direction on the probability of ignition of fuel beds by firebrands. The fuel beds, Douglas-fir particles between 1.3mm and 2.3mm in size, were ignited by a cartridge heater (i.e., surrogate firebrand). Flaming ignition probability and time to ignition were determined for three different wind speeds and three wind directions. CFD calculations were performed to provide additional insights into the flow field leading up to ignition. Increases in wind speed above quiescent conditions reduced the temperature required for flaming ignition. An increase in wind speed to 3.5m/s from quiescent increased the ignition probability of fuel beds from 60% to roughly 100% depending on the wind direction. However, a threshold was observed for some wind directions where a further increase of wind did not increase the ignition probability. Temperatures required for flaming ignition and the time to ignition were sensitive to the wind direction. Ignitions occurred at the lowest temperatures when the wind direction was perpendicular to the surrogate firebrand. High speed images of the ignition process and corresponding CFD calculations indicate that ignition occurred in regions with long residence times. The sensitivity to wind direction is attributed to differences in recirculation zones which changes the residence time of pyrolyzates.

4.2 Introduction

As the severity of wildfires and the number of homes in the wildland urban interface (WUI) increases the need is rising to better protect homes from wildfires [2, 11, 89]. A common way that homes are destroyed during wildfires is by the ignition of fuel beds (e.g., needles, leaves, or landscaping materials) by firebrands. Flames may then spread to and subsequently engulf the structure [68, 90]. A better understanding of how fuel beds ignite around homes is necessary in order to better protect homes from this phenomena. While the overall mechanisms by which ignition by firebrands occur are generally well

understood, predicting when ignition will occur remains elusive [28]. One of the reasons for the limitations of predictive capabilities is the lack of quantification with respect to how changes in the fuel bed and environmental conditions influence the likelihood of ignition [40].

Wind is an environmental factor that can have a significant impact on the spread of fires. First, increases in wind speed increase the size of firebrands produced [91], potentially leading to firebrands of higher energy content. Second, firebrand laden winds flowing around structures can lead to accumulation of firebrands in particular regions [25, 90]. Third, the amount of heat imparted to a fuel bed by firebrands can increase as wind speeds increase [74, 75, 92].

In many studies the presence of wind either increases the probability of ignition by firebrands [32, 34, 35, 93–95], or facilitated ignitions that did not occur without wind [31]. For example, in tests with natural fuel beds (e.g, needles, leaves, and grass) and firebrands (e.g., burning twigs, bark, and cones) increases in ignition probability were observed, in some instances, with increases in wind speeds and changes in wind direction [33]. Similar increases in ignition probability as wind speed increases have been observed in fuel beds with hot metal particles as ignition sources [36]. Increases in ignition propensity have been postulated to be caused by greater oxygen availability and/or increased mixing as a result of the wind speed.

In the aforementioned studies the heat transfer rates from the firebrands to the fuel beds may have changed (likely increased due of faster reaction rates) due to the presence of wind. Changes in the heat transfer rate from the firebrands and changes in the flow field near the fuel bed make it challenging to fully identify cause(s) for wind increasing/altering ignition behavior. As a result it is not clear to what extend changes in ignition behavior are caused by the interaction of the fuel bed with the wind or changes in heat transfer from the firebrands. It is important to decouple these two effects to better understand how each factor impacts ignition. A better understanding of ignition sensitivities to wind can ultimately be used to better design building codes and standards to protect structures near the WUI.

With this background and motivation, the objective of this study is to quantify how changing environmental factors, specifically wind speed and direction, influences ignition of a fuel bed in contact with a firebrand. It is expected that the results of this work will help further the understanding of the influence of wind on fuel bed ignition and may

allow for better protection of structures in the WUI.

4.3 Methodology

4.3.1 Experimental

The probability of flaming ignition for beds of Douglas-fir particles were measured for three different wind speeds and firebrand orientations in a wind tunnel. Douglas-fir particles serve as a surrogate for natural fuels near the WUI. Figure 4.1 shows a representation of the wind tunnel, fuel bed, and the portion of the device for lowing a cartridge heater (i.e., surrogate firebrand) onto the fuel bed. The wind speeds tested were 0.5 m/s, 3.5 m/s, and 5.8 m/s. Higher wind speeds were not tested to avoid material from the fuel bed blowing away. The wind speed was measured with a TSI-IFA300 hot wire probe. Tests were conducted with the heater placed parallel, perpendicular, and 45° relative to the wind direction for each wind speed.

The fuel beds were created in a multi-step process. Kiln dried Douglas-fir lumber was planed, then granulated, and finally screened such that the particles fit through a 2.3mm screen but not a 1.3mm screen. The fuel was placed in a 140mm diameter glass container with a depth of 70mm before insertion into the wind tunnel. The average bulk density of the fuel beds was 74.2kg/m^3.

A minimum of 20 ignition tests were conducted for each experimental condition with a total of 241 tests. The temperature set points of the heater for the various experiments were identified using the three-phase optimal design procedure [96, 97]. The three-phase optimal design is a sequential procedure used to ascertain the probability of a binary outcome (i.e., ignition or non-ignition) with a limited number of tests. The logistic regressions and 95% confidence intervals of the ignition probability were calculated using the scikit-learn python package [88]. A fuel bed was considered to ignite if a flame was observed and persisted after the heater was removed. If flaming ignition was not observed after 3000s of heater contact the heater was removed and the test was considered to have a no-ignition outcome.

The energy imparted to the fuel bed was estimated by applying an energy balance to the heater. Typical heat fluxes to the fuel bed ranged from 5kW/m^2 to 50kW/m^2. Similar values have been reported for studies of heat fluxes from firebrands [74, 75]. The

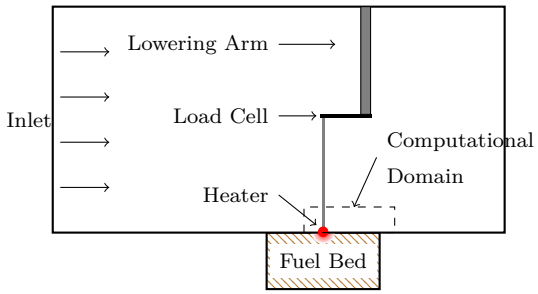

Figure 4.1: Diagram of the experimental wind tunnel apparatus. Air flows through the wind tunnel from left to right. The dashed region represents the domain subset used for computational efforts.

power delivered to the heater was measured using a CR9580-10 current sensor and a ZMPT101B voltage sensor. Temperature distributions, created from infrared images of the heater taken with a FLIR SC6700 camera, were used to estimate heat loss to the ambient. A black body calibration was performed to correlate photon counts from the camera to temperature and produce a longitudinal temperature distribution. The circumferential temperature of the heater was considered uniform.

High speed images of the ignition process were captured using a Phantom VEO 710 camera for select conditions. The images were used to provide insights into differences between ignition processes. Images were collected at 5kHz.

4.3.2 Computational

A simplified computational model was implemented to provide further insights into the processes leading up to ignition for the different configurations. Fluid flow around the heater, heat transfer from the heater to the fluid, and the release of pyrolysis gases into the fluid domain were simulated for the 5.8m/s wind speed and the three heater orientations. Simulations were conducted in two parts. First the average mass flux and average thermal properties of pyrolyzates were estimated. These estimations were conducted through a non-reacting heat transfer model to the fuel bed to obtain an estimate for the mass of fuel bed material above the pyrolysis temperature of 220°C. The thermal properties of the fuel bed were estimated using correlations for porous media [81] and the average bulk density of the fuel beds during the tests. The heat transfer to the fuel bed was

determined from the energy balance for a heater temperature corresponding to the 50% ignition probability.

The temperature evolution of the fuel bed over time was used to estimate the mass of the fuel bed material undergoing pyrolysis. The calculations solved the heat diffusion equation (Equation 4.1) to observe the spatial and temporal evolution of the fuel bed temperatures. Calculations were conducted for 10 seconds for two reasons. First, the assumptions, that are outlined in the following section, reduce the accuracy of the model due to pyrolysis of the fuel bed in the experiment changing the fuel bed properties. Second, in absence of changes in fuel beds due to pyrolysis a simulation time of ten seconds provided sufficient insight into trends observed in the experiments.

$$\frac{\partial\left(\rho h\right)}{\partial t} = \frac{\partial}{\partial x_j}\left(\alpha \frac{\partial h}{\partial x_j}\right) \tag{4.1}$$

The assumptions for the temperature modeling of the fuel bed are as follows:

- Fuel beds were considered to be non reacting.
- Thermal properties of the fuel bed were considered independent of temperature.
- The temperature evolution of the fuel bed is symmetric around the centerline of the heater.
- The heat losses to the ambient are significantly less than the heat transfer from the heater. Thus, the interface between the fuel bed and air was considered insulated.
- The fuel bed was modeled as a solid with the thermal and physical properties either measured or derived from measurements.

The mass of pyrolysis gases released was then estimated using 0D calculations in Cantera. The chemical composition of the fuel bed was estimated from the Bioengineering Feedstock Library database [98]. The BioPox mechanism [57] was used for pyrolysis kinetics in the fuel bed. Species were considered to be released into the flow domain if they existed in the gas phase biomass mechanism Bio1412 [55]. More detail for the species selection process is available in previous work [99]. The Cantera calculations considered the fuel bed material as an insulated fixed mass reactor. The following equations were

solved to obtain the temperature and species concentrations of the pyrolyis products.

$$\frac{\partial m}{\partial t} = 0 \tag{4.2}$$

$$m\frac{\partial \left(mY_k\right)}{\partial t} = \dot{m}_{k,gen} = V\dot{\omega}_k MW_k \tag{4.3}$$

$$mc_v\frac{\partial T}{\partial t} = \dot{Q} - \sum_k \dot{m}_{k,gen}u_k \tag{4.4}$$

Where Y_k, $\dot{m}_k$, and $\dot{\omega}_k$ are the mass fraction, mass generation rate, and generation rate of each species k in the mechanism used. V is the volume of the fuel bed material in the reactor. The species generation rates $\dot{\omega}_k$ are determined from the reactions included in the mechanism. The mechanism used for pyrolysis contains four different types of chemical reactions. The equations used to calculate the reaction rates for an elementary reaction is:

$$k_f = AT^b e^{-E_a/RT} \tag{4.5}$$

$$R_f = [A][B]k_f \tag{4.6}$$

Where R_f is the forward reaction rate, k_f the reaction rate constant, E_a the activation energy, b is the temperature exponent and R is the gas constant. Similarly, the reaction rates for three body reactions are calculated as:

$$R_f = [A][B][M]k_f \tag{4.7}$$

$$[M] = \sum_k \epsilon_k C_k \tag{4.8}$$

Where ϵ_k and C_k are the collision efficiency and concentration of each species, respectively. Falloff reaction rates are calculated using the reduced pressure P defined as:

$$P = \frac{k_0[M]}{k_\infty} \tag{4.9}$$

The reaction reaction rate is then calculated as:

$$k_f(T,P) = k_\infty \left(\frac{P}{1+P}\right) F(T,P) \tag{4.10}$$

Pressure dependent P-Log reaction rates are calculated for intermediate values using a logarithmic interpolation between two reaction rates k_1 and k_2 at pressures P_1 and P_2 as:

$$\log k_f(T,P) = \log k_1(T) + (\log k_2(T) - \log k_1(T)) \frac{\log P - \log P_1}{\log P_2 - \log P_1} \tag{4.11}$$

The overall generation rate of each species ($\dot{\omega}_k$) is defined as the sum of the individual reaction rates R_f for all of the reactions where the species is present. Where ν_i number of each species produced for each reaction. Equation 4.12 results in the source term for Equation 4.3, the solution of which determines the mass fractions of the species that are released into the fluid domain above the fuel bed.

$$\dot{\omega}_k = \sum_i^N \nu_i R_{f,i} \tag{4.12}$$

The second step of the computational effort simulated pyrolysis gas distribution in near the heater using the 3D LES solver FireFOAM implemented in OpenFOAM [84]. The mass, momentum, species, and energy equations for the FireFOAM calculations are shown below.

$$\frac{\partial p}{\partial t} + \frac{\partial \rho u_j}{\partial x_j} = 0 \tag{4.13}$$

$$\frac{\partial (\rho Y_k)}{\partial t} + \frac{\partial (\rho u_j Y_k)}{\partial x_j} = \frac{\partial \mu_{eff}}{\partial x_j} \frac{\partial Y_k}{\partial x_j} \tag{4.14}$$

$$\frac{\partial (\rho u_i)}{\partial t} + \frac{\partial (\rho u_{rj} u_i)}{\partial x_j} + \rho \epsilon_{ijk} \omega_i u_j = -\frac{\partial p_{rgh}}{\partial x_i} - \frac{\partial (\rho g_i x_j)}{\partial x_i} + \frac{\partial}{\partial x_j}\left(\tau_{ij} + \tau_{t_{ij}}\right) \tag{4.15}$$

$$\frac{\partial(\rho h)}{\partial t}+\frac{\partial(\rho u_j h)}{\partial x_j}+\frac{\partial(\rho k)}{\partial t}+\frac{\partial(\rho u_j k)}{\partial x_j}= -\frac{\partial(q_i+q_{ti})}{\partial x_i}+\rho r+q_{rad}+\frac{\partial p}{\partial t}-\rho g_j u_j+\frac{\partial(\tau_{ij}u_i)}{\partial x_j} \quad (4.16)$$

The computational domain used is outlined in Figure 4.1 with a dashed rectangle. A subset of the wind tunnel test section near the heater(s) was considered for the simulation of the flow over the heater(s). For all three heater angles a constant cross section normal to the flow was used. The dimensions of the plane normal to the flow was 110mm wide and 48mm high. The lengths of the domains varied to maintain a domain size of 5D upstream and 14D downstream of the heater. The domain lengths were 170mm for the 45° and parallel configurations and 120mm for the heater perpendicular to the flow. The number of cells for each domain were 420728, 424308, and 307252 for the parallel, 45°, and perpendicular cases. Cell sizes ranged from 0.1mm near the heater to 4mm in the bulk flow region in the center of the domain. For validation the separation angle of the flow was compared to a correlation from literature [100] and was found to predict the angle within 1% of the recommended correlation. Reducing the cell size by a factor of two did not appreciably reduce the error and resulted in a significant increase in computational time. Thus, the calculations were considered of acceptable accuracy to visualize the trends observed in experiments.

The inlet boundary conditions were determined from experimental measurements where the bulk wind speed was 5.8 m/s and the inlet turbulence intensity was 0.14%. The solid surfaces (i.e., cartridge heater, holding rods, fuel bed, and wind tunnel floor) were considered with a no-slip boundary condition and at fixed temperatures. All temperatures except the heater surfaces and pyrolyzate injection were 300K. The cartridge heater was maintained at a fixed uniform temperature corresponding to the temperature estimated to result in 50% ignition probability from experimental tests. The inlet temperature and mass flux of the pyrolysis gases were determined from the fuel bed thermal model and Cantera calculations. The outlet and sides of the domain used a zero gradient boundary condition. The local equivalence ratio was calculated after one second of pyrolysis release. While one second is shorter than average time to ignition, insights are still gained into the distribution of pyrolyzates with respect to the observed ignition locations for the

heater orientations.

4.4 Results and Discussion

The ignition or no ignition outcomes of the tests are shown in Figure 4.2. Individual markers in the plots represent the outcome of each test. The curves are logistic regressions for each of the test groups (i.e., tests with the same wind speed and heater angle) with shaded regions around the curves indicating the 95% confidence interval of the regressions. The tests are grouped such that each plot shows tests of different wind speeds at the same heater orientation. The topmost plot shows results when the heater is parallel to the flow, the middle plot when the heater is 45° to the flow, and the bottom plot when the heater is perpendicular to the flow. The three different sets of data in each plot are the results

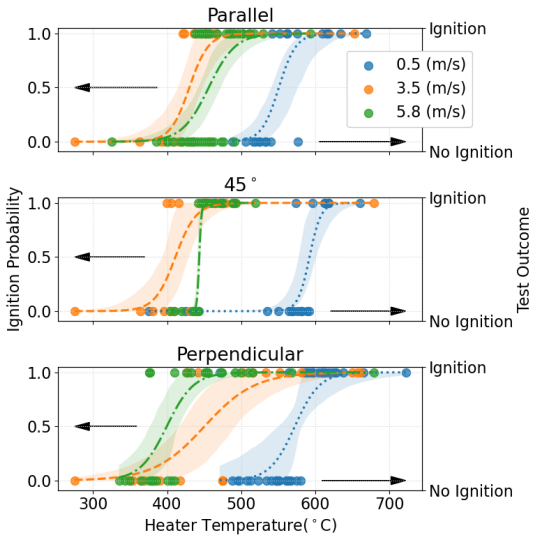

Figure 4.2: Ignition or no ignition outcomes of tests at different bulk wind speeds with respect to heater orientation. Markers indicate the outcome of each test and the curves show the logistic regression of each test group. The shaded regions show 95% confidence intervals for each regression.

for the experiments with three wind speeds. Table 4.1 shows the heater temperatures estimated to produce a 50% ignition probability for the results shown in Figure 4.2. Three observations are noted for the results in Figure 4.2 and Table 4.1. First, the ignition

Table 4.1: Heater temperature required to achieve 50% ignition probability for the wind speeds and heater angles tested.

U_{bulk} (m/s)	0 ° (°C)	45° (°C)	90° (°C)
0.5	551	592	571
3.5	430	411	450
5.8	456	443	399

probability for the 0.5m/s cases are similar to previously published results for a similar fuel bed and apparatus with measured wind speeds of 0.1m/s[99]. Second, increasing the wind speed beyond 0.5m/s increased the ignition probability. This observation is consistent with previously reported work [33, 94] that showed that the presence of wind can increase the likelihood of ignition. What has not been quantified previously is the magnitude of the difference in ignition probability due to wind speed. For example, in tests with the heater oriented parallel to the flow, a heater temperature expected to produce ignition 25% of the time at a wind speed of 0.5m/s is anticipated to produce ignitions for greater than 99% of tests at 3.5m/s and 5.8m/s. The difference is even more pronounced for the 45° and perpendicular orientations where heater temperatures expected to result in ignition less than 1% of tests at 0.5m/s have an ignition probability of over 99% at 5.8m/s. This observation illustrates that an increase in wind speed that is relatively modest (compared to winds often accompanying wildfires) can shift fuel bed ignition risk from minimal to very likely with no other changes in conditions.

The third observation from Figure 4.2 and Table 4.1 is that while an increase in wind speed from 0.5m/s to 3.5m/s resulted in an increase in ignition probability for all heater angles, an increase from 3.5m/s to 5.8m/s does not. For tests where the heater was perpendicular to the flow (90°) an increase in wind speed led to a decrease in heater temperatures required for ignition. For tests with the heater at 45° to the oncoming flow, ignitions were observed at the lowest temperatures in the 3.5m/s case. For the parallel heater case the difference in ignition between the 3.5m/s, and 5.8m/s cases were not statistically significant. These trends in ignition propensity suggest that there is a threshold for ignition enhancement that depends on both wind speed and orientation of the wind with respect to the firebrand. A threshold for an optimum wind speed for inducing ignition has been postulated [95] but this is one of the first studies to confirm its existence and dependence on the orientation of the wind.

Figure 4.3 shows the data reported in Figure 4.2 but organized to more easily highlight sensitivities of ignition behavior for the different heater angles for a constant wind speed. Three observations are noted. First, differences in ignition probability were not statistically significant for the various heater orientations and a wind speed of 0.5m/s. This suggests, as anticipated, that for near quiescent conditions the orientation of the firebrand is less important than the temperature of the firebrand. Second, for the 3.5m/s tests there was not a statistically significant difference in ignition temperatures for the parallel and 45° heater orientations, but there is a statistically significant difference at the 5.8 m/s case. The differences in sensitivities between the two wind speeds is attributed to the lowest temperature required for ignition (maximum ignition enhancement) occurring for a wind speed of 3.5m/s for the 45° orientation. The maximum enhancement of ignition for the perpendicular case appears to occur at a wind speed above 3.5m/s. The third observation is that changing the angle of the heater relative to the wind direction has less of an influence on ignition behavior than changing the wind speed. Thus, for a fixed heater temperature, an increase in wind speed will yield a larger increase in ignition probability when compared to changing the firebrand orientation. This is only true, however, up to the wind speed that produces the greatest likelihood of ignition.

At and above the wind speed that produces the greatest likelihood of ignition for a given firebrand orientation, an increase in ignition will only occur if the angle between the firebrand and wind is increased to become more perpendicular to the flow. The aforementioned observations affirm that both the wind speed and direction can alter the likelihood of flaming ignition of a fuel bed. What is unclear, thus far, are the specific physical processes that promote or retard ignition as the wind speed is increased or the heater angle is changed.

In contrast to the observed sensitivities of wind speed on ignition probability the time to ignition is more sensitive to the heater orientation than the wind speed. Figure 4.4 shows histograms of the time to ignition (i.e., occurrence of flames) for each test where ignition was observed. The wind speed increases from the top plot to the bottom plot and the color of each group in the plot represents the different heater angles. Note that the time to ignition axis is log-scale. Three observations are noted about the time to flaming ignition. First, the times to ignition for the 3.5m/s, and 5.8m/s wind speeds often are sufficiently long (i.e., >100s) enough to suggest that the fuel beds may be igniting in a smoldering mode and then transition to flaming. Second, for the 0.5m/s

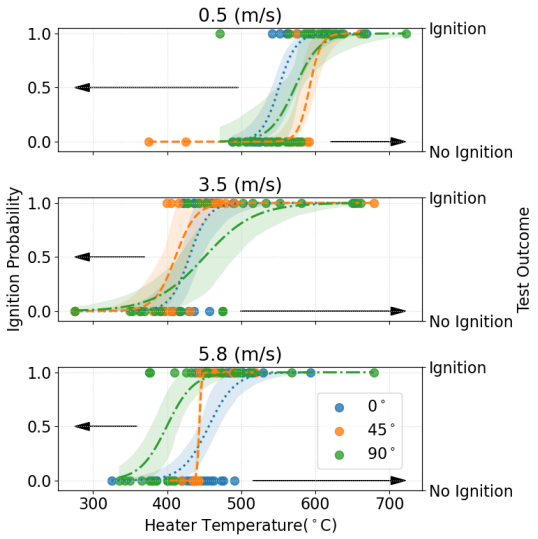

Figure 4.3: Ignition or no ignition outcomes of tests at different heater angles with respect to wind speed. Markers indicate the outcome of each test and the curves show the logistic regression of each test group. The shaded regions show 95% confidence intervals for each regression.

tests the difference in time to ignition between the heater angles are much smaller than for the other two wind speeds. Third, for the 3.5m/s, and 5.8m/s cases ignition times are typically longest when the heater is oriented parallel to the flow. The shortest times to ignition typically occurred when the heater was perpendicular to the flow. The sensitivity of time to ignition to different heater angles suggests that the ignition process changes as the heater angle changes.

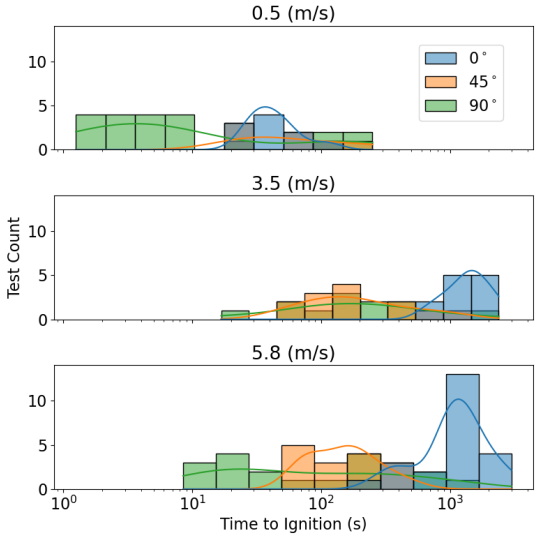

Figure 4.4: Histogram of time to flaming ignition for each test group. Wind speed increased from top to bottom with color indicating different heater angles.

High speed images were recorded for a subset of test configurations to provide more insight into changes in ignition location resulting from changes in heater angle. Figure 4.5 shows images of the initial flame visible during tests of three different heater angles. A heater temperature of 450°C and a wind speed of 5.8m/s were used for all tests. Consistency in the location of ignition was verified by comparing images from three different ignition events for each of the heater angles. For tests where the heater was oriented at either 45° or perpendicular to the flow (Figure 4.5c, 4.5b) ignition was observed to occur on the upwind side of the heater near the fuel bed. For the parallel heater orientation (Figure 4.5a) ignition was observed underneath the heater in a cavity. The cavity was formed by the pyrolysis of the fuel bed. Specifically, ignition occurred at

the downstream side of the cavity in the fuel bed. Differences in ignition location, and subsequent changes in ignition times, are attributed to changes in the velocity field around the heater as the orientation relative to the wind changes. As the heater is rotated from parallel to perpendicular to the flow, pyrolyzates are more likely to remain near the hottest part of the heater (approximately the center) due to the recirculation zones that form on the upwind side of the heater. When the heater is parallel to the flow pyrolyzates tend to advect away from the heater. Thus, for the perpendicular heater the recirculation zone is anticipated to have the longest pyrolyzate residence time. The pyrolyzates are also anticipated to remain near the highest temperature region of the heater. This explantion is consistent with the observation that tests where the heater is oriented perpendicular to the flow typically ignited at lower temperatures than the other orientations, as shown in Figure 4.3.

Considering the aforementioned importance of pyrolyzate residence time on ignition enhancement, it is not immediately clear how the threshold for ignition is lowered with an increase of wind for tests where the heater is parallel to the wind direction. When the heater is positioned parallel to the flow with wind, the pyrolyzates tend to advect away from the hot regions of the heater. However, as previously noted, ignitions for the parallel case occur inside a cavity that forms underneath the heater. The fluid flow that develops with this cavity is anticipated to lead to longer residence times for pyrolyzates. The absence of a sufficient residence times until a cavity of sufficient size forms appears to be the major reason for differences in the time to ignition for the various heater orientations.

Further insights into recirculation zones that form near the heater and the impact on residence times of pyrolyzates are gained from computational results. Figure 4.6 shows streamlines passing though the pyrolysis release zones and the temperature distribution for regions where pyrolyzates are present (i.e., ϕ >0.05) for the three heater orientations at a wind speed of 5.8m/s. The images shown in Figure 4.6 correspond to 1s after the release of pyrolyzates. While typical ignition times are significantly longer than 1s, the results still provide insight into the controlling fluid mechanics. The streamlines shown in Figure 4.6 confirm that a recirculation zone is present near the hottest region of the heater when the orientation is perpendicular or 45° with respect to the wind direction. The presence of recirculation zones is further supported by the presence of pyrolyzates upstream of the heater in Figures 4.6b,4.6c. Perhaps unexpected are the characteristics of the region of the fluid anticipated to be capable of ignition ($\Phi > 0.85$). For both the

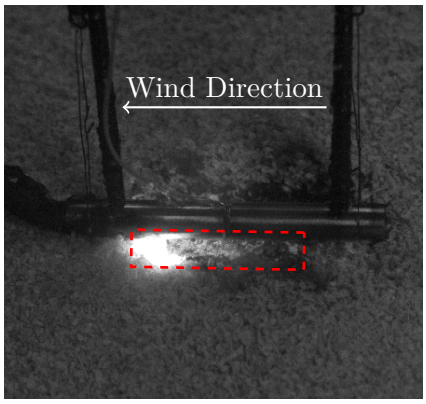

(a) Parallel

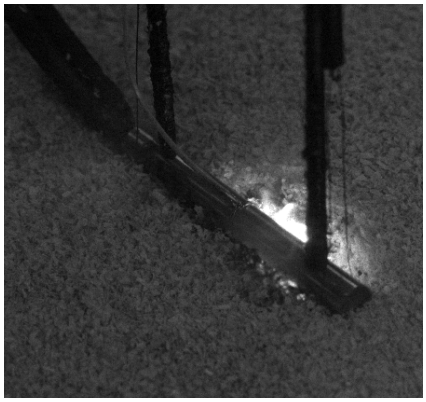

(b) 45°

(c) Perpendicular

Figure 4.5: Representative images of the location of flaming ignition for three different heater angles with a heater temperature of 450°C and a wind speed of 5.8m/s from right to left. The dotted rectangle in 4.5a highlights the cavity formed under the heater during tests.

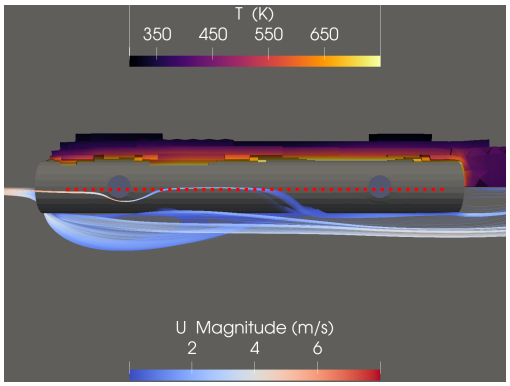

(a) Parallel

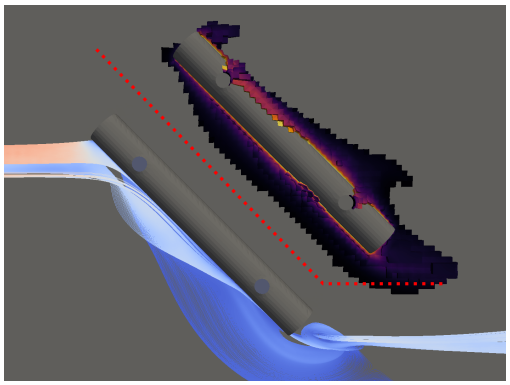

(b) 45°

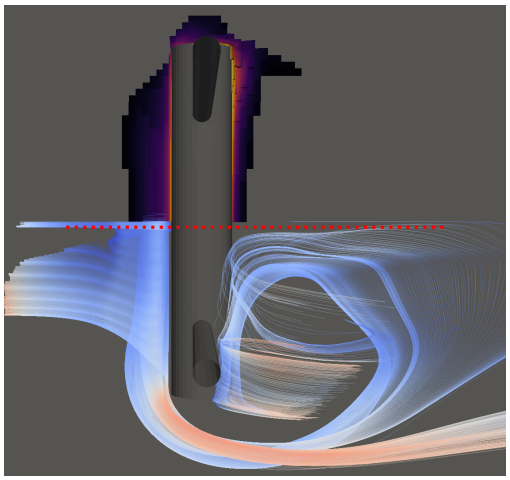

(c) Perpendicular

Figure 4.6: CFD results showing pyrolyzate distribution and streamlines for a wind speed of 5.8m/s. The top half of each image shows the temperature distribution of pyrolyzates in regions where pyrolyzates are present (i.e., ϕ >0.05). The bottom half of each image shows the streamlines, with the color scale representing velocity magnitude, passing through the pyrolyzate release region. Panel 4.6b shows a duplicated heater across the dotted line.

parallel and 45° heater orientation the total volume of ignitable pyrolyzates are between 4 and 6 times larger than the perpendicular heater orientation. The average temperature 3%-5% larger in the parallel and 45° heater orientations. These results suggest that the gas and temperature conditions favor ignition when the heater is not perpendicular to the flow. However, the residence time of the flammable mixture favors ignition when the heater is perpendicular to the flow. Estimates of residence time are made using the ratio of the average velocity magnitude of the pyrolysis gases with $\Phi > 0.85$ and the mass release rate of the pyrolyzates from the fuel bed estimates. The average velocity of the pyrolyzates serves as a proxy for removal of combustible gases from the high temperature zone near the heater. The estimated residence time of the pyrolyzates in the perpendicular heater orientation is more than 25 times longer when compared to the parallel heater orientation and 15 times longer when compared to the 45° heater orientation. The differences in residence times for the three heater orientations align with those for ignition probability supporting the previous assertion that combinations of wind and geometry that facilitate long residence times ignite more readily.

The correlation between time to ignition, ignition temperatures, and ignition locations indicates that ignition events are sensitive to the residence time of pyrolyzates in a high temperature zone. In other words, a firebrand is much more likely to ignite a fuel bed if the wind speed and geometry of the firebrand or firebrands promote extended residence times of pyrolyzates in a low velocity recirculation zone near the firebrand.

4.5 Summary and Conclusions

Flaming ignition tests were conducted for surrogate fuel beds made of Douglas-fir particles. Ignition was induced by a cartridge heater, which served as a surrogate firebrand. The heater was maintained at a fixed temperature throughout each test, thus allowing sensitivities of ignition to wind speed and orientation to be further understood. The ignition probability, time to ignition, high speed imagery, and CFD results were used to quantify sensitivities to ignition related to fluid mechanics around the firebrand and fuel bed as controlled by the wind speed and heater angle. The specific conclusions of this work are as follows:

1. An increase in wind speed above quiescent conditions reduces the temperature required for the flaming ignition of a fuel bed. For example, an increase in wind

speed of 3.5m/s from quiescent increases the ignition probability of a fuel bed from under 30% to roughly 100%. However, a linear increase in wind speed does not result in a linear increase in ignition probability. Thresholds in wind speed exist above which temperatures required to achieve ignition actually increase. For example, when the wind is oriented 45° from the heater centerline increasing the wind from quiescent to 3.5m/s reduces the temperature required for ignition probability by 30%. However, increasing the wind speed from quiescent to 5.8m/s reduces the temperature required for ignition by only 25%. Presumably these thresholds occur because of reductions in residence time.

2. The temperatures at which ignition occurs for porous fuel beds is sensitive to the orientation of a firebrand relative to the wind direction. Higher temperatures are typically required for ignition for a heater parallel to the flow compared to 45° and perpendicular to the flow. This sensitivity attributed to differences in recirculation zones and residence times of air and pyrolyzates near the hottest region of the heater. Thus, predictions of ignition probabilities that consider wind may need to include both wind speed and orientation to obtain sufficient accuracy.

3. Times to flaming ignition of porous fuel beds are sensitive to the firebrand/heater angle in the presence of wind. The parallel heater orientation ignites at the longest time followed by the 45° case with the perpendicular cases igniting in the shortest amount of time. High speed images indicate that ignition typically occurrs in regions where recirculation zones occur, as shown in CFD calculations. The heightened propensity to ignition is attributed to increased residence times of pyrolyzates in the recirculation zones as supported by calculations.

The conclusions of this work show that ignition is favored when a firebrand(s) land on a fuel bed under wind speeds and orientations that promote greater residence times of pyrolyzates near a high temperature region of firebrands. It was observed that increases of wind speed, of a magnitude that may commonly occur during wildfires, can increase the probability of fuel bed ignition from very unlikely to a near certainty regardless of the ember orientation to the wind. This highlights the increased risk of spot fires due to ignition of fuel beds that accompanies wind in a wildfire.

Chapter 5: Effect of Fuel Bed Composition on Flaming Ignition Probability

Derek Bean, David L. Blunck

My contributions to this work included the design of the experiments, fabrication of the experimental apparatus, collecting data, data analysis, and preparation of the manuscript.

Status: In Preparation

Target Journals: Fire Safety Science, Fire Safety Journal, or Fire Technology

5.1 Abstract

The increasing severity of wildfires and the expansion of the wildland urban interface have placed a greater number of homes at risk of being destroyed by wildfires. Ignition of fuel beds on or near homes by firebrands is a significant source of fire spread and structure loss. Fire prevention and suppression efforts lack an expedient method for estimating the likelihood of ignition for the wide variety of materials around homes. In this study, the effects of fuel bed chemical composition on the temperature threshold for flaming ignition was considered. Fuel beds of six different species were heated with a cartridge heater as a surrogate firebrand. Tests were conducted in both quiescent and windy conditions. Fuel beds with high lignin content (i.e., Douglas-fir bark and pine park) were not observed to ignite at the maximum temperature at either wind speed. Increasing the wind speed decreased the ignition threshold for Douglas-fir wood and pine wood but increased the threshold for oak wood. Decreases in the ignition threshold are attributed to recirculation zones near the fuel bed and firebrand interface. However, the increase in ignition threshold for oak wood suggests that chemical sensitivities may inhibit ignition enhancement due to wind. This work suggests that areas of high risk of firebrand exposure may reduce the risk of ignition by using materials high in lignin content.

5.2 Introduction

After a firebrand lands on a fuel bed, the parameters that determine if ignition occurs can be broken down into three categories. The first category contains the properties of the firebrand that lands. The second category considers the heat transfer between the firebrand, fuel bed, and the surroundings. The last category is how the fuel bed responds to the heat transfer from the firebrand. The response of the fuel bed to the heat transfer from the firebrand is influenced by the morphology and chemical composition of the particles in the fuel bed. Fuel bed materials present in wildfires vary significantly in both morphology and chemical composition, and knowledge of the effects of each on ignition is qualitative, at best. A previous study evaluated the impact of particle morphology [99], and this work seeks to identify how differences in the chemical composition of a fuel bed under attack by firebrands influence the probability of flaming ignition.

Fuel beds at risk for ignition by firebrands vary significantly in chemical composition, which may result in differences in thermal properties and the chemical species produced during pyrolysis. Works considering ignition of fuel beds with varying concentrations of constituents have found significant variation in ignition characteristics. Cellulose fuel beds have been observed to have a lower ignition threshold when compared to grass and pine needles when put in contact with hot metal particles [73]. Interestingly, cellulose undergoes pyrolysis at either higher temperatures or later in the heating process than both lignin and hemicellulose [63, 87]. This suggests that the lower ignition temperature of cellulose is not due to pyrolysis occurring at lower temperatures but to the flammability of pyrolyzates produced.

One method to evaluate the effects of chemical composition on the flammability of pyrolyzates produced, and thus ignition propensity, is through modeling of the pyrolysis process. Efforts to characterize the pyrolysis of biomass have continually improved the understanding of the chemical processes that occur in both the solid and gas phase of pyrolysis products. Recently, more inclusive pyrolysis models have been developed that improve on the initial single step Arrhenius reactions [58] and more closely approximate the reactions occurring during combustion of biomass [55–57] based on the initial chemical composition of the fuels. With the development of models that are applicable to a wide range of chemical compositions and environmental factors, the possibility of modeling pyrolysis and ignition of fuel beds is possible. Coupling these models with databases, such as the Bioenergy Feedstock Library [98] (which contains the chemical composition information for a wide variety of materials that may be vulnerable to firebrand attack during a wildfire), predictions of ignition potential may be possible without data from ignition experiments. While currently available tools, like combustion models and composition databases, may be useful individually for understanding fuel bed ignition and pyrolysis, a framework linking the individual resources and knowledge to provide a general model of fuel bed ignition is lacking. Unfortunately, the current level of knowledge on the ignition threshold of materials of variable composition does not facilitate such a framework.

Studies considering ignition have primarily focused on the influence of heat transfer and fuel bed conditions when identifying ignition parameters. The observed sensitivities to fuel bed properties are attributed to heat transfer and chemistry-related processes. The probability of ignition generally increases as the energy content of a firebrand increases [39]. However, further research has indicated that energy content alone is not a sufficient

indicator of ignition as a minimum firebrand temperature (a driver of heat flux rates) is also necessary [72]. Additionally, heat loss from firebrands to the surroundings has a significant effect on ignition [38]. While the previous efforts have focused primarily on identifying the impact of firebrand properties on ignition, efforts focused on the properties of the fuel bed have shown sensitivities to fuel bed material type and particle size [73].

Additionally, for fuel beds of constant particle size, an increase in the packing density of the fuel bed results in a decrease in the critical heat flux needed for ignition [77, 78, 101]. The observed sensitivities to fuel bed properties are likely caused by differences in both heat transfer and chemistry-related processes. Changes in the particle size may impact the contact area (e.g., a ball resting on fine sawdust compared to a pile of pine needles) between the firebrand and fuel bed, potentially reducing the amount of heat transferred through conduction as the contact area decreases. Additionally, when considering a fixed particle size fuel bed, changes in chemical composition may change the heat transfer and heating rate of the materials due to changes in the thermal conductivity of the material affecting the ignition properties of the material. For these reasons, knowledge of the effects of chemical composition on ignition, as it relates to thermal and chemical processes, must be addressed to accurately represent ignition properties for the wide range of materials found in fires resulting in home loss.

The objective of this work is to identify how changes in the chemical composition of fuel bed materials affect the probability of flaming ignition. It is anticipated that knowledge gained from this study may be used to improve the understanding of fuel bed ignition for different fuels and help build a framework for estimating ignition probabilities of different fuels without the need for extensive laboratory testing.

5.3 Methods

The 50% probability of flaming ignition with respect to the surface temperature of a resistance heater was determined for five different materials in quiescent conditions and at a wind speed of 5.8m/s. The fuel bed materials used were Douglas-fir wood, Douglas-fir bark, pine wood, pine bark, wheat straw, and oak wood. These materials were chosen to represent a range of chemical compositions and are materials that may be subject to firebrand attack in a wildland urban interface fire. Table 5.1 shows the estimated chemical composition of the materials based on the Bioenergy Feedstock Library [98]. To

create fuel beds of consistent particle size, materials were granulated and then sorted such that the particles fit through a screen with openings of 2.1mm but not through openings of 0.85mm. Once sorted, the materials were oven-dried at 103°C. Two experimental

Table 5.1: Proportion of cellulose, hemicellulose, and lignin of the materials tested estimated from the Bioenergy Feedstock Library [98]

Material	Cellulose (%)	Hemicellulose (%)	Lignin (%)	Other (%)
Oak Wood	45	22	24	9
Douglas-fir Wood	44	22	28	6
Wheat Straw	44	27	19	10
Pine Wood	40	30	20	10
Pine Bark	39	17	37	7
Douglas-Fir Bark	26	11	59	4

Table 5.2: Average bulk density of materials for each material and wind speed.

Material	U_{bulk} = 0.1m/s (kg/m^3)	U_{bulk} = 5.8m/s (kg/m^3)
Oak Wood	344	428
Douglas-fir Wood	99	74
Wheat Straw	85	85
Pine Wood	114	115
Pine Bark	215	172
Douglas-Fir Bark	131	146

apparatus were used to conduct ignition experiments. The experimental apparatus used for the tests in quiescent conditions is shown in Figure 5.1. The quiescent apparatus used a lever arm to hold the cartridge heater in a fixed position for the duration of the test. The heater was inserted into the fuel bed approximately half of the heater diameter (3mm). Tests conducted with a wind speed of m/s were performed using the apparatus shown in Figure 5.2. This apparatus was operated inside of a wind tunnel where the heater was lowered using an automated lowering device that maintained a constant pressure equivalent to that of a 10g firebrand landing on the fuel bed. The pressure was monitored and adjusted using a PID control system with force measured by a load cell. For all tests the cartridge heater (firebrand surrogate) used was a 50mm long 6.35mm diameter cartridge heater. The temperature of the heater was recorded with a type-K thermocouple for the duration of each test. The temperature of the heater ranged from 250°C to 750°C

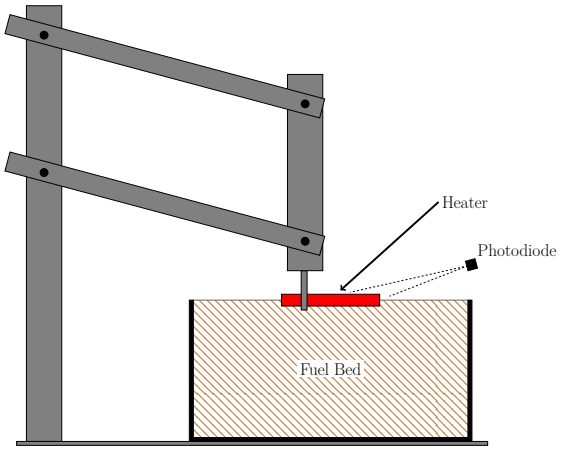

Figure 5.1: Experimental apparatus for the ignition tests. The lever arm used to lower the apparatus into the fuel bed, the fuel bed size relative to the heater, and the location of the photodiode are illustrated.

and was controlled using PID control logic implemented in LabVIEW. The PID controller kept the heater temperature within 6% of the setpoint for the duration of the tests. The temperature setpoints of the resistance heater were determined using the three-phase optimal design procedure to efficiently determine the desired ignition probability for the number of tests conducted [96]. For tests where flaming ignition did not occur, data was recorded for 3000s or until the reaction front of the smoldering material reached the edge of the test container. The fixed position of the cartridge heater and the use of the cartridge heater was implemented to maintain consistency between tests of the same material and between test series of different materials. The use of the cartridge heater and the fixed position is not necessarily representative of a burning firebrand landing on the fuel bed, but the consistency of surface temperatures, ability to record temperature, and consistent contact with the fuel bed is essential for comparing results across test series and materials. For the quiescent tests, flaming ignition was detected with the use of a BPX 65 photodiode sampled at 1 kHz. If the intensity detected rose above a set threshold, flaming ignition was said to occur. For the wind tunnel tests, flaming ignition was determined from the rising temperature of the cartridge heater in the presence of flame. Visual detection of flames was also used in cohort with the photodiode measurements. The 50% probability of ignition was determined from a logistic regression on the outcomes of 25

ignition tests conducted for each of the materials for which flaming ignition was observed. The scikit-learn python package [88] was used to perform the logistic regressions used to predict ignition probabilities. Table 5.3 shows the estimated thermal properties for

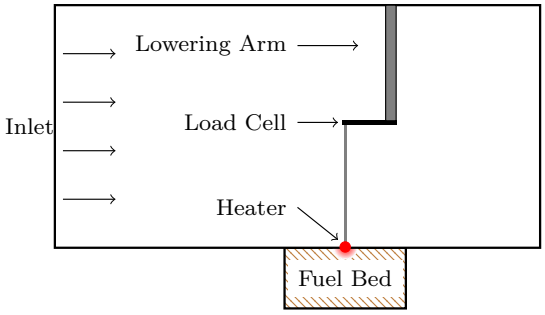

Figure 5.2: Diagram of the experimental wind tunnel apparatus. Air flows through the wind tunnel from left to right.

solid materials, as obtained from literature. The thermal conductivity of the porous fuel

Table 5.3: Estimated material properties the fuel beds tested. The properties of the solid materials were obtained from literature. The thermal conductivity (k_{bed}) and thermal diffusivity (α_{bed}) were calculated.

Material	k_{solid} (W/(m K))	ρ_{solid} (kg/m^3)	c_{solid} (kJ/(kg K))
Douglas-fir Wood	0.12 [82]	510 [99]	1.26 [82]
Pine Wood	0.10 [82]	400 [102]	1.36 [82]
Oak Wood	0.15 [82]	600 [102]	1.23 [82]
Wheat Straw	0.16 [103]	1038 [104]	1.34 [105]
Pine Bark	0.21 [106]	350 [102]	1.36 [106]
Douglas-Fir Bark	0.21 [106]	440 [102]	1.36 [106]

bed materials was calculated using correlations for porous media from literature [81]. Equation 5.1 shows the correlation used where ϵ is defined as the proportion of volume occupied by air, as is shown in Equation 5.2.

$$k_{eff} = \frac{1}{2}\left(\frac{1}{(1-\epsilon)/k_{solid} + \epsilon/k_{air}} + \epsilon k_{air} + (1-\epsilon)\, k_{solid}\right) \tag{5.1}$$

$$\epsilon = 1 - \frac{\rho_{solid}}{\rho_{bed}} \tag{5.2}$$

The specific heat of the porous media was determined using the respective proportions of solid and air, as defined by ϵ, using the values obtained from literature.

$$c_{bed} = \epsilon\ c_{air} + (1 - \epsilon)\ c_{solid} \tag{5.3}$$

The calculated thermal conductivity (k_{bed}) and diffusivity values (α_{bed}) are shown in Table 5.4.

Table 5.4: Calculated thermal conductivity (k_{bed}) and thermal diffusivity (α_{bed}) for the materials tested at both wind speeds.

Material	$U_{bulk} = 0.1$m/s		$U_{bulk} = 5.8$m/s	
	k_{bed} (W/(m K))	$\alpha_{bed}\cdot10^{-7}$ (m^2/s)	k_{bed} (W/(m K))	$\alpha_{bed}\cdot10^{-7}$ (m^2/s)
Douglas-fir Wood	0.038	4.72	0.035	5.49
Pine Wood	0.040	4.87	0.040	4.84
Oak Wood	0.074	5.07	0.089	7.17
Wheat Straw	0.033	4.20	0.033	4.20
Pine Bark	0.098	11.7	0.081	9.18
Douglas-Fir Bark	0.058	6.25	0.062	6.30

5.4 Results and Discussion

The flaming or non-flaming ignition outcome of each test and the logistic regression results for Douglas-fir wood, oak wood, and pine wood are shown in Figure 5.3 for the quiescent tests. The circular markers represent the outcome of each test, either flaming or no ignition. The logistic regression for each material is shown as a solid line with the shaded regions representing the 95% confidence interval for each regression. Douglas-fir bark, pine bark, and wheat straw are not shown in Figure 5.3 because flaming ignition was not observed for five tests at the maximum heater temperature of 750°C. The heater temperature estimated to produce 50% ignition probability from the logistic regressions for each material is shown in Figure 5.5. Anecdotally, self-sustained smoldering was observed for all five materials at temperatures lower than the flaming ignition temperature. The heater temperature corresponding to the onset of smoldering ignition was not measured in this study. Two aspects of the ignition results are of note from the quiescent cases.

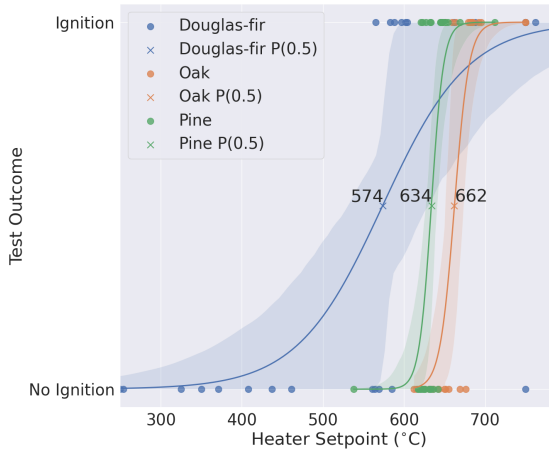

Figure 5.3: Test results for materials where flaming ignition was observed. The circular markers denote individual tests. The solid lines represent the logistic regression and the shaded zones the 95% confidence interval with the 'x' denoting the temperature for 50% ignition probability.

Differences in the heater temperature estimated to produce 50% ignition probability suggest that significant differences in ignition occur across a range of materials in the same apparatus and experimental conditions. Second, the transition between no ignition and flaming is less abrupt (i.e., the 95% confidence interval of the regression spans a much larger temperature range) in the Douglas-fir results when compared to oak wood and pine wood. This is significant because it may cause more difficulty predicting the ignition of materials that ignite at lower temperatures. Lower confidence in predicting ignition for more easily ignitable materials would be detrimental to the usefulness of a model or predictive tool that may be implemented from this testing methodology. It is, however, unclear if the ignition to no ignition transition in other materials of similarly low ignition temperature will behave similarly to that of Douglas-fir. Characterization of additional materials is needed to determine if the ignition to no ignition transition becomes less abrupt as the ignition threshold decreases.

Figure 5.4 shows the averaged cellulose, hemicellulose, and lignin concentrations for each material according to the samples recorded in the Bioenergy Feedstock Library, as shown in Table 5.1. The marker colors for each material correspond to the calculated 50%

ignition probability for the quiescent tests except for the wheat straw and Douglas-fir bark, which are denoted as 800°C to indicate that the 50% ignition probability was higher than the temperatures tested. Note that due to scaling inherent to a ternary projection, the proportion of the fuels that are not cellulose, hemicellulose, or lignin, causes a shift in the data. For example, the wheat straw and Douglas-fir are estimated to have the same cellulose content but do not lie on the same iso-line of 44% cellulose. Nonetheless, the relative proportions of each constituent are retained, and comparisons may still be made. From the data shown in Figure 5.4 a local minimum ignition threshold exists near the concentration of Douglas-fir wood. If the apparent local minimum persists with additional materials, it could be used to rapidly identify materials less conducive to ignition, which would be a powerful tool for choosing appropriate materials on and around homes in areas at risk of ember attack.

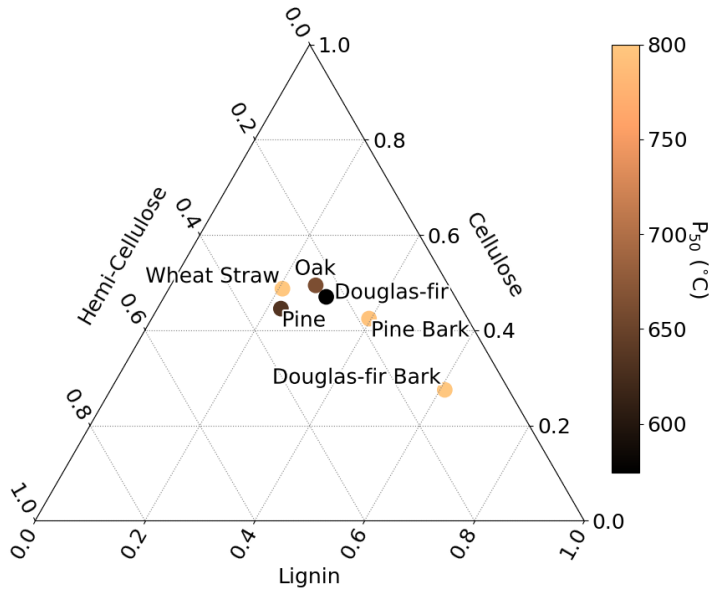

Figure 5.4: Estimated chemical composition of each material tested with the marker color representing the estimated 50% ignition probability. Note that the materials where flaming ignition did not occur are represented as 800°C to show that the temperature of ignition was not achieved.

The 50% ignition probability results for the 5.8m/s wind speed tests are shown

in Table 5.5 along with the results for the 0.1m/s tests. From these results, there are three observations of note. First, the increase of wind lowered the threshold for ignition probability for the Douglas-fir wood and Pine wood by approximately 30%. The decreased threshold for ignition is attributed to the formation of recirculation zones near the heater. This is consistent with results presented in Chapter 4. Second, in contrast to the Douglas-fir and Pine wood results, an increase in wind resulted in an increase in the ignition threshold for oak wood. Flaming ignition was observed for some tests of oak wood under wind. However, the predicted threshold for ignition was above 750°C. Third, the materials that did not ignite in the quiescent tests were also not observed to ignite in the presence of wind. The trends for Douglas-fir wood and pine wood match those presented in Chapter 4 and trends reported in other studies of pine needle ignition [36] and eucalyptus bark [31, 32]. However, the decreasing ignition probability of the oak wood contradicts those observed in the aforementioned studies and this study. A decrease in the ignition in the presence of wind is not unprecedented. An ignition study of various litter layer types ignited by different types of firebrands observed sensitivity to firebrand location. Ignition probability was reduced when the firebrand landed on top of the fuel bed when compared to embedded firebrands [95]. The decrease in ignition probability was attributed to increased heat loss due to wind. In this study, however, the location of the cartridge heater was consistent across all materials, the energy is not a function of the wind speed, and the flow field around the firebrands is consistent. Considering the

Table 5.5: Heater temperature required for 50% probability of ignition for the materials and conditions tested.

Material	0.1 m/s(°C)	5.8 m/s (°C)	ΔT (°C)
Douglas-fir Wood	574	391	-185
Pine Wood	634	430	-204
Oak Wood	663	>750	87
Wheat Straw	>750	>750	-
Pine Bark	>750	>750	-
Douglas-Fir Bark	>750	>750	-

consistent ignition heat source and environmental conditions, the remaining differences that may be driving factors for ignition trends of oak wood are material properties or changes in pyrolyzate ignition due to wind. The most accessible material property to

quantify and compare is the bulk density of the materials. However, there is no clear correlation between density and the probability of ignition. Consider first the wheat straw, which did not ignite at either wind speed, had a bulk density between pine wood and Douglas-fir wood, which ignited in both wind conditions. Based on bulk density, wheat straw is anticipated to ignite at a temperature between these two materials. Similarly, oak wood has a bulk density higher than the Douglas-fir bark and pine bark but was observed to ignite in the low wind speed cases. Clearly, the bulk density of the material is not sufficient to differentiate between cases where ignition does or does not occur.

The thermal diffusivity of the fuel bed materials may provide insight into ignition trends that bulk density does not capture. From the thermal diffusivity values presented in Table 5.4 the fuel bed materials with the highest thermal diffusivity values (pine bark, Douglas-fir bark, and oak wood in a wind speed of 5.8m/s) were not observed to ignite. While there appears to be a correlation between thermal diffusivity and ignition, the wheat straw had a lower thermal diffusivity than both pine wood and Douglas-fir wood but was not observed to ignite in any tests. It is possible that, similar to the chemical composition results, an ideal thermal diffusivity for ignition exists near the thermal diffusivity of Douglas-fir wood and pine wood; however, a more likely cause is the error from the multiple correlations used to estimate values or differences in measurements across the multiple studies from which properties were collected. Thus, neither the bulk density nor the thermal diffusivity estimates made here are sufficient to explain differences in ignition, leaving differences in chemical composition as the remaining predictor.

Douglas-fir bark and pine bark, with the highest lignin content, were not observed to ignite for the conditions tested. This suggests that materials with high lignin contents may be the least likely to experience flaming ignition when exposed to firebrands and thus are the safest with respect to risk around homes. However, this observation does not consider the potential for smoldering ignition and a subsequent smoldering to flaming transition that may occur. Thermogravimetric analysis experiments have shown that while lignin begins to decompose at the lowest temperature of the three primary components, it decomposes at the slowest rate and over a much wider range of temperatures [87]. It was also observed that the peak gas production of CO, CO_2, and CH_4 occurs at higher temperatures than hemicellulose and cellulose. In contrast to Douglas-fir bark, wheat straw had the lowest estimated lignin concentration but was also not observed to ignite. When comparing wheat straw to Douglas-fir wood, the higher lignin concentration sug-

gests that Douglas-fir wood is likely to have a higher ignition temperature than wheat straw. This discrepancy in observed ignition behavior and what is expected based lignin content is attributed to two material attributes. First, the pyrolysis process is complex, and there is not a clear linear relationship between the composition of the fuel and flaming ignition. It appears that materials of different compositions are capable of producing gaseous products of near equal ignitability. However, the proportion of each constituent for which ignition occurs most readily is unclear. Second, the thermal conductivity of the materials likely varies significantly, which impacts the temperature gradients and mass of the material above the pyrolysis temperature, further obfuscating the effect of composition on ignition.

5.5 Conclusions

Flaming ignition tests were conducted for fuel beds of six different materials at two different wind speeds. Ignition of fuel beds was induced by a cartridge heater that served as a firebrand surrogate. The temperature of the heater was maintained at a fixed temperature throughout each test, allowing sensitivities of ignition to fuel bed composition to be evaluated. The ignition probability and chemical composition were used to evaluate the influence of the chemical composition of the fuel bed and observe differences in ignition probabilities in the presence of wind and in quiescent conditions. The specific conclusions of this work are as follows:

1. Of the six materials tested, only three were able to be ignited below the 750°C maximum temperature of the firebrand surrogate. Two of the three materials for which ignition was not observed were bark. The higher ignition threshold of the bark materials is attributed to higher lignin concentrations. The resistance to ignition present in these materials suggest that using materials high in lignin in locations at risk for firebrand attack in wildfires may reduce ignitions and subsequent losses of structures. It is acknowledged that these results are for flaming ignition only, and high lignin materials may pose a significant risk if smoldering or the smoldering to flaming transition occurs.

2. For Douglas-fir and pine wood, an increase in wind speed decreased the temperature required for ignition. However, for oak wood, an increase in wind speed inhibited

ignition. Increases in ignition propensity with an increase in wind are attributed to the formation of recirculation zones near the ignition source. In the case of oak wood, the formation of recirculation zones inhibits ignition. The root cause of the dichotomy in ignition trends is unclear; however, differences in the flammability of pyrolysis products corresponding to changes in chemical composition are most likely.

3. A direct correlation between the fuel bed composition and the ignition propensity was not observed. This is attributed to the complexity of biomass pyrolysis. However, a local minimum ignition threshold near the composition of Douglas-fir wood is present that warrants further investigation.

The conclusions of this work show that ignition is sensitive to the chemical composition of fuel beds in both quiescent conditions and under wind. An increase in wind was observed to increase ignition probability for some materials; however, this was not universally the case. Materials high in lignin were among the least likely to ignite and more suitable for placement in areas where firebrands are likely to land or accumulate in a WUI environment. Further and more targeted analysis of the differences in pyrolysis products for each material will likely yield further insight.

Chapter 6: Influence of Multiple Firebrands on the Ignition of Fuel Beds

Derek Bean, David L. Blunck

My contributions to this work included the design of the experiments, fabrication of the experimental apparatus, collecting data, data analysis, modelling efforts, and preparation of the manuscript.

Status: In Preparation

Target Journals: Fire Safety Science, Fire Safety Journal, or Fire Technology

6.1 Abstract

The increase in wildfire severity and the expansion of the wildland urban interface have increased the need to protect homes from igniting during fires. Firebrand ignition is a significant source of home loss in wildfires. Firebrands often accumulate on or near structures, and an understanding of how multiple firebrands interact with the fuel, environmental factors (i.e., wind), and other firebrands is necessary to better predict ignition and protect homes effectively. This study evaluates changes in the ignition propensity of a fuel bed when two surrogate firebrands are introduced as ignition sources. The fuel beds consisted of Douglas-fir particles between 1.3mm and 2.3mm in size. Cartridge heaters were used as surrogate firebrands. Four different heater configurations were tested at two different wind conditions. Two heater spacings were used with either two actively heated firebrand surrogates or one inert and one actively heated. A simplified CFD model was implemented to provide additional insights into conditions leading up to ignition. Increasing the wind speed reduced the temperature required for flaming ignition between 20% and 60%. Ignition thresholds were largely independent of firebrand surrogate configuration at the high wind speed. However, at the low wind speed, interactions between the firebrand surrogates significantly influenced ignition. Results from the CFD model indicate that ignition occurred in regions where recirculation zones were present. The location of recirculation zones where ignition was initiated was not always located near the firebrand surrogate. More broadly, this work suggests that at low wind speeds or in quiescent conditions, thermal interactions between firebrands has a significant impact on ignition, but higher wind speeds, fluid dynamic effects control ignition.

6.2 Introduction

The increase of both wildfire severity and the number of homes on the Wildland Urban Interface (WUI) has increased the occurrence of home loss due to wildfires since the turn of the century [89]. Ignition of fuels by firebrands that in turn leads to the loss of a structure is a primary source of home loss [18, 20, 69], and in some fires, has been the source of 2/3 of structure ignitions [68]. Thus, it is important to understand the ignition of fuel beds by firebrands in order to mitigate the risk of structure ignition [90]. Ideally, the understanding of the ignition process would result in a predictive model that

would enable homeowners, firefighters, and other risk management personnel to determine location-specific strategies for preventing ignition before and during a fire. Unfortunately, such a model does not currently exist due to critical shortfalls in the current knowledge of fuel bed ignition. For example, if a burning twig or cone landed on needles accumulated in a gutter of a home, there is no model that can quantitatively predict whether or not ignition occurs, and therefore the risk of that structure being lost to ignition from the ember cannot be determined. The consequences of limited risk assessment and mitigation for structures are numerous. For example, in WUI fires, firefighting resources are often used to harden structures against firebrand ignition, but without an accurate prediction of risk, each home must be treated equally, which in turn expends fixed resources on homes that don't need assistance at the detriment to those at highest risk.

Processes that influence ignition begin within the fire when a firebrand (e.g., branch, bark, cone, etc.) is ignited and lofted into the air by wind. The combusting firebrand is then transported to and lands on a fuel bed near or on a structure. Energy is then transferred to the fuel bed, and if the energy is sufficient, the fuel bed will undergo pyrolysis and produce flammable gases, which may then ignite and begin flaming. These flames may then spread and destroy the structure. Each of these processes, firebrand generation, transport, and ignition, require additional research before a predictive model is possible. This work focuses on the processes that occur during ignition of the fuel bed.

An additional risk factor for the ignition of structures is the accumulation of firebrands on fuel beds. The geometry of homes often promotes the accumulation of firebrands by creating recirculation zones that promote the deposition of firebrands. The accumulation of firebrands poses an increased risk of home ignition in multiple ways. First, since ignition is largely a stochastic process, the more firebrands that land on an area, the larger the probability of ignition. Second, firebrands that accumulate close to one another may depart more energy onto a fuel bed than a single firebrand alone. In work conducted by Hakes et al. [74] an increase in firebrand pile mass increased the total energy imparted to an instrumented surface. The increase in energy release was attained by a longer duration of energy release as the pile mass increased.

The accumulation of firebrands near structures also requires the presence of wind which has also been shown to influence ignition. Thus, considering ignition by multiple firebrands also requires the consideration of wind on the process. In work conducted by Suzuki and Manzello [25] when wind was increased from 6m/s to 8m/s the number of

firebrands required for ignition of the wood much fuel bed decreased. Similar observations of wind lowering the ignition threshold have been observed in multiple studies with single firebrands. Wang et al. [36] reported decreases in ignition times as wind speed increased for hot metal particles dropped on pine needle fuel beds. Ellis reported that the addition of wind increased the threshold of fuel moisture content where ignition was observed for natural firebrands deposited on eucalypt forest litter. The trends observed by Ellis agreed with those observed by Ganteaume et al. [33] and Pulcinski and Anderson [95] where the addition of wind increased ignition probability. From these studies, an increase in wind increases the danger of fuel bed ignition near homes, but the mechanism(s) that cause the increased ignition probability are unclear.

For single firebrands, it has been postulated that the primary enhancement of wind is due to increased oxygen to the firebrand and fuel bed. From these works it was unclear if the ignition enhancement was due to increased heat release from the firebrand, increased mixing and oxygen in the pyrolyzates, or some combination of both. Results from the work outlined in Chapter 4 show that in the presence of an ignition source where the heat release is not influenced by wind an increase of wind increases the ignition probability. The increase in ignition probability was attributed to the accumulation of pyrolysis products near the energy source (cartridge heater) suggesting that fluid flow near the firebrand is a significant controlling parameter for ignition.

The addition of multiple firebrands in close proximity adds additional layers of complexity with respect to both heat release and fluid dynamics. Hakes et al. [74] identified re-radiation and reheating as key processes that differentiate single firebrands from multiple firebrands and have significant influence on energy deposited to the fuel bed. The presence of multiple firebrands may also create disturbances in the fluid flow around the firebrands that influence recirculation zones and alter the ignition propensity. What is unclear from these conclusions is the magnitude of the effect that re-radiation and flow disturbances have on ignition. Understanding the magnitude of these processes on the probability of ignition is imperative to creating accurate ignition models.

With this background and motivation, the objective of this study is to quantify the influence of multiple firebrands on the ignition propensity of a fuel bed. It is anticipated that the results of this work will help further the understanding of the difference in ignition propensity between a single firebrand and multiple firebrands that may interact through fluid and thermal processes. A more complete understanding of these processes

can ultimately be used to increase the accuracy of ignition models and enable better protection of structures in the WUI.

6.3 Methodology

6.3.1 Experimental

The probability of flaming ignition for fuel beds consisting of Douglas-fir particles was measured for eight configurations of two firebrands in a wind tunnel. The wind tunnel was operated at either 0.5 m/s or 5.8 m/s for each test series. The wind speed was measured with a TSI-IFA300 hot wire probe. Figure 6.1 shows a representation of the wind tunnel, fuel bed, and the automated lowering device. Table 6.1 shows the test matrix for each series of tests. For all of the tests the heaters were oriented perpendicular to the flow and the downstream heater was heated. For tests where both heaters were heated the temperatures of both heaters were maintained at the same temperature.

The combinations of heater spacing and hot or ambient upstream heater were chosen to represent different levels of fluid and thermal interactions between the heaters and the fuel bed. The heater spacing of five diameters was chosen such that minimal interaction between the heaters occurs as preliminary CFD calculations indicated that the recirculation zone of the upstream heater is approximately five diameters when the heater is in a wind of 5.8 m/s and an orientation perpendicular to the flow. Preliminary thermal calculations also indicated that the pyrolysis fronts created by each heater are unlikely to interact within previously observed times to ignition. The heater spacing of one diameter was chosen for a high level of interaction between both the fluid disturbances and thermal fronts of each firebrand. The one diameter spacing places the downstream heater inside the recirculation zone of the upstream heater under wind, and the preliminary heat transfer calculations indicated that the thermal fronts of each heater will merge before the anticipated time to ignition.

The chosen heater orientations also represent potential scenarios that may be encountered in a wildfire. The configuration with two heaters both heated is representative of a multi firebrand attack where the one diameter spacing approximates a firebrand pile and the five diameter spacing approximates two firebrands falling in close proximity but not within each others region of influence. The configuration with only the downstream

heater heated is representative of a firebrand falling near an object (e.g., twig, rock, or cone) that disturbs the flow and may act as a heat sink for the energy deposited to the firebrand with the one and five diameter spacing representing a firebrand falling both within and outside of the region of influence of the firebrand. The configuration where the upstream heater is not heated and five diameters is also considered a control for comparison to previous single heater ignition results.

Table 6.1: Test matrix

Test Series	Heater Spacing	Upstream Heater	U_{bulk} (m/s)
1	1	Ambient	0.5
2	1	Ambient	5.8
3	1	Hot	0.5
4	1	Hot	5.8
5	5	Ambient	0.5
6	5	Ambient	5.8
7	5	Hot	0.5
8	5	Hot	5.8

The cartridge heaters used had diameters of 6.4mm and lengths of 51mm. The heater sizes were chosen to represent large firebrands with a high potential to ignite a fuel bed in a wildfire [107]. The heater temperatures were controlled using a PID temperature controller implemented in LabVIEW. Heater temperatures ranged from 250°C to 750°C. Heater temperatures were measured using a type-K thermocouple attached to the center of each heater opposite the fuel bed. Controlling the temperature of the heater provides an advantage over natural burning or smoldering firebrands and pre-heated particles by removing the temperature variability of the heat source and enabling real-time data logging of the heat source temperature. Controlling the temperature of the firebrand also removes some complexity of calculating the energy imparted to the fuel bed. The heater was lowered onto the fuel bed with an automated lowering device. The lowering device included a load cell and a PID controller to maintain a force equivalent to a two 10g firebrands throughout the experiment. To minimize flow disruptions due to apparatus, the heaters were each attached to two 4-40 threaded rods that extended approximately 100mm below the load cell.

The fuel bed material was processed from kiln-dried Douglas-fir lumber. The lumber was first planed to generate shavings. The wood shavings were then granulated and

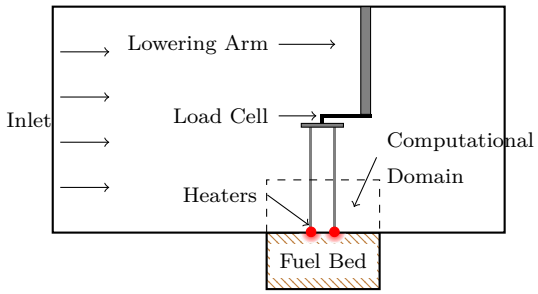

Figure 6.1: Diagram of the experimental wind tunnel apparatus. Air flows through the wind tunnel from left to right. The dashed region represents the domain subset used for computational efforts.

screened such that the particles passed through a 2.3mm screen but not through a 1.3mm screen. The particles were then dried in an oven at 103°C to remove any remaining moisture content. During tests, the fuel was placed in a 140mm diameter glass container with a depth of 70mm and then inserted into the wind tunnel. The average density of the fuel beds was 93kg/m^3.

6.3.2 Computational

A simplified model was implemented to obtain further insight into the fluid mechanics and heat transfer processes that influence the trends observed in the experimental efforts. The model was implemented in three parts. First, a thermal model of the fuel bed was used to estimate the mass of the fuel bed above the pyrolysis temperature and the average temperature. Second, the mass of the fuel bed material converted from solid fuel to gaseous pyrolysis products was estimated. In the third and final step, the fluid flow and heat transfer between the heaters, air, and released pyrolyzates was modeled. The modeling efforts were conducted for a 10s interval to ensure proper characterization of the flow field and maintain an accurate representation of the fuel bed. As mass is lost from the fuel bed due to pyrolysis, the contact area between the heater and the fuel bed changes as does the surface shape of the fuel bed. It was observed during experiments that the contact between the heat and the fuel bed and the shape of the fuel bed itself began to deviate significantly from the model domain at approximately 10s. Considerations of changes in contact area and changing geometry due to pyrolysis is out of the scope of this

work. Nonetheless, the treatment of each configuration equally and within the limited time frame is still anticipated to produce insight into the influence of the thermal and fluid processes on ignition.

The 2-D thermal model of the fuel bed was conducted using OpenFOAM [84]. The calculations solved the heat diffusion equation (Equation 6.1) to observe the spatial and temporal evolution of the fuel bed temperatures.

$$\frac{\partial\left(\rho h\right)}{\partial t}=\frac{\partial}{\partial x_j}\left(\alpha\frac{\partial h}{\partial x_j}\right) \tag{6.1}$$

Figure 6.2 shows the computational domain of the fuel bed. The thermal diffusivity of the fuel bed materials was estimated using correlations from literature for the thermal conductivity [81] and published values of specific heat [108]. Equation 6.2 shows the correlation for effective thermal conductivity where ϵ, as defined in Equation 6.3, is the proportion of the fuel bed that is air. The bulk density of the fuel bed material (ρ_{bed}) and the solid wood (ρ_{solid}) were obtained from experimental samples.

$$k_{eff}=\frac{1}{2}\left(\frac{1}{\left(1-\epsilon\right)/k_{solid}+\epsilon/k_{air}}+\epsilon k_{air}+\left(1-\epsilon\right)k_{solid}\right) \tag{6.2}$$

$$\epsilon=1-\frac{\rho_{solid}}{\rho_{bed}} \tag{6.3}$$

Average cell sizes for the domain ranged between 0.02mm near the heater to 0.2mm near the insulated boundary. The mesh consisted of 500,000 cells. The interface between the fuel bed and air and the radial edge of the domain were treated as insulated. The centerline was treated as a symmetric boundary condition. The insulated radial edge and symmetric boundary conditions are consistent with boundary conditions in the actual experiment since the 25mm distance ensure no temperature change during 10s of heating modeled, and the heater temperature has been observed to be circumferentially consistent with infrared imaging. The insulated interface with the air does not account for radiation and convective heat losses from the surface of the fuel bed as it is heated. However, the magnitude of the heat losses from the fuel bed is estimated to be significantly smaller in magnitude than the heat transfer from the heater. Reactions, mass loss due to pyrolysis, and changes in contact area due to changing fuel bed geometry are not considered in the temperature analysis. While the aforementioned assumptions and limitations reduce the

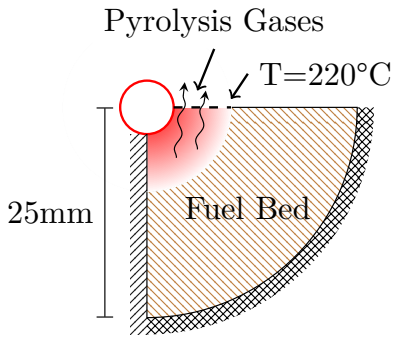

Figure 6.2: Diagram of the computational domain where black lines indicate domain boundaries and red lines are boundaries defined by the heater. The arrows denote flow of pyrolysis products from the fuel bed into the air above the fuel bed.

accuracy of the model in comparison to the experimental conditions, the temperature distributions still provide insights into differences in the mass of the fuel bed material that undergoes pyrolysis and provides insight to better interpret the experimental results.

The velocity of pyrolyzates entering the fluid domain from the fuel bed was determined in a two-step process. First, the mass of material in the fuel bed undergoing pyrolysis was estimated. All material over a temperature of 220°C was considered to undergo pyrolysis. This temperature was chosen as 220°C corresponds to the minimum temperature for the pyrolysis of hemicellulose and is considered the onset of pyrolysis [87]. The amount of mass estimated to depart the fuel bed was determined to be the proportion of fuel bed material that converted to gas-phase products when reacted at the average temperature of the material above the pyrolysis threshold from the thermal model. Reactions were conducted using the BioPOx mechanism [57], and mass was assumed to depart the fuel bed if it existed in the gas phase. Species were considered to be gas-phase if they were present in the Bio1412 mechanism [55, 86] since the Bio1412 mechanism considers the gas-phase reaction of pyrolysis products. The reaction calculations were conducted in Cantera [85]. The Cantera calculations were 0D which necessitated using the average temperatures of the fuel bed for the pyrolysis calculations rather than spatially resolved temperatures. The Cantera calculations considered the fuel bed material as an insulated fixed mass reactor. The following equations were solved to obtain the temperature and

species concentrations of the pyrolyis products.

$$\frac{\partial m}{\partial t} = 0 \tag{6.4}$$

$$m\frac{\partial \left(mY_k\right)}{\partial t} = \dot{m}_{k,gen} = V\dot{\omega}_k MW_k \tag{6.5}$$

$$mc_v\frac{\partial T}{\partial t} = \dot{Q} - \sum_k \dot{m}_{k,gen}u_k \tag{6.6}$$

Where Y_k, $\dot{m}_k$, and $\dot{\omega}_k$ are the mass fraction, mass generation rate, and generation rate of each species k in the mechanism used. V is the volume of the fuel bed material in the reactor. The species generation rates $\dot{\omega}_k$ are determined from the reactions included in the mechanism. The mechanism used for pyrolysis contains four different types of chemical reactions. The equations used to calculate the reaction rates for an elementary reaction is:

$$k_f = AT^b e^{-E_a/RT} \tag{6.7}$$

$$R_f = [A][B]k_f \tag{6.8}$$

Where R_f is the forward reaction rate, k_f the reaction rate constant, E_a the activation energy, b is the temperature exponent and R is the gas constant. Similarly, the reaction rates for three body reactions are calculated as:

$$R_f = [A][B][M]k_f \tag{6.9}$$

$$[M] = \sum_k \epsilon_k C_k \tag{6.10}$$

Where ϵ_k and C_k are the collision efficiency and concentration of each species, respectively. Falloff reaction rates are calculated using the reduced pressure P defined as:

$$P = \frac{k_0[M]}{k_\infty} \tag{6.11}$$

The reaction reaction rate is then calculated as:

$$k_f(T,P) = k_\infty \left(\frac{P}{1+P}\right) F(T,P) \tag{6.12}$$

Pressure dependent P-Log reaction rates are calculated for intermediate values using a logarithmic interpolation between two reaction rates k_1 and k_2 at pressures P_1 and P_2 as:

$$\log k_f(T,P) = \log k_1(T) + (\log k_2(T) - \log k_1(T)) \frac{\log P - \log P_1}{\log P_2 - \log P_1} \tag{6.13}$$

The overall generation rate of each species ($\dot{\omega}_k$) is defined as the sum of the individual reaction rates R_f for all of the reactions where the species is present. Where ν_i number of each species produced for each reaction. Equation 6.14 results in the source term for Equation 6.5, the solution of which determines the mass fractions of the species that are released into the fluid domain above the fuel bed.

$$\dot{\omega}_k = \sum_i^N \nu_i R_{f,i} \tag{6.14}$$

Where ν_i number of each species produced for each reaction.

The mass flux of the gases exiting the fuel bed was determined by averaging the total mass of gaseous pyrolysis products produced over the 10s interval. The exit velocity was then determined as the mass flux through the distance between the heater edge and the pyrolysis threshold, as shown by the dotted line in Figure 6.2. The calculated velocity and injection area was then used as an input for calculations conducted in the flow field.

A 2D RANS model of the flow above the fuel bed and around the heaters was implemented in OpenFOAM. The area of the computational domain with respect to the experimental apparatus is shown as the dashed line in Figure 6.1. The 2D slice of the domain modeled was considered to pass through the center of the heaters and corresponds to the location of the highest temperature of the heater, which also typically coincides with the ignition location. The mass, momentum, species, and energy equations for the calculations are shown below [109].

$$\frac{\partial \bar{\rho}}{\partial t} + \frac{\partial}{\partial x_i}(\bar{\rho}\tilde{u_i}) = 0 \tag{6.15}$$

$$\frac{\partial(\bar{\rho}\tilde{u}_i)}{\partial x_t} + \frac{\partial}{\partial x_i}(\bar{\rho}\tilde{u}_i\tilde{u}_j) + \frac{\partial \bar{p}}{\partial x_j} = \frac{\partial}{\partial x_i}(\bar{\tau}_{ij} - \widetilde{\bar{\rho}u_i''u_j''}) \tag{6.16}$$

$$\frac{\partial(\bar{\rho}\tilde{Y}_k)}{\partial t} + \frac{\partial}{\partial x_i}(\bar{\rho}\tilde{u}_i\tilde{Y}_k) = -\frac{\partial}{\partial x_i}\left(\overline{V_{k,i}Y_k} + \widetilde{\bar{\rho}u_i''Y_k''}\right) + \dot{\omega}_k \tag{6.17}$$

$$\frac{\partial \bar{\rho}\tilde{h}_s}{\partial t} + \frac{\partial}{\partial x_i}(\bar{\rho}\tilde{u}_i\tilde{h}_s) = \bar{\omega_T} + \frac{\bar{D}p}{Dt} + \frac{\partial}{\partial x_i}\left(\overline{\lambda\frac{\partial T}{\partial x_i}} - \overline{\rho u_i''h_s''}\right) + \overline{\tau_{ij}\frac{\partial u_i}{\partial x_j}} - \frac{\partial}{\partial x_i}\left(\overline{\rho\sum_{k=1}^{n}V_{k,i}Y_kh_{s,k}}\right) \tag{6.18}$$

where

$$\frac{\bar{D}p}{Dt} = \frac{\partial \bar{p}}{\partial t} + \tilde{u_i}\frac{\partial \bar{p}}{\partial x_i} + \overline{u_i''\frac{\partial p}{\partial x_i}} \tag{6.19}$$

The domain used for all calculations performed was 125mm long and 75mm high. For the cases where the heaters were spaced one diameter apart a total of 13206 cells with characteristic lengths from 0.05mm in the region surrounding the heaters to 1.5mm in the free stream above the heaters. For the cases where the heaters were spaced five diameters apart a total of 21948 cell with characteristic lengths from 0.06mm in the region surrounding the heaters to 1.6mm in the free stream above the heaters. For both cases the fine mesh spacing extended between the heaters accounting for the increased cell count for the five diameter spaced case. Refinement of the mesh by a factor of three resulted in a shift in separation angle for the upstream heater of 0.2%. Thus, the calculations were considered of acceptable accuracy to visualize the trends observed in experiments.

The inlet boundary conditions were determined from experimental measurements where the bulk wind speeds were 5.8 m/s, 3.5 m/s, 0.5 m/s with corresponding inlet turbulence intensities of 0.14%, 0.2% and 1.6% respectively. Turbulence parameters were determined from measurements taken of the experimental apparatus with a TSI IFA-300 hot wire anemometer. The k-ϵ turbulence model was used with values of $1.4{\cdot}10^{-4}\mathrm{m}^2/\mathrm{s}^2$ and $9.5{\cdot}10^{-6}\mathrm{m}^2/\mathrm{s}^3$ for k and ϵ respectively. Calculations were conducted for 10s and were then averaged to observe differences in temperature and velocity characteristics between the different configurations. The solid surfaces (i.e., cartridge heater, fuel bed, and wind

tunnel floor) were considered with a no-slip boundary condition at fixed temperatures. All temperatures except the heater surfaces and pyrolyzate inlets were 300K. The inlet temperature and inlet velocity of the pyrolysis gases were determined from the fuel bed thermal model and Cantera calculations. The cartridge heater was maintained at a fixed uniform temperature corresponding to the temperature estimated to result in 50% ignition probability from experimental tests. The outlet and tap of the domain used a zero gradient boundary condition.

6.4 Results and Discussion

The flaming ignition or non-ignition result of each test is shown in Figure 6.3. The markers show the result of each test, and the curves show the logistic regression for each of the heater configurations as defined in Table 6.1. The shaded regions around the curves represent the 95% confidence intervals of each regression. The top plot in Figure 6.3 shows configurations where the downstream heater is actively heated and the upstream heater is at ambient conditions. The bottom plot in Figure 6.3 shows results for configurations where both heaters are actively heated to the same temperature. Table 6.2 shows the heater temperatures estimated to result in a 50% ignition probability from the logistic regressions shown in Figure 6.3 as well Temperature values for the corresponding wind speed and orientation from the single heater study in Chapter 4 are shown in the column titled "Single" for comparison.

Table 6.2: Heater temperature required to achieve 50% ignition probability for the configurations tested with 95% confidence intervals shown in parentheses. The column "Unheated" refers to cases where the upstream heater was not temperature controlled. Hence the temperature corresponds to the temperature of the hot heater. "Heated" refers to cases where both upstream and downstream heaters were maintained at the setpoint temperature. The single heater column shows predicted ignition temperatures from the study in Chapter 4 for a single heater.

U_{bulk} (m/s)	Spacing (D)	Unheated (°C)	Heated (°C)	Single (°C)
0.5	1	750 (644, 850)	533 (527, 541)	571
0.5	5	578 (565, 583)	601 (597, 604)	571
5.8	1	423 (417, 429)	406 (397, 416)	399
5.8	5	438 (421, 454)	396 (387, 407)	399

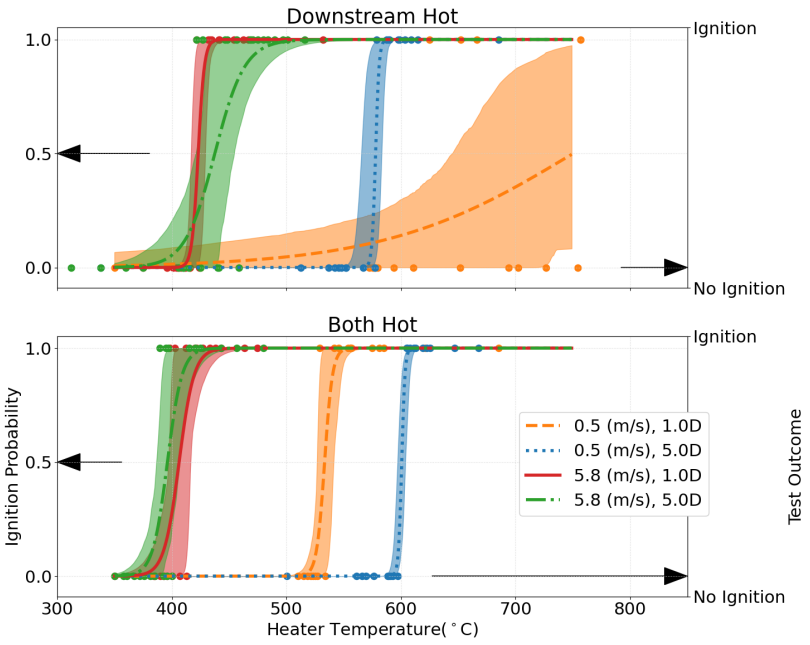

Figure 6.3: Ignition or no ignition outcomes of tests with different heater configurations. The circular markers indicate outcomes of individual tests and the curves represent logistic regressions of each test series. The shaded region shows the 95% confidence interval for each regression.

Considering first the cases where both heaters are actively heated (Figure 6.3 bottom panel and Table 6.2 "Heated" column) there are three observations of note. First, in both the one and five heater diameter spacing cases an increase in wind from *0.5*m/s to *5.8*m/s resulted in a lower temperature threshold for ignition. The 50% ignition threshold decreased 24% (127°C) for the one diameter spacing and 34% (205°C) for the five diameter spacing configuration. These results are similar to the 35% decrease in the ignition threshold for the single heater results presented in Chapter 4. The reduction in ignition temperature is attributed to an increased residence time of pyrolyzates near the heater in recirculation zones. The second observation for the 0.5m/s wind speed tests is that decreasing the heater spacing from five heater diameters to one heater diameter resulted in an 11% decrease in the temperature required to achieve a 50% ignition probability. The shift in ignition probabilities is attributed to increased heat transfer between the closely spaced heaters. Anecdotally, the shift in ignition probability observed by moving the heaters closer together was accompanied by a shift in ignition mode. Specifically, as the heater temperature was reduced below the 50% ignition threshold for a single heater, ignition was observed only after the smoldering fronts between the heaters merged (based on the visible location of char). Flaming ignition then occurred in the plume of pyrolyzates that established between the heaters. The lower threshold for ignition when both heaters were hot, and only one diameter apart is attributed to increased heat transfer to the pyrolyzates as they depart the fuel bed. However, due to the multiple parallel processes that may be influenced by the increased heat transfer, the root cause mechanism for the increase in ignition probability is not clear. Possibilities include an increased temperature of pyrolyzates departing between the heaters due to enhanced radiative and convective heat transfer, preheating of air as it flows over the upstream heater before mixing, increased mass flux of pyrolyzates from the fuel bed, or a combination of effects. In contrast to the change in ignition probability between configurations at a wind speed of 0.5m/s, the differences in ignition probability were not statistically significant at 5.8m/s irrespective of heater configuration. This suggests that the enhanced heat transfer between the cartridge heaters is not influential in windy conditions. Anecdotally, in cases under wind, ignitions occurred on the upstream side of the upstream cartridge heater suggesting that ignition is more favorable in the recirculation zones on the upstream side of the heater even with the addition of heat.

Now considering the cases where only the downstream heater was actively heated

("Unheated" column of Table 6.2), there are three observations of note. First, similar to the dual heated and single heater results from Chapter 4 an increase of wind from from 0.5m/s to 5.8m/s significantly lowered the ignition threshold. Second, for cases with a wind speed of 5.8m/s, changing the spacing between the heaters did not have a significant influence on the temperature required for ignition, which aligns with the trends observed for the cases where both heaters were hot. Third, decreasing the spacing from five diameters to one diameter in low wind speed conditions increased the temperature required for ignition by greater than 30%, which is the opposite trend observed for cases where both heaters were hot. This notable deviation from trends is attributed to the unheated heater acting as a heat sink requiring significantly more energy for ignition.

Further insight into the influence of heater configuration and wind speed on ignition is gained from the results of the computational efforts. Figure 6.4 shows the averaged velocity streamlines and temperature distribution in the fluid flow around the heaters for each heater configuration. Air flows from left to right in Figure 6.4. The solid black lines separate the figure into quadrants with the same heater spacing and wind speed. Each quadrant contains two images, one where both heaters are actively heated and one where only the downstream heater is actively controlled. The numbers inside the circular heater boundaries correspond to the assigned temperature of the heater during the calculation. The assigned surface temperatures correspond to the heater temperature anticipated to produce a 50% probability of ignition for the wind speed and heater conditions. Heater boundaries with blue circles inside them correspond to cases where the heater was not heated and acted as an inert object. The arrows indicate the observed location of ignition when observed. Ignition locations were not observed for every case. However, sufficient ignition locations were recorded to provide insight into controlling parameters.

The computational results for the 0.5m/s cases are represented in rows 1 and 2 of Figure 6.4 and the results for the 5.8m/s cases are represented in rows 3 and 4 of Figure 6.4. Recall, from the experimental results that the increase in wind speed from 0.5m/s to 5.8m/s had the most significant decrease in ignition threshold. When comparing differences between the streamlines for the two different wind speeds, the cases with a wind speed of 5.8m/s have recirculation zones near the intersection of the fuel bed and the heater and the 0.5m/s cases do not. Figure 6.5 shows an enlarged images of the streamlines for panels (A, 2) and (A, 4) from Figure 6.4 where both heaters are active and spaced one diameter apart. Considering the regions on the upstream (left) side of the

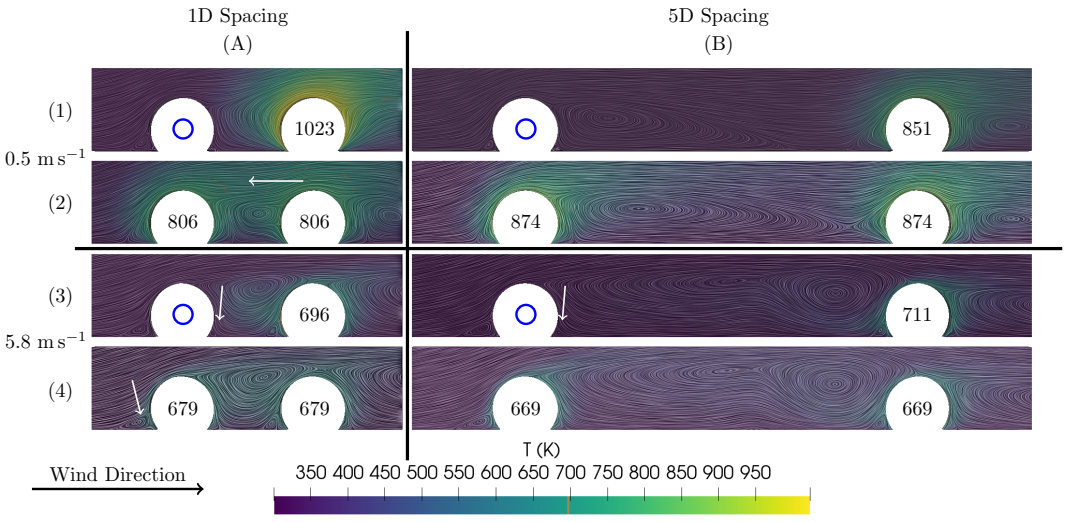

Figure 6.4: Time averaged velocity streamlines and temperature profiles for each configuration. The numbers inside the heater boundaries identify the surface temperature of the heater. Blue circles indicate that the heater was unheated. Arrows show typical ignition locations in experiments.

heaters the 5.8m/s case shown in Figure 6.5b has distinct recirculation zones. Notably, ignition observed during experiments that correspond to Figure 6.5b and Figure 6.4 panel (A, 4) was observed to occur on the upstream side of the upstream heater, which corresponds to the leftmost recirculation zone in Figure 6.5b. This is perhaps unexpected as the leading edge of the downstream heater also has a recirculation zone near the fuel bed, and a secondary recirculation zone exists between the heaters that create a large region of fluid at temperatures above ambient which would facilitate ignition. Instead, it appears that the conditions in the furthest upstream recirculation zone are more favorable. A similar location for ignition was observed for single heater configurations in Chapter 4. The similar observations of ignition location and the similarities in ignition threshold between the single and double heater cases suggest that in the prescience of wind, fluid dynamic effects are more influential than thermal effects. Considering the cases where

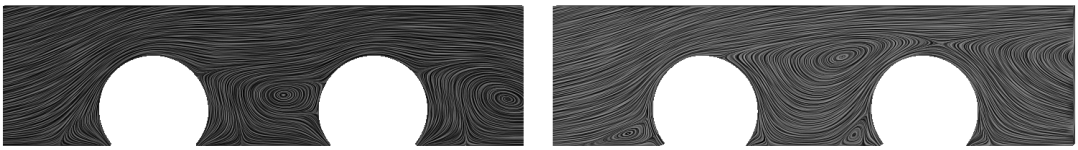

(a) 0.5m/s (b) 5.8m/s

Figure 6.5: Comparison of streamlines for two different wind speeds with heaters spaced one diameter apart. Air flows from left to right. Images correspond to the panels (A, 2) and (A, 4) in Figure 6.4

the wind speed was 5.8m/s but the upstream heater was not heated and is effectively an inert flow obstruction (Figure 6.4 row 3). Following the trends of the previous case where both heaters were heated, ignition would be expected to occur in the recirculation zone upstream of the actively heated heater. However, in these configurations, ignition occurred on the downstream side of the upstream heater as indicated in Figure 6.4 row 3 and as shown in Figure 6.6. Figure 6.6 shows images of the fuel beds shortly after ignition occurred for both the one diameter and five diameter spaced cases. In both heater cases, ignition occurred on the downstream side of the upstream heater after the pyrolysis front of the fuel bed propagated upstream and reached the inert heater. Effectively by not heating the upstream heater, the location of ignition shifted from the upstream side of the upstream heater to the downstream side of the upstream heater. This is perhaps counterintuitive since ignition occurred in recirculation zones when both heaters were

(a) 1D Spacing (b) 5D Spacing

Figure 6.6: Images of fuel beds shortly after ignition near the upstream (left) heater. In both cases the wind speed was 5.8m/s and the upstream heater is unheated/inert. Air is travelling from left to right in both images.

heated, but the ignition locations for the inert upstream heater do not coincide with recirculation zones in the computational results shown in Figure 6.4 row 3. In addition to ignition in an area that lacks recirculation, in these cases, ignition is also occurring further from the heat source than in the other heater configurations and wind speeds. Ignition far from the heat source, especially in the five diameter spaced case, suggests that the fuel bed is undergoing a smoldering to flaming transition. Ignition away from the heat source was not observed in the single heater cases presented in Chapter 4 suggesting that the upstream heater appears to be facilitating this transition. The smoldering to flaming transition near the inert heater is attributed to changes in the local fluid flow field as the smoldering front approaches the heater. Studies of the smoldering to flaming transition have found that the mass flux rate of smoldering fuel bed is sensitive to wind speed [110] and that the accumulation of pyrolyzates increases the likelihood of flaming [111]. As the smoldering front approaches the upstream heater, both a change in wind speed and an accumulation of pyrolyzates may occur, creating a perturbation that ultimately results in ignition. Another potential contributor to ignition is the heater acting as an overhang which may contribute to the smoldering to flaming transition. Unfortunately, little information is available regarding the influence of overhangs on the smoldering to flaming transition, but in this case overhangs seem to promote ignition [112]. Despite the different ignition locations between the heater configurations with a wind speed of 5.8m/s the temperature required for a 50% ignition probability differs by less than 10% between

all four heater configurations and spacings and in comparison to the single heater results from Chapter 4. Thus, for the configurations tested, an increase of wind speed from 0.5m/s to 5.8m/s has a more significant effect than the number, spacing, and whether or not both heaters are hot.

6.5 Conclusions

Flaming ignition tests have been conducted for porous Douglas-fir fuel beds with two firebrand surrogates in various configurations. Eight different configurations of heater spacing (1D or 5D), wind speed (0.5m/s or 5.8m/s), and heater condition (actively heated or inert) were tested. Cylindrical resistive cartridge heaters were used as firebrand surrogates. The ignition or no ignition outcomes of tests for each configuration were used to determine the temperature required for 50% ignition probability. A simplified model of heat transfer, pyrolysis product release, and fluid flow over the fuel beds was implemented to gain insights into differences in ignition propensity between the configurations. The specific conclusions of this work are as follows:

1. Increasing the wind speed lowers the threshold for ignition. However, the magnitude of the change in ignition threshold is sensitive to the spacing and temperatures of cartridge heaters used. The ignition threshold may reduce between 20% and 60% depending on the heater configurations.

2. At wind speeds of 5.8m/s the ignition threshold is largely independent of thermal interactions between firebrand surrogates. The lack of sensitivity to inter-firebrand effects is attributed to the ignition being largely controlled by the fluid dynamics around the firebrand surrogates. Ignition is largely controlled by the propensity of pyrolysis products to accumulate and is independent of thermal interactions with nearby objects, whether they are energy sources or sinks.

3. In low wind conditions (e.g., 0.5m/s), the ignition threshold is more sensitive to thermal interactions between the firebrand surrogates than in higher wind conditions. For example, when the firebrand was spaced one diameter apart, the difference between ignition thresholds when the upstream firebrand is inert or an energy source is 34%. When the firebrand surrogates were spaced such that they did not thermally interact (five diameters apart), the difference in ignition threshold was

4%. Thus, at low wind speeds or in quiescent conditions, ignition is sensitive to thermal interactions with nearby objects. Ignition is promoted if nearby objects supply energy and inhibited if thermal sinks are nearby.

4. In configurations where the firebrand is downstream of a flow obstacle, ignition may occur via the smoldering to flaming transition. The smoldering to flaming transition appears to be facilitated by either accumulation of pyrolysis gases in the downstream edge of the flow obstruction or by the formation of an overhang as the fuel bed recedes underneath the obstruction. This phenomenon produces ignition at similar temperatures to other configurations and may not be important for ignition predictions but may be of interest to smoldering research.

The conclusions of this work show that ignition of a fuel bed is more likely when a firebrand or firebrand lands on a fuel bed under conditions that promote recirculation zones near locations where pyrolysis gases are released from the fuel bed. It was observed that under windy conditions, ignition is less sensitive to nearby embers or inert objects than at low wind speeds. These observed sensitivities highlight the increased risk of fuel bed ignition in windy conditions and in cases where firebrands may accumulate in all wind conditions.

Chapter 7: Conclusions & Ignition Model

The preceding chapters of this document presented findings from studies evaluating the influence of various parameters on the probability of ignition of fuel beds in wildfires. The specific objectives of this work are as follows:

1. Determine the effects of particle morphology on ignition propensity
2. Ascertain ignition dependence on heating location(s), mode, and rate
3. Identify and quantify the influence of environmental conditions on ignition propensity.
4. Identify the influence of fuel bed chemical composition on flaming ignition.

The conclusions of each effort are restated in the following sections, followed by a discussion of the implications of the results as they pertain to each specific objective and the overall objective of this work.

7.1 Sensitivities of Porous Beds and Plates to Ignition by Firebrands

1. Smaller particles ignite more readily in porous beds than larger particles when heat transfer from the heater is primarily through conduction. This was evident by higher ignition probabilities, in general, of the smaller particles for a fixed heater temperature. As particle sizes increase, radiant heat transfer becomes more important, and fuel beds with larger particles were more likely than smaller particles to ignite at extended times (>100s) due to the increased importance of radiant ignition.
2. Douglas-fir plates ignite at times where conduction is the dominant mode of heat transfer (<10s) due to the higher thermal conductivity of the solid plates. The ignition probability of plates was the most similar to the larger particle, in particular at lower heater temperatures, due to dispersed heating of the porous fuel bed

through radiation and the increased thermal conductivity of the plates creating similar temperature profiles. The rise in ignition probability over a smaller heater temperature range time with temperature results from more consistent contact between the heater and plate surface.

3. Heat flux delivered to the fuel bed, when compared to heater temperature, is more indicative of ignition likelihood and ignition time for porous fuel beds. Heat flux is a more significant predictor of ignition because it captures differences in heat transfer modes and particle contact that heater temperature values do not. While this finding is not new, what is novel is that the mixed mode of heating (conduction and radiation) has a significant impact on the flaming ignition of fuel beds.

4. Consideration of the transport characteristics of pyrolyzate gases near the high-temperature source can be important for more fully predicting ignition propensity. A Da of ignition, in relation to the measured heat flux and thermal diffusivity of the fuel beds, is a promising relationship for predicting ignition for the porous fuel beds.

Further work is needed to verify that the Da may be used to predict ignition for solid surfaces and for porous fuel beds with varying chemical compositions. If proven valid, the (Da), measured/predicted heat fluxes, and fuel bed properties may be used to help predict the ignition of fuel beds both in and out of the WUI, ultimately helping to increase the effectiveness of fire prevention and suppression efforts.

7.2 Influence of Wind on Flaming Ignition of Porous Wood Fuel Beds

1. An increase in wind speed above quiescent conditions reduces the temperature required for the flaming ignition of a fuel bed. For example, an increase in wind speed of 3.5m/s from quiescent increases the ignition probability of a fuel bed from under 30% to roughly 100%. However, a linear increase in wind speed does not result in a linear increase in ignition probability. Thresholds in wind speed exist above which temperatures required to achieve ignition actually increase. For example, when the wind is oriented 45° from the heater centerline, increasing the wind from quiescent to 3.5m/s reduces the temperature required for ignition probability by

30%. However, increasing the wind speed from quiescent to 5.8m/s reduces the temperature required for ignition by only 25%. Presumably, these thresholds occur because of reductions in residence time.

2. The temperature at which ignition occurs for porous fuel beds is sensitive to the orientation of a firebrand relative to the wind direction. Higher temperatures are typically required for ignition for a heater parallel to the flow compared to 45° and perpendicular to the flow. This sensitivity is attributed to differences in recirculation zones and residence times of air and pyrolyzates near the hottest region of the heater. Thus, predictions of ignition probabilities that consider wind may need to include both wind speed and orientation to obtain sufficient accuracy.

3. Times to flaming ignition of porous fuel beds are sensitive to the firebrand/heater angle in the presence of wind. The parallel heater orientation ignites at the longest time, followed by the 45° case, with the perpendicular cases igniting in the shortest amount of time. High-speed images indicate that ignition typically occurs in regions where recirculation zones occur, as shown in CFD calculations. The heightened propensity to ignition is attributed to increased residence times of pyrolyzates in the recirculation zones, as supported by calculations.

The conclusions of this work show that ignition is favored when a firebrand(s) land on a fuel bed under wind speeds and orientations that promote greater residence times of pyrolyzates near a high-temperature region of firebrands. It was observed that increases in wind speed, of a magnitude that may commonly occur during wildfires, can increase the probability of fuel bed ignition from very unlikely to a near certainty regardless of the ember orientation to the wind. This highlights the increased risk of spot fires due to ignition of fuel beds that accompanies wind in a wildfire.

7.3 Effect of Fuel Bed Composition on Flaming Ignition Probability

1. Of the six materials tested, only three were able to be ignited below the 750°C maximum temperature of the firebrand surrogate. Two of the three materials for which ignition was not observed were bark. The higher ignition threshold of the bark materials is attributed to higher lignin concentrations. The resistance to ignition

present in these materials suggest that using materials high in lignin in locations at risk for firebrand attack in wildfires may reduce ignitions and subsequent losses of structures. It is acknowledged that these results are for flaming ignition only, and high lignin materials may pose a significant risk if smoldering or the smoldering to flaming transition occurs.

2. For Douglas-fir and pine wood, an increase in wind speed decreased the temperature required for ignition. However, for oak wood, an increase in wind speed inhibited ignition. Increases in ignition propensity with an increase in wind are attributed to the formation of recirculation zones near the ignition source. In the case of oak wood, the formation of recirculation zones inhibits ignition. The root cause of the dichotomy in ignition trends is unclear; however, differences in the flammability of pyrolysis products corresponding to changes in chemical composition are most likely.

3. A direct correlation between the fuel bed composition and the ignition propensity was not observed. This is attributed to the complexity of biomass pyrolysis. However, a local minimum ignition threshold near the composition of Douglas-fir wood is present that warrants further investigation.

The conclusions of this work show that ignition is sensitive to the chemical composition of fuel beds in both quiescent conditions and under wind. An increase in wind was observed to increase ignition probability for some materials; however, this was not universally the case. Materials high in lignin were among the least likely to ignite and more suitable for placement in areas where firebrands are likely to land or accumulate in a WUI environment. Further and more targeted analysis of the differences in pyrolysis products for each material will likely yield further insight.

7.4 Influence of Multiple Firebrands on the Ignition of Fuel Beds

1. Increasing the wind speed lowers the threshold for ignition. However, the magnitude of the change in ignition threshold is sensitive to the spacing and temperatures of cartridge heaters used. The ignition threshold may reduce between 20% and 60% depending on the heater configurations.

2. At wind speeds of 5.8m/s the ignition threshold is largely independent of thermal interactions between firebrand surrogates. The lack of sensitivity to inter-firebrand effects is attributed to the ignition being largely controlled by the fluid dynamics around the firebrand surrogates. Ignition is largely controlled by the propensity of pyrolysis products to accumulate and is independent of thermal interactions with nearby objects, whether they are energy sources or sinks.

3. In low wind conditions (e.g., 0.5m/s), the ignition threshold is more sensitive to thermal interactions between the firebrand surrogates than in higher wind conditions. For example, when the firebrand was spaced one diameter apart, the difference between ignition thresholds when the upstream firebrand is inert or an energy source is 34%. When the firebrand surrogates were spaced such that they did not thermally interact (five diameters apart), the difference in ignition threshold was 4%. Thus, at low wind speeds or in quiescent conditions, ignition is sensitive to thermal interactions with nearby objects. Ignition is promoted if nearby objects supply energy and inhibited if thermal sinks are nearby.

4. In configurations where the firebrand is downstream of a flow obstacle, ignition may occur via the smoldering to flaming transition. The smoldering to flaming transition appears to be facilitated by either accumulation of pyrolysis gases in the downstream edge of the flow obstruction or by the formation of an overhang as the fuel bed recedes underneath the obstruction. This phenomenon produces ignition at similar temperatures to other configurations and may not be important for ignition predictions but may be of interest to smoldering research.

The conclusions of this work show that ignition of a fuel bed is more likely when a firebrand or firebrand lands on a fuel bed under conditions that promote recirculation zones near locations where pyrolysis gases are released from the fuel bed. It was observed that under windy conditions, ignition is less sensitive to nearby embers or inert objects than at low wind speeds. These observed sensitivities highlight the increased risk of fuel bed ignition in windy conditions and in cases where firebrands may accumulate in all wind conditions.

7.5 Ignition Model

The overall objective of this work is to identify parameters and processes that control the ignition of a fuel bed when an ember lands on it with an anticipated impact of enabling the creation of a simplified model that may be used to determine the likelihood of ignition quickly. A model was created to predict ignition to evaluate the effectiveness of this work in meeting those goals. The code for the model and the data used for training and training can be accessed here. The model was then applied to the results of other studies that utilized different fuel bed materials and ignition sources to determine cross-study applicability.

After the completion of the experimental efforts outlined in the previous chapters the results were aggregated into a single dataset containing the results from the 1086 tests conducted. The parameters included in the model and the corresponding units are as follows:

- Wind speed (m/s)
- Wind direction relative to longitudinal firebrand axis (°)
- Ratio of characteristic lengths between particle size and ember size (-)
- Chemical composition: mass fractions of Cellulose, Hemicellulose, Lignin, Tannins, and Triglycerides (-)
- Fuel bed bulk density (kg/m^3)
- Fuel bed thermal diffusivity (m^2/s)
- Average temperature of the firebrand(s) (°C)
- Number of firebrands (-)
- Spacing between firebrands as multiple of characteristic length (-)

The aggregated data was then used to create a Random Forest Classifier model using the scikit-learn package in python [88] to estimate ignition outcomes for each test. A 0.75/0.25 test-train split was used for training the models, meaning that 25% of the data was used to train the model, and the remaining 75% was used to test the model accuracy.

The R^2 validation score for the model with an out-of-bag score of 0.83, which means that the model predicts ignition correctly 80% of the time. While the accuracy of the model is likely acceptable if such a model was to be used as an indicator or predictor of ignition during a fire or to inform preventative measures, it would be beneficial to reduce the number of inputs required. An examination of the most important input parameters and refinement of the model found that accuracy was not degraded if the number of parameters was reduced to include only the following variables:

- Average temperature of the firebrands
- Fuel bed bulk density
- Wind speed
- Ratio of characteristic lengths between particle size and ember size
- Wind direction

Reducing the model to include only the five characteristics above maintained the 80% prediction accuracy. While it is beneficial to have an accurate predictive model for a single set of experiments in a similar apparatus, a model capable of predictions across different firebrands, fuel beds, and environmental conditions is far more valuable for preventing home loss. The model was applied to select studies from the literature to evaluate the accuracy across studies. The authors and relevant parameters from each study are shown in Table 7.1. Three of the studies presented in Table 7.1 used hot metal particles dropped onto fine fuel beds of processed material. The studies by Hadden et al. and Urban et al. used pure cellulose as the fuel bed, and the study by Zak et al. used a blend of grasses processed into a powder. The fourth study, conducted by Filkov et al., used multiple bark embers of various sizes dropped onto dried but otherwise unprocessed pine needle duff. A wind direction of 0° was used for the not metal particle studies since the geometry of the metal particles is anticipated to produce recirculation zones similar to that of a cylindrical heater parallel to the flow. A wind direction of 45° was used for the pine bark embers since the embers provided a more significant flow disruption than the metal particles but were dropped randomly and therefore not considered to be normal to the flow in all cases. The average temperature was defined as the average of the initial temperature and ambient temperature for the hot metal particles. More

sophisticated estimates of the average temperature based on the average time to ignition and estimated heat losses from the ember were conducted, but the model accuracy was not improved. Thus, a simpler metric was chosen. The average temperature of the bark embers was estimated from measurements of similar embers in the literature [94, 113]. The first approach used was to apply a reduced model created from only the data

Table 7.1: Data inputs for the model from selected studies.

Authors	$\bar{T}$ (°C)	$\bar{\rho}_{bed}$ (kg/m^3)	U (m/s)	L_p/L_e (-)	Θ_{wind} (°)	Citation
Hadden et al.	260 - 560	200	0.5	0.02 - 0.45	0	[39]
Urban et al.	285 - 560	282	0.5	0.06 - 0.25	0	[73]
Zak et al.	310 - 560	338	0.5	0.04 - 0.15	0	[72]
Filkov et al.	407	105	1, 1.5, 2	0.17 - 2.60	45	[93]

generated from studies in this dissertation and predict ignition for each of the studies in the literature. The accuracy of the model at predicting ignition for other studies was 50%, which is entirely unusable for any type of predictive modeling. However, when the model was retrained using the same five parameters but including 25% subsets of the Zak et al. and the Filkov et al. data, in conjunction with the results of this work, the predictive accuracy increased to 98% for the Zak et al. study, 94% for the Hadden et al. study, 81% for the Urban et al. study and 74% for the Filkov et al. study. The increase in accuracy suggests that predictions can be made across differences in experimental conditions, ember types, and fuel bed types using as few as five parameters. Predictions across experimental conditions have been one of the biggest hurdles to creating a general predictive model. Identifying the primary controlling parameters of ignition in this work has created a framework for bridging the predictive gap across various configurations.

Chapter 8: Future Work

The results in this work have identified controlling parameters for ignition and provided a framework for creating models with capabilities to predict various ignition scenarios. Significant additional work is needed to refine the proposed framework and explore different ignition parameters.

- The moisture content of the fuel bed was not considered in this work but is a well-studied parameter that significantly affects ignition. Extension of the experiments or a meta-analysis of literature is necessary to determine how moisture content fits into the proposed framework. The change in fuel bed bulk density due to moisture may sufficiently characterize the difference, but that remains to be seen.

- Additional tests with well-characterized smoldering or flaming embers would significantly enhance the knowledge gained in this work. Typical temperatures of physically combusting firebrands are higher than those capable by the apparatus used in this work [113]. The higher temperatures may influence the ignition propensity. However, combusting embers are susceptible to heat losses and environmental factors where the firebrand surrogates used in this work are mainly independent of these factors. It is unclear how or if the addition of energy sources that react with the environment will shift the parameters identified to be most influential to ignition. A series of highly instrumented and controlled experiments focused on the coupled interactions between a reacting ember, a reacting fuel bed, and changing environmental conditions would provide novel and valuable insight into ignition processes. I applaud the patience and perseverance of those who may undertake this endeavor in the future.

- Relatively limited data is available regarding the thermal properties of porous biomass media. The lack of available information is likely due to the significant variation in solid biomass material properties and the endless configurations (e.g., porosity and particle orientation) in the natural environment. A series of targeted studies determining the thermal properties of common fuel bed materials would

likely increase the understanding of how ignition changes between different materials or even similar materials under various packing conditions.

- In addition to the limited data available for thermal properties of fuel bed materials, the chemical composition of materials and the influence of chemical changes on the pyrolysis and subsequent ignition would provide valuable insight into the differences in ignition between materials and environmental conditions.

Bibliography

[1] N Levin, M Yebra, and S Phinn, "Unveiling the factors responsible for Australia's black summer fires of 2019/2020", Fire **4**, 10.3390/fire4030058 (2021) 10.3390/fire4030058.

[2] JR Marlon, PJ Bartlein, DG Gavin, CJ Long, RS Anderson, CE Briles, KJ Brown, D Colombaroli, DJ Hallett, MJ Power, EA Scharf, and MK Walsh, "Long-term perspective on wildfires in the western USA", Proceedings of the National Academy of Sciences of the United States of America **109**, 535–543 (2012) 10.1073/pnas.1112839109.

[3] JE Keeley and JG Pausas, "Distinguishing disturbance from perturbations in fire-prone ecosystems", International Journal of Wildland Fire, 282–287 (2019) 10.1071/WF18203.

[4] VC Radeloff, DP Helmers, H Anu Kramer, MH Mockrin, PM Alexandre, A Bar-Massada, V Butsic, TJ Hawbaker, S Martinuzzi, AD Syphard, and SI Stewart, "Rapid growth of the US wildland-urban interface raises wildfire risk", Proceedings of the National Academy of Sciences of the United States of America **115**, 3314–3319 (2018) 10.1073/pnas.1718850115.

[5] RB Hammer, SI Stewart, and VC Radeloff, "Demographic trends, the wildland-urban interface, and wildfire management", Society and Natural Resources **22**, 777–782 (2009) 10.1080/08941920802714042.

[6] S Suzuki and SL Manzello, "Ignition vulnerabilities of combustibles around houses to firebrand showers: Further comparison of experiments", Sustainability (Switzerland) **13**, 1–14 (2021) 10.3390/su13042136.

[7] SL Manzello, S Suzuki, MJ Gollner, and AC Fernandez-Pello, "Role of firebrand combustion in large outdoor fire spread", Progress in Energy and Combustion Science **76**, 100801 (2020) 10.1016/j.pecs.2019.100801.

[8] V Babrauskas, *Ignition Handbook* (Fire Science Publishers, Issaquah, WA, 2003).

[9] VC Radeloff, DP Helmers, HA Kramer, MH Mockrin, PM Alexandre, A Bar Massada, V Butsic, TJ Hawbaker, S Martinuzzi, AD Syphard, and SI Stewart, *The 1990-2010 wildland-urban interface of the conterminous United States - geospatial data. 2nd Edition.* 2017, https://doi.org/10.2737/RDS-2015-0012-2.

[10] CAL FIRE, *Top 20 Most Destructive California Wildfires.* 2022.

[11] K Barrett, *Wildfires destroy thousands of structures each year*, 2020.

[12] AI Filkov, T Ngo, S Matthews, S Telfer, and TD Penman, "Impact of Australia's catastrophic 2019/20 bushfire season on communities and environment. Retrospective analysis and current trends", Journal of Safety Science and Resilience **1**, 44–56 (2020) 10.1016/j.jnlssr.2020.06.009.

[13] SL Manzello, R Blanchi, MJ Gollner, D Gorham, S McAllister, E Pastor, E Planas, P Reszka, and S Suzuki, "Summary of workshop large outdoor fires and the built environment", Fire Safety Journal **100**, 76–92 (2018) 10.1016/j.firesaf.2018.07.002.

[14] S Suzuki and SL Manzello, "Ignition vulnerabilities of combustibles around houses to firebrand showers: Further comparison of experiments", Sustainability (Switzerland) **13**, 1–14 (2021) 10.3390/su13042136.

[15] WE Mell, SL Manzello, A Maranghides, D Butry, and RG Rehm, "The wildland-urban interface fire problem - Current approaches and research needs", International Journal of Wildland Fire **19**, 238–251 (2010) 10.1071/WF07131.

[16] SL Manzello, K Almand, E Guillaume, S Vallerent, S Hameury, and T Hakkarainen, "FORUM position paper: The growing global wildland urban interface (WUI) fire Dilemma: Priority needs for research", Fire Safety Journal **100**, 64–66 (2018) 10.1016/j.firesaf.2018.07.003.

[17] A Westhaver, *Why some homes survived: Learning from the Fort McMurray wildland/urban interface fire disaster*, tech. rep. 56 (Institute for Catastrophic Loss Reduction, Toronto, 2017), p. 81.

[18] ME Roberts, AA Rawlinson, and Z Wang, "Ember risk modelling for improved wildfire risk management in the peri-urban fringes", Environmental Modelling and Software **138**, 104956 (2021) 10.1016/j.envsoft.2020.104956.

[19] A Maranghides and W Mell, "A Case Study of a Community Affected by the Witch and Guejito Wildland Fires", Fire Technology **47**, 379–420 (2011) 10.1007/s10694-010-0164-y.

[20] AD Syphard and JE Keeley, "Factors Associated with Structure Loss in the 2013 – 2018 California Wildfires", Fire **2**, 1–15 (2019).

[21] TR Hudson, RB Bray, DL Blunck, W Page, and B Butler, "Effects of fuel morphology on ember generation characteristics at the tree scale", International Journal of Wildland Fire **29**, 1042–1051 (2020) 10.1071/WF19182.

[22] S Adusumilli, JE Chaplen, and DL Blunck, "Firebrand Generation Rates at the Source for Trees and a Shrub", Frontiers in Mechanical Engineering **7**, 1–13 (2021) 10.3389/fmech.2021.655593.

[23] N Sardoy, JL Consalvi, B Porterie, and AC Fernandez-Pello, "Modeling transport and combustion of firebrands from burning trees", Combustion and Flame **150**, 151–169 (2007) 10.1016/j.combustflame.2007.04.008.

[24] Matvienko, O V A, Filkov, A I, and A Grishin, "Computational investigation of the transport of burning particles", Journal of Engineering Physics and Thermophysics **89**, 1315–1324 (2016).

[25] S Suzuki and SL Manzello, "Role of accumulation for ignition of fuel beds by firebrands", Applications in Energy and Combustion Science **1-4**, 100002 (2020) 10.1016/j.jaecs.2020.100002.

[26] S Suzuki and S Manzello, "Experimental investigation of firebrand accumulation zones in front of obstacles", Fire Safety Journal **94**, 1–7 (2017) 10.1016/j.firesaf.2017.08.007.

[27] S Suzuki, SL Manzello, K Kagiya, J Suzuki, and Y Hayashi, "Ignition of Mulch Beds Exposed to Continuous Wind-Driven Firebrand Showers", Fire Technology **51**, 905–922 (2015) 10.1007/s10694-014-0425-2.

[28] AC Fernandez-Pello, "Wildland fire spot ignition by sparks and firebrands", Fire Safety Journal **91**, 2–10 (2017) 10.1016/j.firesaf.2017.04.040.

[29] S Suzuki and SL Manzello, "Garnering understanding into complex firebrand generation processes from large outdoor fires using simplistic laboratory-scale experimental methodologies", Fuel **267**, 117154 (2020) 10.1016/j.fuel.2020.117154.

[30] TE Waterman, *Experiemntal Study of Firebrand Generation*, tech. rep. (Engineering Mechanics Division IIT Research Institute, Chicago, Il, 1969), pp. 1–36.

[31] PFM Ellis, "Fuelbed ignition potential and bark morphology explain the notoriety of the eucalypt messmate 'stringybark' for intense spotting", International Journal of Wildland Fire **20**, 897–907 (2011) 10.1071/WF10052.

[32] PF Ellis, "The likelihood of ignition of dry-eucalypt forest litter by firebrands", International Journal of Wildland Fire **24**, 225–235 (2015) 10.1071/WF14048.

[33] A Ganteaume, C Lampin-Maillet, M Guijarro, C Hernando, M Jappiot, T Fonturbel, P Ṕrez-Gorostiaga, and JA Vega, "Spot fires: Fuel bed flammability and capability of firebrands to ignite fuel beds", International Journal of Wildland Fire **18**, 951–969 (2009) 10.1071/WF07111.

[34] SL Manzello, TG Cleary, JR Shields, and JC Yang, "On the ignition of fuel beds by firebrands", Fire and Materials **30**, 77–87 (2006) 10.1002/fam.901.

[35] SL Manzello, TG Cleary, JR Shields, and JC Yang, "Ignition of mulch and grasses by firebrands in wildlandurban interface fires", International Journal of Wildland Fire **15**, 427–431 (2006) 10.1071/WF06031.

[36] S Wang, X Huang, H Chen, and N Liu, "Interaction between flaming and smouldering in hot-particle ignition of forest fuels and effects of moisture and wind", International Journal of Wildland Fire **26**, 71–81 (2017) 10.1071/WF16096.

[37] JL Urban, CD Zak, J Song, and C Fernandez-Pello, "Smoldering spot ignition of natural fuels by a hot metal particle", Proceedings of the Combustion Institute **36**, 3211–3218 (2017) 10.1016/j.proci.2016.09.014.

[38] AC Fernandez-Pello, C Lautenberger, D Rich, C Zak, J Urban, R Hadden, S Scott, and S Fereres, "Spot Fire Ignition of Natural Fuel Beds by Hot Metal Particles, Embers, and Sparks", Combustion Science and Technology **187**, 269–295 (2015) 10.1080/00102202.2014.973953.

[39] RM Hadden, S Scott, C Lautenberger, and CC Fernandez-Pello, "Ignition of Combustible Fuel Beds by Hot Particles: An Experimental and Theoretical Study", Fire Technology **47**, 341–355 (2011) 10.1007/s10694-010-0181-x.

[40] MA Finney, JD Cohen, SS McAllister, and WM Jolly, "On the need for a theory of wildland fire spread", International Journal of Wildland Fire **22**, 25 (2013) 10.1071/WF11117.

[41] J Fjellerup, U Henriksen, AD Jensen, PA Jensen, and P Glarborg, "Heat transfer in a fixed bed of straw char", Energy and Fuels **17**, 1251–1258 (2003) 10.1021/ef030036n.

[42] J Yang, S Wang, and H Chen, "Effect of interface thermal resistance on ignition of reactive material by a hot particle", International Journal of Heat and Mass Transfer **97**, 146–156 (2016) 10.1016/j.ijheatmasstransfer.2016.01.070.

[43] J Zinn, "Initiation of explosions by hot spots", The Journal of Chemical Physics **36**, 1949 (1962) 10.1063/1.1701302.

[44] PH Thomas, "A Comparison of Some Hot Spot Theories", Combustion and Flame **9**, 369–372 (1965).

[45] UI Gol'dshleger, "Ignition of a condensed explosive by a hot object of finite dimensions", Combustion, Explosion, and Shock Waves **9**, 99–102 (1973).

[46] P Yin, N Liu, H Chen, JS Lozano, and Y Shan, "New Correlation Between Ignition Time and Moisture Content for Pine Needles Attacked by Firebrands", Fire Technology **50**, 79–91 (2014) 10.1007/s10694-012-0272-y.

[47] MI Nelson, J Brindley, and A McIntosh, "The dependence of critical heat flux on fuel and additive properties: a critical mass flux model", Fire Safety Journal **24**, 107–130 (1995) 10.1016/0379-7112(95)00013-J.

[48] D Rich, C Lautenberger, JL Torero, JG Quintiere, and C Fernandez-Pello, "Mass flux of combustible solids at piloted ignition", Proceedings of the Combustion Institute **31**, 2653–2660 (2007) 10.1016/j.proci.2006.08.055.

[49] BL Yashwanth, B Shotorban, S Mahalingam, and DR Weise, "An Investigation of the Influence of Heating Modes on Ignition and Pyrolysis of Woody Wildland Fuel", Combustion Science and Technology **187**, 780–796 (2015) 10.1080/00102202.2014.973948.

[50] S McAllister, "Critical mass flux for flaming ignition of wet wood", Fire Safety Journal **61**, 200–206 (2013) 10.1016/j.firesaf.2013.09.002.

[51] J Dai, MA Delichatsios, L Yang, and J Zhang, "Piloted ignition and extinction for solid fuels", Proceedings of the Combustion Institute **34**, 2487–2495 (2013) 10.1016/j.proci.2012.07.021.

[52] C Di Blasi, "Heat, Momentum, and Mass Transport Through A Shrinking Biomass Particle Exposed to Thermal Radiation", Chemical Engineering Science **51**, 1121–1132 (1996).

[53] Y Ding, C Wang, and S Lu, "Modeling the pyrolysis of wet wood using FireFOAM", Energy Conversion and Management **98**, 500–506 (2015) 10.1016/j.enconman.2015.03.106.

[54] JL Torero, JI Gerhard, MF Martins, MA Zanoni, TL Rashwan, and JK Brown, "Processes defining smouldering combustion: Integrated review and synthesis", Progress in Energy and Combustion Science **81**, 10.1016/j.pecs.2020.100869 (2020) 10.1016/j.pecs.2020.100869.

[55] E Ranzi, A Cuoci, T Faravelli, A Frassoldati, G Migliavacca, S Pierucci, and S Sommariva, "Chemical kinetics of biomass pyrolysis", Energy and Fuels **22**, 4292–4300 (2008) 10.1021/ef800551t.

[56] PEA Debiagi, C Pecchi, G Gentile, A Frassoldati, A Cuoci, T Faravelli, and E Ranzi, "Extractives Extend the Applicability of Multistep Kinetic Scheme of Biomass Pyrolysis", Energy and Fuels **29**, 6544–6555 (2015) 10.1021/acs.energyfuels.5b01753.

[57] A Dhahak, R Bounaceur, C Le Dreff-Lorimier, G Schmidt, G Trouve, and F Battin-Leclerc, "Development of a detailed kinetic model for the combustion of biomass", Fuel **242**, 756–774 (2019) 10.1016/j.fuel.2019.01.093.

[58] C Di Blasi, "Modeling and simulation of combustion processes of charring and non-charring solid fuels", Progress in Energy and Combustion Science **19**, 71–104 (1993) https://doi.org/10.1016/0360-1285(93)90022-7.

[59] I Haberle, Ø Skreiberg, J Łazar, and NEL Haugen, "Numerical models for thermochemical degradation of thermally thick woody biomass, and their application in domestic wood heating appliances and grate furnaces", Progress in Energy and Combustion Science **63**, 204–252 (2017) 10.1016/j.pecs.2017.07.004.

[60] C Lautenberger and C Fernandez-Pello, "A model for the oxidative pyrolysis of wood", Combustion and Flame **156**, 1503–1513 (2009) 10.1016/j.combustflame.2009.04.001.

[61] K McGrattan, S Hostikka, R McDermott, J Floyd, C Weinschenk, and K Overholt, "Fire Dynamics Simulator Technical Reference Guide (Sixth Edition)", NIST Special Publication **1**, 1–147 (2021).

[62] BL Yashwanth, B Shotorban, S Mahalingam, CW Lautenberger, and DR Weise, "A numerical investigation of the influence of radiation and moisture content on pyrolysis and ignition of a leaf-like fuel element", Combustion and Flame **163**, 301–316 (2016) 10.1016/j.combustflame.2015.10.006.

[63] B Shotorban, BL Yashwanth, S Mahalingam, and DJ Haring, "An investigation of pyrolysis and ignition of moist leaf-like fuel subject to convective heating", Combustion and Flame **190**, 25–35 (2018) 10.1016/j.combustflame.2017.11.008.

[64] C Lautenberger and AC Fernandez-Pello, "Spotting ignition of fuel beds by firebrands", WIT Transactions on Modelling and Simulation **48**, 603–612 (2009) 10.2495/CMEM090541.

[65] Cal Fire, *Top 20 Largest California Wildfires*, 2019.

[66] US DOI/USDA, "Federal Firefighting Costs (Suppression Only) [table]", U.S. Department of Interior/U.S. Department of Agriculture, Forest Service (2019).

[67] CDo Insurance, *Wildfire insurance losses from November 2018 blazes top $12 billion*, 2019.

[68] A Maranghides, D McNamara, W Mell, J Trook, and B Toman, *NIST Technical Note 1796 A: A Case Study of a Community Affected by the Witch and Guejito Fires: Report #2 – Evaluating the Effects of Hazard Mitigation Actions on Structure Ignitions*, tech. rep. (NIST, 2013).

[69] E Koo, PJ Pagni, DR Weise, and JP Woycheese, "Firebrands and spotting ignition in large-scale fires", International Journal of Wildland Fire **19**, 818–843 (2010) 10.1071/WF07119.

[70] SL Manzello, TG Cleary, JR Shields, A Maranghides, W Mell, and JC Yang, "Experimental investigation of firebrands: Generation and ignition of fuel beds", Fire Safety Journal **43**, 226–233 (2008) 10.1016/j.firesaf.2006.06.010.

[71] JL Urban, J Song, S Santamaria, and C Fernandez-Pello, "Ignition of a spot smolder in a moist fuel bed by a firebrand", Fire Safety Journal **108**, 102833 (2019) 10.1016/j.firesaf.2019.102833.

[72] CD Zak, JL Urban, and C Fernandez-Pello, "Characterizing the flaming ignition of cellulose fuel beds by hot steel spheres", Combustion Science and Technology **186**, 1618–1631 (2014) 10.1080/00102202.2014.935612.

[73] JL Urban, CD Zak, and C Fernandez-Pello, "Spot Fire Ignition of Natural Fuels by Hot Aluminum Particles", Fire Technology **54**, 797–808 (2018) 10.1007/s10694-018-0712-4.

[74] RS Hakes, H Salehizadeh, MJ Weston-Dawkes, and MJ Gollner, "Thermal characterization of firebrand piles", Fire Safety Journal **104**, 34–42 (2019) 10.1016/j.firesaf.2018.10.002.

[75] Z Tao, B Bathras, B Kwon, B Biallas, and MJ Gollner, "Effect of firebrand size and geometry on heating from a smoldering pile under wind", Fire Safety Journal, 103031 (2020) 10.1016/j.firesaf.2020.103031.

[76] ED Bearinger, JL Hodges, F Yang, CM Rippe, and BY Lattimer, "Localized heat transfer from firebrands to surfaces", Fire Safety Journal **120**, 103037 (2021) 10.1016/j.firesaf.2020.103037.

[77] N Hernández, A Fuentes, JL Consalvi, and JC Elicer-Cortés, "Spontaneous ignition of wildland fuel by idealized firebrands", Experimental Thermal and Fluid Science **95**, 88–95 (2018) 10.1016/j.expthermflusci.2018.01.037.

[78] J Rivera, N Hernández, JL Consalvi, P Reszka, J Contreras, and A Fuentes, "Ignition of wildland fuels by idealized firebrands", Fire Safety Journal, 10.1016/j.firesaf.2020.103036 (2020) 10.1016/j.firesaf.2020.103036.

[79] Z Wang, Y Zhang, J Huang, Z Liang, L Zheng, and J Lu, "Ignition method effect on detonation initiation characteristics in a pulse detonation engine", Applied Thermal Engineering **93**, 1–7 (2016) 10.1016/j.applthermaleng.2015.09.064.

[80] Watlow, *Heat Loss Factors and Graphs*, 2020.

[81] F Incropera, D Dewitt, T Bergman, and A Lavine, *Fundamentals of heat and mass transfer*, 7th ed. (Wiley, Hoboken, NJ, 2011), pp. 119–121.

[82] FP Laboratory, *Wood Handbook-Wood as an engineering material*, tech. rep. (U.S. Department of Agriculture, Madison, 2010), p. 508.

[83] F Asdrubali, AL Pisello, F D'Alessandro, F Bianchi, M Cornicchia, and C Fabiani, "Innovative cardboard based panels with recycled materials from the packaging industry: Thermal and acoustic performance analysis", Energy Procedia **78**, 321–326 (2015) 10.1016/j.egypro.2015.11.652.

[84] TO Foundation, *OpenFOAM*, 2020.

[85] DG Goodwin, Raymond L. Speth, and Harry K. Moffat, *Cantera*, 2020, 10.5281/zenodo.1174508.

[86] E Ranzi, M Dente, A Goldaniga, G Bozzano, and T Faravelli, "Lumping procedures in detailed kinetic modeling of gasification, pyrolysis, partial oxidation and combustion of hydrocarbon mixtures", Progress in Energy and Combustion Science **27**, 99–139 (2001) 10.1016/S0360-1285(00)00013-7.

[87] H Yang, R Yan, H Chen, DH Lee, and C Zheng, "Characteristics of hemicellulose, cellulose and lignin pyrolysis", Fuel **86**, 1781–1788 (2007) 10.1016/j.fuel.2006.12.013.

[88] F Pedregosa, G Varoquaux, A Gramfort, V Michel, B Thirion, O Grisel, M Blondel, P Prettenhofer, R Weiss, V Dubourg, J Vanderplas, A Passos, D Cournapeau, M Brucher, M Perrot, and E Duchesnay, "Scikit-learn: Machine Learning in Python", Journal of Machine Learning Research **12**, 2825–2830 (2011).

[89] SL Manzello, T Yamada, A Jeffers, Y Ohmiya, K Himoto, and A Carlos Fernandez-Pello, "Summary of workshop for fire structure interaction and urban and wildland-urban interface (WUI) Fires-operation Tomodachi-fire research", Fire Safety Journal **59**, 122–131 (2013) 10.1016/j.firesaf.2013.03.021.

[90] SL Manzello, "Enabling the investigation of structure vulnerabilities to wind-Driven firebrand showers in wildland-Urban Interface (WUI) fires", Fire Safety Science **11**, 83–96 (2014) 10.3801/IAFSS.FSS.11-83.

[91] S Suzuki, SL Manzello, and Y Hayashi, "The size and mass distribution of firebrands collected from ignited building components exposed to wind", Proceedings of the Combustion Institute **34**, 10.1016/j.proci.2012.06.061 (2013) 10.1016/j.proci.2012.06.061.

[92] H Salehizadeh, RS Hakes, and MJ Gollner, "Critical ignition conditions of structural materials by cylindrical firebrands", Frontiers in Mechanical Engineering, 1–13 (2021) 10.3389/fmech.2021.630324.

[93] A Filkov, D Kasymov, V Zima, and O Matvienko, "Experimental investigation of surface litter ignition by bark firebrands", AIP Conference Proceedings **1698**, 10.1063/1.4937859 (2016) 10.1063/1.4937859.

[94] OVA Matvienko, DPA Kasymov, and AI Filkov, "Simulation of fuel bed ignition by wildland firebrands", International Journal of Wildland Fire **27**, 550–561 (2018) 10.1071/WF17083.

[95] MP Plucinski and WR Anderson, "Laboratory determination of factors influencing successful point ignition in the litter layer of shrubland vegetation", International Journal of Wildland Fire **17**, 628–637 (2008) 10.1071/WF07046.

[96] CF Wu and Y Tian, "Three-phase optimal design of sensitivity experiments", Journal of Statistical Planning and Inference **149**, 1–15 (2014) 10.1016/j.jspi.2013.10.007.

[97] S Burke and L Truett, *Test Strategies for Experiments with a Binary Response and Single Stress Factor Best Practice*, tech. rep. June (Air Force Institute of Technology, Dayton, OH, USA, 2017).

[98] Idaho National Laboratory, *Bioenergy Feedstock Library*, tech. rep. (U.S. Department of Energy, 2020).

[99] D Bean and DL Blunck, "Sensitivities of Porous Beds and Plates to Ignition by Firebrands", Frontiers in Mechanical Engineering **7**, 1–11 (2021) 10.3389/fmech.2021.653810.

[100] H Jiang, "Separation angle for flow past a circular cylinder in the subcritical regime", Physics of Fluids **32**, 10.1063/1.5139479 (2020) 10.1063/1.5139479.

[101] P Mindykowski, A Fuentes, JL Consalvi, and B Porterie, "Piloted ignition of wildland fuels", Fire Safety Journal **46**, 34–40 (2011) 10.1016/j.firesaf.2010.09.003.

[102] PD Miles and WB Smith, "Specific Gravity and Other Properties of Wood and Bark for 156 Tree Species Found in North America", Res. Note. NRS-38, 35 (2009).

[103] PE Mason, LI Darvell, JM Jones, and A Williams, "Comparative Study of the Thermal Conductivity of Solid Biomass Fuels", Energy and Fuels **30**, 2158–2163 (2016) 10.1021/acs.energyfuels.5b02261.

[104] PS Lam, S Sokhansanj, X Bi, S Mani, CJ Lim, AR Womac, M Hoque, J Peng, T Jayashankar, LJ Nalmi, and S Nayaran, "Physical characterization of wet and dry wheat straw and switchgrass - Bulk and specific density", 2007 ASABE Annual International Meeting, Technical Papers **11 BOOK**, 10.13031/2013.23552 (2007) 10.13031/2013.23552.

[105] M Stenseng, A Jensen, and K Dam-johansen, "Investigation of biomass pyrolysis by thermogravimetric analysis and differential scanning calorimetry", Journal of Analytical and Applied Pyrolysis **58**, 765–780 (2001).

[106] M Gupta, J Yang, and C Roy, "Specific heat and thermal conductivity of softwood bark and softwood char particles", Fuel **82**, 919–927 (2003) 10.1016/S0016-2361(02)00398-8.

[107] SL Manzello, A Maranghides, and WE Mell, "Firebrand generation from burning vegetation", International Journal of Wildland Fire **16**, 458–462 (2007) 10.1071/WF06079.

[108] WJ Parker, "Prediction of the Heat Release Rate of Wood.", 207–216 (1986) 10.3801/iafss.fss.1-207.

[109] H Versteeg and W Malalasekera, *An Introduction to Computational Fluid Dynamics: The Finite Volume Method*, 2nd (Pearson, 2007), 10.1007/978-3-030-72884-7.

[110] TJ Ohlemiller, "Force Smolder Propagation and the Transition to Flaming in Cellulosic Insulation", Combustion and Flame **81**, 354–365 (1990).

[111] SI Stoliarov, O Zeller, AB Morgan, and S Levchik, "An experimental setup for observation of smoldering-to-flaming transition on flexible foam/fabric assemblies", Fire and Materials **42**, 128–133 (2018) 10.1002/fam.2464.

[112] MA Santoso, EG Christensen, J Yang, and G Rein, "Review of the Transition From Smouldering to Flaming Combustion in Wildfires", Frontiers in Mechanical Engineering **5**, 10.3389/fmech.2019.00049 (2019) 10.3389/fmech.2019.00049.

[113] V Fateev, M Agafontsev, S Volkov, and A Filkov, "Determination of smoldering time and thermal characteristics of firebrands under laboratory conditions", Fire Safety Journal **91**, 791–799 (2017) 10.1016/j.firesaf.2017.03.080.